UNIVERSIDADE FEDERAL DE SÃO CARLOS

CENTRO DE CIÊNCIAS EXATAS E TECNOLOGIA

PROGRAMA DE PÓS-GRADUAÇÃO EM ENGENHARIA QUÍMICA

Catalytic hydrogenation: novel process for valorization of 3-hydroxybutyric acid and advanced in situ infrared spectroscopy applied to CO_2 conversion

João Lucas Marques Barros

São Carlos, SP

2026

UNIVERSIDADE FEDERAL DE SÃO CARLOS

CENTRO DE CIÊNCIAS EXATAS E TECNOLOGIA

PROGRAMA DE PÓS-GRADUAÇÃO EM ENGENHARIA QUÍMICA

Catalytic hydrogenation: novel process for valorization of 3-hydroxybutyric acid and advanced in situ infrared spectroscopy applied to CO_2 conversion

Tese de Doutorado apresentada ao Programa de Pós-Graduação em Engenharia Química da Universidade Federal de São Carlos como requisito para a obtenção do título de Doutor em Engenharia Química.

Orientador: Prof. Dr. José Maria Corrêa Bueno

São Carlos, SP

2026

UFSCar

UNIVERSIDADE FEDERAL DE SÃO CARLOS

Folha de Aprovação

Defesa de Tese de Doutorado do candidato João Lucas Marques Barros, realizada em 26/02/2026.

Comissão Julgadora:

Prof. Dr. José Maria Corrêa Bueno (UFSCar)

Prof. Dr. João Batista Oliveira dos Santos (UFSCar)

Dr. Davi Petrolini (UFSCar)

Profa. Dra. Adriana Maria da Silva (INMETRO)

Profa. Dra. Daniela Zanchet (UNICAMP)

O Relatório de Defesa produzido pelos membros da Comissão Julgadora encontra-se arquivado junto ao Programa de Pós-Graduação.

APOIO FINANCEIRO

O presente trabalho foi realizado com apoio da Coordenação de Aperfeiçoamento de Pessoal de Nível Superior – Brasil (CAPES) – Código de Financiamento 001. Agradecemos também às agências de fomento Conselho Nacional de Desenvolvimento Científico e Tecnológico (CNPq, 160761/2022-0) e Fundação de Amparo à Pesquisa do Estado de São Paulo (FAPESP, 2018/01258-5) pelo apoio financeiro. Também à empresa PHB Industrial S.A. pelo fornecimento de reagentes e apoio financeiro.

AGRADECIMENTOS

Primeiramente aos meus pais, Loide e Cleomar, ao meu irmão Thiago e meu cunhado André, meus exemplos de pessoas batalhadoras, por me apoiar durante toda minha vida pessoal e acadêmica até o presente momento. Essas pessoas me mostraram a valiosa lição de que grandes conquistas só são possíveis com sacrifícios, sendo a minha ausência ao lado deles durante longos períodos de tempo o maior de todos na minha vida até hoje.

Ao meu orientador Prof. Dr. José Maria pela paciência na supervisão, por compartilhar sua sabedoria e pela confiança no meu trabalho durante o doutorado, resultando no profissional que sou hoje. Ao Prof. Dr. João Batista pelo suporte fundamental para nossa pesquisa, pelo auxílio na resolução dos mais diversos problemas e pelo companheirismo. Á minha orientadora do mestrado, colaboradora e amiga Dra. Adriana Maria por ter me iniciado na catálise, me guiado nos primeiros passos dessa trajetória, participar ativamente na minha carreira até hoje e pelas caracterizações deste trabalho. Aos meus grandes amigos e colegas de laboratório José Lucas e Gustavo pelo acolhimento quando cheguei em São Carlos, pelas várias discussões que tanto enriqueceram meu conhecimento e pela construção do Pagode Catalítico. Aos meus colegas do DEQ Arnaldo, Henrique, Mariana, Vitor, Daiara, Davi, Gabi, Yasmin e Breno por toda a parceria que tivemos no laboratório, somos a prova do poder da colaboração ao realizar a pesquisa e desenvolver o nosso laboratório, trabalhar com eles foi não só um prazer mas um previlégio. Também ao Prof Dr. Marco Daturi pela oportunidade do estágio na França e pelo treinamento em infravermelho in situ e à Prof. Dra. Daniela Zanchet e meu amigo Dr. Leonardo da Silva pelo auxílio na construção do sistema de modulação. Á Dra. Carla Ramos Moreira e ao LABNANO/CBPF pelas análises de HRTEM e ao Prof. Dr. Jean Gallo por disponibilizar o sistema de reação batelada em alta pressão e o HPLC.

Aos vários colegas e amigos que conheci em São Carlos, Alessandra, Christian, Ana Laura, Daniel, Jão, Wilhamis, Karoll, Marcus, Paulo, Danielly, Simon, Breno, Angélica, Fernando, Julio, Gilberto, Balena, Fabi, Josias e Douglas. Sou muito grato pelo melhor ambiente de trabalho do mundo e por trazer tanta alegria para esse doutorado. Agradeço também à equipe técnica, administrativa, de segurança e limpeza do departamento por tornar tudo isso possível.

Finalmente aos meus amigos de infância, meus segundos irmãos Leonardo, Renato, Alexandre, Matheus e Tiago e minhas primas Danielly e Gabriela, pelos vários momentos

maravilhosos que passamos juntos e por me fazer não me sentir completamente sozinho mesmo nos momentos mais difíceis. Aos colegas e amigos que fizeram parte da minha vida durante a graduação em Toledo, em especial ao meu falecido amigo Kennedy, a quem dedico esta tese. Também às pessoas incríveis que conheci no mestrado em Cachoeira Paulista.

CONTEXTUALIZAÇÃO

Este trabalho teve como foco reações de hidrogenação catalítica, sendo o primeiro capítulo relacionado à valorização do ácido 3-hidróxibutírico, enquanto os capítulos dois e três abordam a conversão de CO_2. Ao longo dos anos, as reações de hidrogenação vem sendo amplamente estudadas, desenvolvidas e implementadas na indústria, devido a vasta gama de produtos de valor agregado que podem ser obtidos e o potencial para converter gases de efeito estufa.

O estudo destaca a importância da compreensão dos mecanismos reacionais envolvidos nos processos de catálise heterogênea. Dado o caráter inovador da reação de hidrogenação do ácido 3-hidróxibutírico a 1,3-butanodiol em meio aquoso, foi realizada investigação das rotas de degradação do produto nas condições reacionais utilizadas, permitindo identificar os desafios para se obter alta seletividade. Por outro lado, no caso da hidrogenação de CO_2 a literatura a respeito dos mecanismos é vasta, principalmente estudos utilizando a técnica de espectroscopia no infravermelho in situ. Entretanto, mesmo com o avanço da pesquisa, diversos aspectos das rotas reacionais atualmente ainda são tema de debate e controvérsia.

Os desafios se dão pelas limitações intrínsecas da técnica convencional, visto que durante o monitoramento in situ da superfície do catalisador são observados sinais de intermediários da reação, mas também de espécies espectadoras, ou seja, espécies que se acumulam na superfície do material mas não participam de fato da reação, o que pode acarretar em conclusões errôneas a respeito do caminho reacional. Nesse sentido, o trabalho apresenta a implementação da técnica avançada de modulação excitação acoplada com detecção sensitiva de fases, utilizando um sistema convencional de infravermelho in situ. Este método transiente permite diferenciar espécies ativas de espectadores, além de fornecer informação a respeito da cinética relativa dos intermediários. Com isso, foi demonstrado o potencial da técnica por meio do estudo da hidrogenação de CO_2 sobre catalisadores Cu/ZrO_2 e $Cu\text{-}ZrO_2/SiO_2$, com a identificação de intermediários da reação e as etapas lentas do mecanismo.

Summary

CHAPTER I: NOVEL AQUEOUS-PHASE PROCESS FOR CONVERSION OF 3-HYDROXYBUTYRIC ACID TO 1,3-BUTANEDIOL: EFFECTS OF TEMPERATURE, HYDROGEN PRESSURE, AND NATURE OF Ru-SUPPORTED CATALYSTS ON SELECTIVE HYDROGENATION

ABSTRACT

A novel aqueous-phase hydrogenation reaction was developed for the conversion of 3-hydroxybutyric acid (HBA) to 1,3-butanediol (1,3-BDO) over catalysts composed of Ru supported on TiO_2, SiO_2, and C. Analyses using XRD and Raman spectroscopy indicated strong metal-oxide interaction in the Ru/TiO_2 samples, while weak interaction of Ru with SiO_2 led to crystallization of the Ru species. Preliminary catalytic tests with a commercial Ru/C catalyst showed that higher H_2 pressure and low temperature (130 ºC) enabled selective hydrogenation of HBA to 1,3-BDO. Compared to the commercial catalyst, the synthesized Ru/TiO_2 and Ru/SiO_2 catalysts were more selective towards 1,3-BDO, achieving 38% selectivity with a catalyst composed of 2.0% Ru supported on TiO_2. The SiO_2-supported catalyst was significantly more active (62% HBA conversion at 150 ºC) than the TiO_2-supported counterpart, but was also more prone to side reactions leading to 2-propanol and 2-butanol. Stability experiments with the 1,3-BDO product revealed that the Ru-based catalysts promoted side reactions originating from 1,3-BDO, especially over the SiO_2-supported catalyst, which could explain the lower selectivity observed in the catalytic HBA hydrogenation. A mechanistic investigation indicated that 1,3-BDO could undergo dehydration to 2-butanol and dehydrogenation to 4-hydroxy-2-butanone, a possible intermediate in the formation of 2-propanol by a C-C cleavage pathway.

INTRODUCTION

Worldwide concerns about pollution of the environment by plastics released from different sources have led to increased research into the development of sustainable alternatives, such as bioplastics. One widely studied bioplastic is the polymer poly(3-hydroxybutyrate) (PHB), which

can be used to produce the 3-hydroxybutyric acid (HBA) monomer by means of microbial, enzymatic, and chemical methodologies [1, 2].

The HBA monomer presents antimicrobial, insecticidal, and antiviral activities, and has applications in the synthesis of fine chemicals, antibiotics, and vitamins [3]. One potential synthesis route that has received little attention is the catalytic hydrogenation of HBA to 1,3-butanediol (1,3-BDO), a high value-added product with known nutritional benefits, currently being studied in food ingredient research. 1,3-BDO can also be used as a building block in the production of butadiene, polyester resins, and plasticizers, among other substances [4, 5]. Hence, it is highly desirable to develop catalysts that are active and selective in the hydrogenation of HBA to 1,3-BDO [6], since this pathway could add to the wide range of applications for HBA.

However, it remains a challenge to selectively hydrogenate the carboxyl group (COOH-) of the HBA, while preserving the hydroxyl group (OH-). Under hydrogenation conditions, the formation of alcohols and diols from the corresponding carboxylic acids and esters occurs by cleavage of the acyl bonds [7]. Nevertheless, the selective formation of 1,3-BDO from HBA is hindered by possible side reactions involving OH- hydrogenolysis, in addition to the formation of hydrocarbons, acids, and ethers [8]. Therefore, the optimization of catalyst properties is fundamental for enhancing activity in the selective hydrogenation of the carbonyl group.

The primary products may also undergo further conversion reactions, such as the formation of butadiene from 1,3-BDO, for which an established route involves consecutive dehydration steps of both primary and secondary hydroxyl groups of 1,3-BDO [9-11]. The dehydrogenation of 1,3-BDO has also been reported, yielding unsaturated compounds such as 3-hydroxybutanal and 4-hydroxy-2-butanone, which, in turn, may be converted to shorter carbon chain saturated alcohols by cleavage of carbon bonds [12-14] and hydrogenation pathways [15-18]. Although these reactions involving 1,3-BDO usually require strong Brönsted acidity and high temperatures, it has been demonstrated that the reactions can also proceed over a Cu/SiO_2 catalyst, at mild temperatures (~250 ºC) [19]. It is notable that most of the studies cited provide catalytic test data obtained using gas-phase continuous fixed-bed reactors, so little information is available regarding the mechanisms of liquid-phase reactions with 1,3-BDO. Furthermore, due to the novel aspect of the hydrogenation of HBA, no data concerning side reactions involving the acid have so far been reported.

Given the challenge of achieving selective hydrogenation of the carboxylic group, while preserving the hydroxyls, the hydrogenation of HBA to 1,3-BDO requires the development of an effective catalyst. Among the systems utilized in the hydrogenation of carboxylic acids, supported Ru catalysts have attracted attention, since they offer superior activity in selectively hydrogenating carbonyl (C=O) groups. Ru-based catalysts have been employed in the hydrogenation of carboxylic acids including lactic acid and butyric acid, which have structures similar to that of HBA [20-23]. Lee et al. [20] synthesized ZnO-supported catalysts for the hydrogenation of butyric acid to n-butanol, achieving almost complete selectivity using materials with Ru content as low as 1%, when a small amount of Sn (2%) was introduced in the catalyst. In recent work concerning the hydrogenation of lactic acid to 1,2-propanediol (1,2-PDO), TiO_2 was observed to have a beneficial effect on the selectivity to 1,2-PDO, when compared to other supports including carbon and oxides such as SiO_2, CeO_2, and Al_2O_3, which was explained in terms of improved Ru reducibility, due to the acid-base properties of TiO_2 [22]. There is also theoretical evidence of heterolytic H_2 dissociation over Ru/TiO_2, ascribed to interfacial sites of Ru and TiO_2 [24]. Furthermore, a comparative study with different metals supported on SiO_2 found that superior 1,2-propanediol yields were obtained using Ru, compared to Pt, Ni, Cu, and other metals [23].

Research on the selective hydrogenation of carboxylic and dicarboxylic acids/esters to produce the corresponding unsaturated alcohols and diols has shown the superior performance of TiO_2 for selective reduction of the COOH- group [25, 26]. The effect of TiO_2 has been linked to the generation of Lewis acid centers, such as non-stoichiometric TiO_x, by interaction with O^{2-} of the carboxyl groups. Most of the research concerning Ru and TiO_2 reported in the literature is related to unsaturated compounds such as aldehydes, carboxylic acids/esters, and dicarboxylic acids/esters [27], while few studies have addressed the selective hydrogenation of keto dicarboxylic acids or esters.

The present work reports a novel aqueous-phase catalytic hydrogenation of 3-hydroxybutyric acid to 1,3-butanediol over catalysts composed of Ru supported on C, TiO_2, and SiO_2. Evaluation was made of the effects of Ru loading, type of support, and the reaction conditions. The challenges in the novel reaction are highlighted, together with provision of product stability data and insights into the conversion mechanism.

METHODOLOGY

Synthesis of the catalysts

The Ru/TiO_2 catalysts containing 0.1% and 2.0% of Ru were synthesized by incipient wetness impregnation, according to the procedure described by Liu et al. [22], with adaptations. Firstly, commercial TiO_2 (Degussa P-25) was dried in an oven at 110 ºC for 24 h. An aqueous solution of the $RuCl_3.xH_2O$ (Sigma) precursor was agitated for 0.5 h, at 150 rpm and room temperature, and was then added to the dried support. The slurry mixture was stirred at 250 rpm for 4.5 h. The product was dried at 80 ºC for 2.0 h and then at 110 ºC overnight. The prepared catalyst was activated for 2.0 h, at 350 ºC, under a flow of pure H_2 (30 mL/min).

The SiO_2 support was prepared by treatment of tetraethyl orthosilicate with HNO_3 and NH_4OH, followed by calcination for 5.0 h, at 500 ºC, under an air atmosphere, using a heating rate of 3 ºC/min. The 0.1% Ru/SiO_2 catalyst was also synthesized by incipient impregnation, following the same synthesis and activation procedures described above. For comparison, a commercial 5.0% Ru/C (Sigma) catalyst was employed, without any pretreatment.

Characterizations

X-ray diffraction (XRD) analyses were performed using a Shimadzu XRD 6000 instrument operating with Cu Kα radiation, in the 2θ range from 10º to 80º, with step size of 0.02º. Chemical composition analyses were performed by X-ray fluorescence (XRF), using a Shimadzu EDX-720 instrument. Raman spectra were acquired using a Witec Alpha-300 R spectrometer integrated with a confocal optical microscope. Spectra were obtained for specific regions of interest in the samples, as observed under the microscope. Given the spot-sized nature of the Raman analysis, multiple regions of the samples were examined, since catalyst surfaces often present heterogeneity. The laser excitation wavelength used was 532 nm. The experiments were performed at INMETRO.

High resolution transmission electron microscopy (HRTEM) analyses were performed using a JEOL JEM 2100F instrument operating at 200 kV at LABNANO/CBPF. The samples were suspended in ethanol and dispersed ultrasonically for 5 min. Drops of the suspension were then deposited on a copper grid (#200) coated with a holey carbon film. Particle size measurements

were performed using ImageJ software (version 1.54d). For statistical purposes, more than 200 particles were considered.

Catalytic tests

The catalytic experiments employed a stainless-steel batch reactor (70 mL) at the Chemistry Department (DQ – UFSCar). In a typical test, the equipment was loaded with 20 mL of an aqueous reactant solution (at 0.1 mol/L) and 150 mg of previously reduced catalyst, followed by purging with Ar and then with H_2. The reactor was then pressurized with pure H_2 to obtain a pressure of 70 bar at the different reaction temperatures used (130, 150, or 170 ºC). The entire system was then placed in a thermal oil bath maintained at the desired reaction temperature. After the transient period, the reaction was allowed to proceed under this condition for 5 h. Finally, the resulting mixture was analyzed using a Shimadzu HPLC system equipped with a refractive index detector (RID). The analyses were typically performed with the column oven maintained at 65 ºC. The equations used to determine HBA conversion (Equation 1), products selectivity (Equation 2), and 1,3-BDO yield (Equation 3) are presented below.

$$X_{HBA} = \frac{C^0_{HBA} - C_{HBA}}{C^0_{HBA}} .100 \quad (1)$$

$$S_i = \frac{C_i}{C^0_{HBA} - C_{HBA}} .100 \quad (2)$$

$$Y_{1,3BDO} = \frac{C_{1,3BDO}}{C^0_{HBA}} .100 \quad (3)$$

where, C^0_{HBA} and C_i are the concentration of HBA at the start of the reaction and the concentration of the product i after the reaction, respectively.

RESULTS AND DISCUSSION

Characterization

The Ru loading of the samples was determined by XRF, the results are presented in Table 1, denoting at low Ru content the impregnation process was more efficient. The sample names defined are used throughout the text.

Table 1. Ru loading of the samples determined by XRF.

Catalyst	Ru loading (wt. %)	Sample name
0.1% Ru/SiO_2	0.1	$0.1Ru/SiO_2$
0.1% Ru/TiO_2	0.1	$0.1Ru/TiO_2$
2.0% Ru/TiO_2	1.7	$2.0Ru/TiO_2$
5.0%Ru/C	5.0	5.0Ru/C

X-ray diffractograms of SiO_2 and Ru/SiO_2 are shown in Figure 1. For SiO_2, a broad peak between 2θ of 12º and 40º corresponded to the amorphous SiO_2 phase, while for Ru/SiO_2, low intensity peaks at 2θ of 38º, 42.2º, and 44.1º could be attributed to the (1 0 0), (2 0 0), and (1 0 1) planes of Ru^0, respectively [30, 31]. The diffractogram for the commercial 5.0% Ru/C material presented the Ru^0 diffraction lines, together with broad peaks related to poorly-organized carbon at 2θ of around 26º and 43º, corresponding to the (0 0 2) and (1 0 1) planes, respectively.

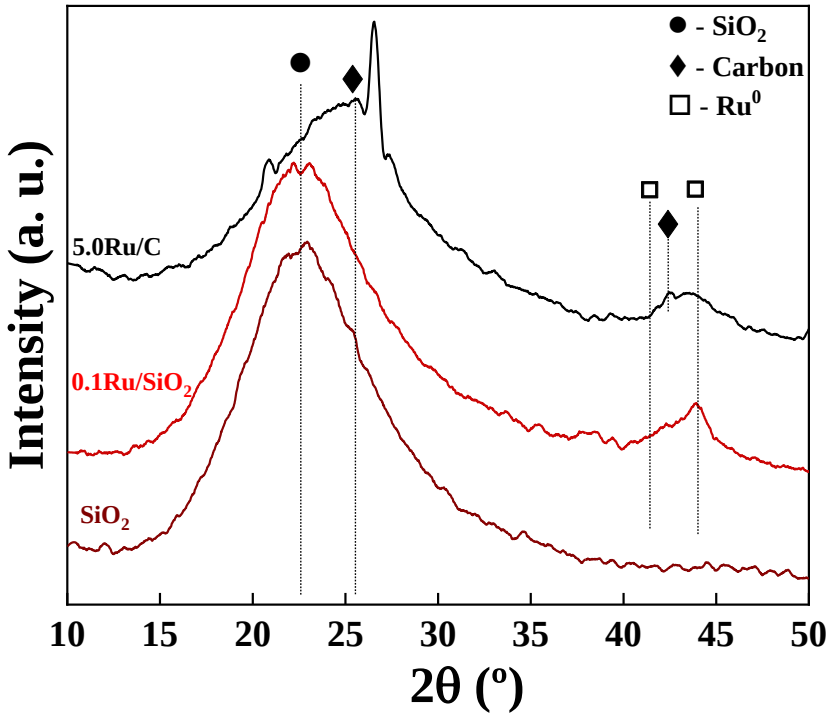

Figure 1. Powder X-ray diffractograms for the SiO_2 support and the 0.1Ru/SiO_2 and 5.0Ru/C catalysts.

X-ray diffractograms of the TiO_2 support and the Ru/TiO_2 catalysts are shown in Figure 2. The diffractogram for TiO_2 presented Bragg reflections corresponding to the anatase and rutile phases, as expected for the commercial P-25 with nominal anatase:rutile composition of 80:20 [28]. Nevertheless, the coexistence of anatase and rutile is complex, involving both amorphous and crystallized phases that can share the lattice of the same crystal, as well as exist as distinct layers [28, 29]. The main diffraction lines of Ru^0 were overlapped with TiO_2 phases, at 2θ of 38º, 42.2º, and 44.1º, attributed to the (1 0 0), (2 0 0), and (1 0 1) planes of Ru^0. Comparison of the diffractograms for the Ru/TiO_2 systems with that for the pure TiO_2 revealed no new features or increases of the peak intensities, indicating that the metal was highly dispersed on the support or existed as very small particles. Figure 2(b) shows an amplification of the main anatase TiO_2 peak, revealing that no peak shift occurred with Ru addition, which was plausible, given that the amount of Ru was insufficient to alter the TiO_2 lattice.

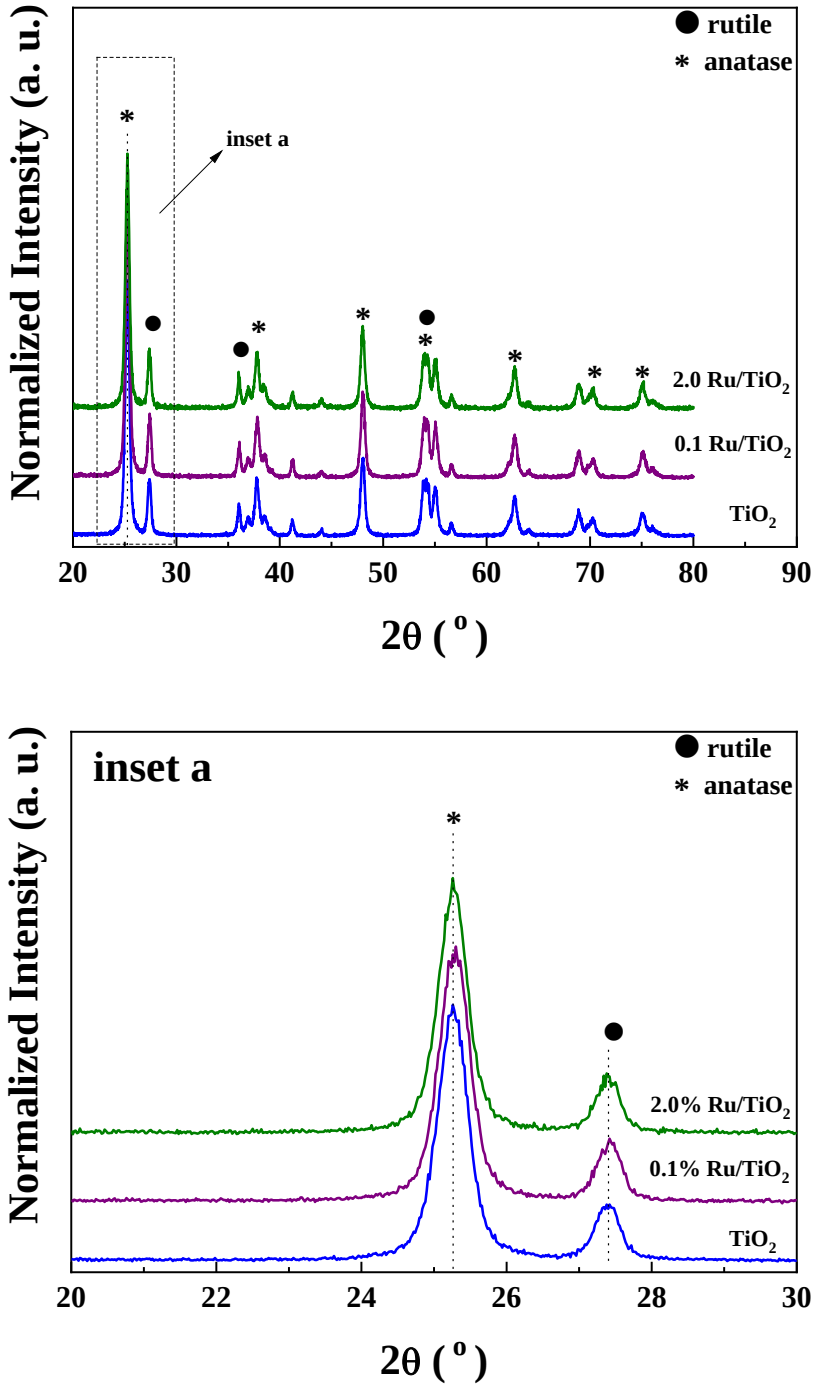

Figure 2. (a) Powder X-ray diffractograms for the TiO_2 support and the Ru/TiO_2 catalysts, and (b) amplification of the region between 2θ of 20º and 30º.

The samples were also characterized by Raman spectroscopy to identify different Ru oxide species and obtain additional structural information related to the catalyst components. The spectra obtained are shown in Figures 3 and 4.

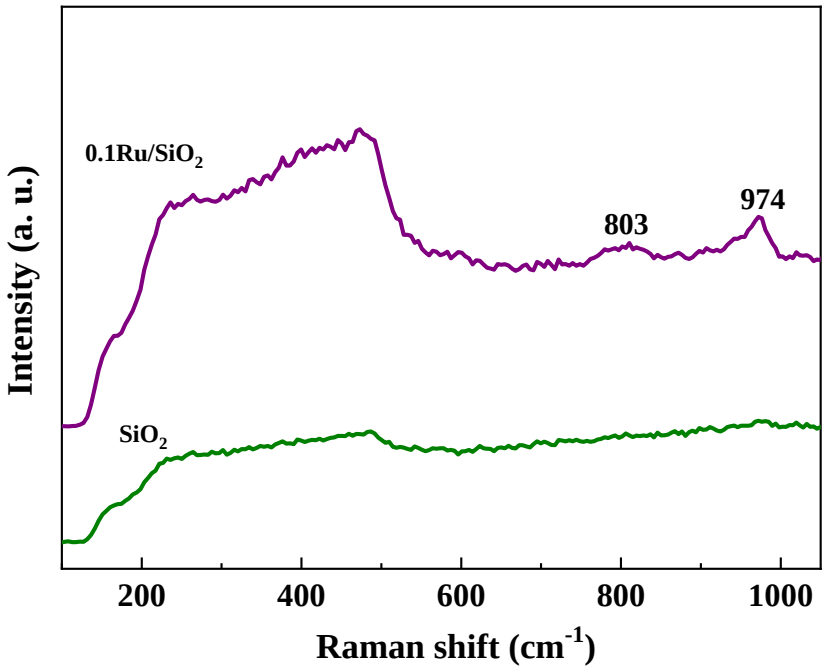

Figure 3. Raman spectra of the SiO_2 support and the 0.1Ru/SiO_2 catalyst.

Raman spectra typically show bands related to RuO_x and $RuCl_3$ in the range from 100 to 700 cm^{-1}, with features reported for RuO_2 at 641, 703, and 520 cm^{-1}. However, in the spectrum for Ru/SiO_2, the bands related to Ru species overlapped with those for SiO_2 in the range from 100 to 550 cm^{-1}, making the attribution unfeasible. The spectrum for the Ru/SiO_2 catalyst presented bands at 800 and 974 cm^{-1}, attributed to SiO_2 [32]. In the absence of Ru, no features were observed in the Raman spectrum. The presence of vibrations associated with SiO_2 in the Ru/SiO_2 catalyst suggested some degree of SiO_2 crystallization, probably resulting from the thermal treatment during reduction. Despite this evidence, the structure was predominantly amorphous, in agreement with the XRD results.

The Raman spectra of both the TiO_2 and Ru/TiO_2 samples (Figure 4) exhibited characteristic vibrations of the anatase phase (at 392, 507, and 623 cm^{-1}) and the rutile phase (at 235 and 445 cm^{-1}). Additionally, a distinct feature at 143 cm^{-1} could be attributed to crystalline

TiO_2. This band at 143 cm^{-1} is often attributed to the anatase phase of TiO_2, although the rutile phase exhibits a similar band near this wavenumber. The exact assignment was hindered by the presence of a mixture of phases, requiring detailed spectral analysis and comparison with reference spectra for the pure phases, which was beyond the scope of this study. Bands in the Raman spectra corresponding to RuO_2, at 523 and 640 cm^{-1}, overlapped with signals for anatase TiO_2, while the band at 708 cm^{-1} was not detected in the Ru/TiO_2 spectra. This was consistent with the fact that the samples were reduced, so most of the Ru was present as Ru^0, and/or suggested the presence of highly dispersed Ru oxides. The Raman spectra corroborated the XRD results, indicating high dispersion of metallic Ru in the samples. In addition, for the Ru/TiO_2 samples, there was a clear trend of peak broadening as the amount of Ru increased, compared to the P-25 samples, which could be explained by the creation of localized defects resulting from the removal of oxygen during the reduction under H_2 [33, 36], with oxygen vacancies leading to the generation of TiO_x, facilitated by the presence of Ru.

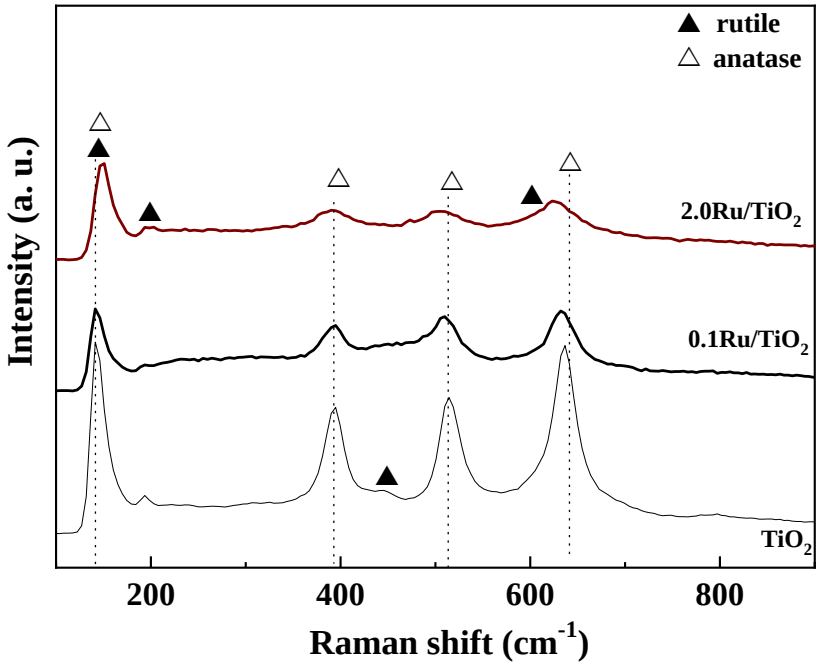

Figure 4. Raman spectra of the TiO_2 support and the $0.1/TiO_2$ and $2.0Ru/TiO_2$ catalysts.

Hence, the surface interaction between Ru nanoparticles and TiO_2, together with electronic perturbations caused by the presence of Ru atoms in the TiO_2 electronic structure, could result in both broadening and shifts of the vibration frequencies. Overall, the simultaneous occurrence of broadening and red shift of the anatase phase features in the Raman spectra of Ru/TiO_2, as the Ru content increased, reflected the complex interplay among the structural, electronic, and surface properties of these composite materials. These findings were consistent with Ru/TiO_2 catalysts being prone to strong metal-support interactions (SMSI), especially when subjected to reduction temperatures close to 400 ºC [34].

High-resolution transmission electron microscopy (HRTEM) was used to investigate the distributions of the Ru nanoparticles over the supports, as well as to acquire additional crystallographic information. Figure 5 shows HRTEM micrographs of the catalysts, together with the corresponding particle size distribution histograms. For all the catalysts, it was possible to observe Ru nanoparticles (dark dots). The Ru particles generally presented spherical geometry, although some hexagonal particles were also detected. The micrographs of the samples based on SiO_2 and C (Figure 5(a,b)) showed the predominance of amorphous phases. On the other hand, for the TiO_2-supported catalysts (Figure 5(c,d)), there was the presence of titania crystalline planes, as evidenced by well-organized rows of atomic planes surrounded by amorphous phase. In all cases, the HRTEM images corroborated the XRD and Raman results for the studied samples. Due to the very low metal content, the 0.1Ru/TiO_2 catalyst exhibited highly dispersed Ru nanoparticles, with a relatively narrow size distribution profile. When the metal content was increased to 2.0%, the average particle size increased from 0.9 to 1.8 nm, with broadening of the size distribution. Despite having a higher Ru content, the commercial 5.0Ru/C catalyst presented smaller particles than both the 2.0Ru/TiO_2 and 0.1Ru/SiO_2 systems, possibly related to a higher surface area of the carbon and/or a synthesis process that promoted metal dispersion.

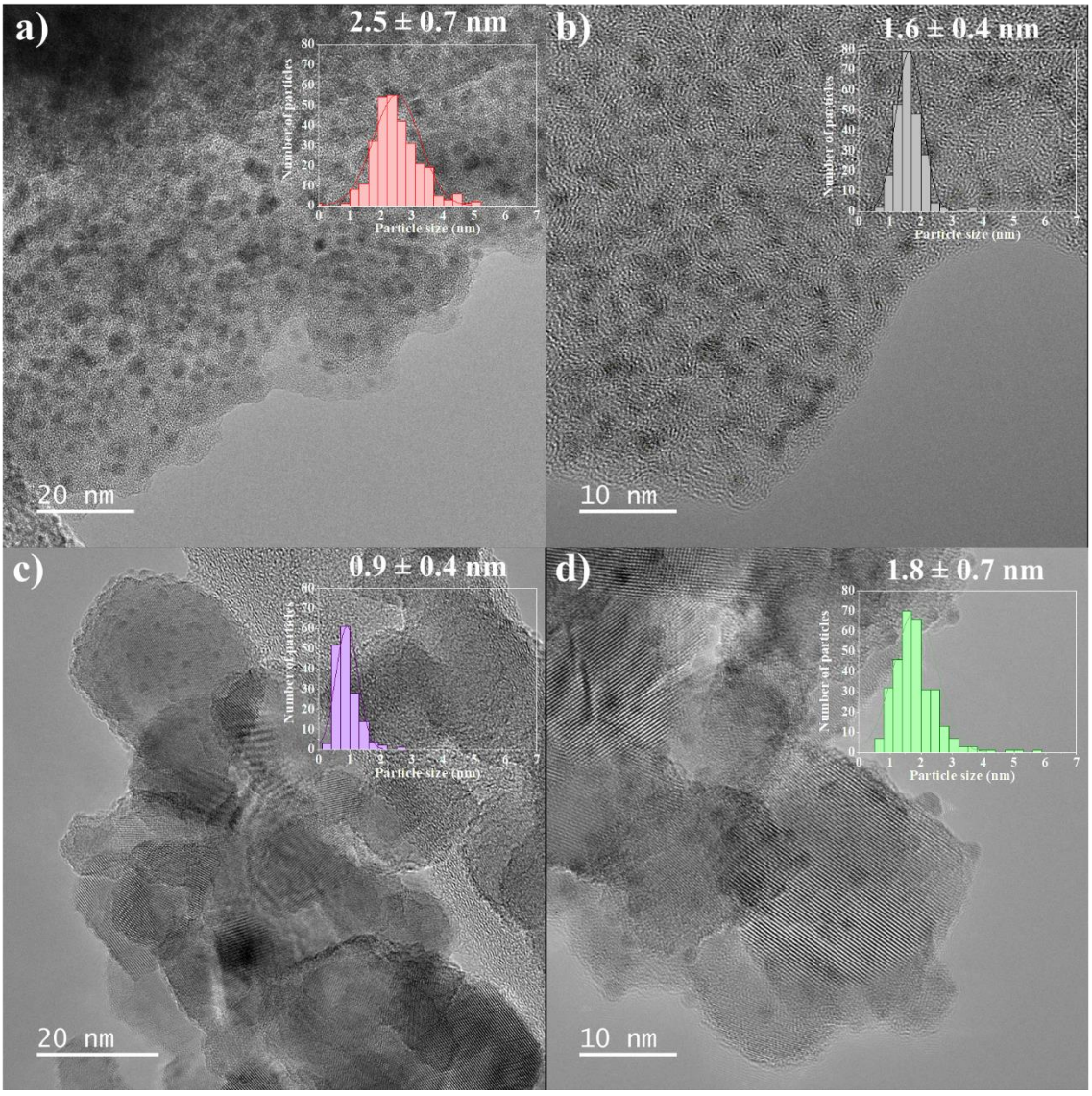

Figure 5. HRTEM micrographs of the catalysts: **a)** 0.1Ru/SiO_2, **b)** 5.0Ru/C, **c)** 0.1Ru/TiO_2, and **d)** 2.0Ru/TiO_2. Also shown are the corresponding size distribution histograms and the average particle sizes.

A substantial difference in Ru average particle size and size distribution was observed between the samples with 0.1% Ru supported on SiO_2 (2.5 ± 0.7 nm) and on TiO_2 (0.9 ± 0.4 nm), in agreement with the XRD and Raman analyses. The presence of diffraction lines for Ru in the diffractogram for the 0.1% Ru/SiO_2 sample (Figure 1) indicated the crystallization of Ru particles, even with small amounts of Ru. This could have been due to poor interaction between the Ru

precursor and the SiO_2 sites, resulting in weakly bonded Ru on the support. Consequently, the Ru particles were significantly larger on SiO_2 than on TiO_2, as shown by the HRTEM analyses.

Effects of temperature and H_2 pressure

To select the reaction parameters employed in this study, the effects of reaction temperature and H_2 pressure were firstly investigated using the commercial 5.0Ru/C catalyst. The results (Figures 6 and 7) revealed that the 1,3-BDO yield showed a continuous increase with pressure (Figure 6), at 130 ºC, while the selectivity towards 2-propanol (2-PrOH), the major side product, decreased. The selectivity towards 2-butanol (2-ButOH), the other side product identified, remained approximately constant at higher pressures (35-70 bar), suggesting that it was formed by a different mechanism than 2-PrOH.

Additionally to the catalytic tests of 3-hydroxybutyric acid (HBA) hydrogenation, blank experiments and tests with the supports were performed, the results are presented in Table 2. The tests demonstrate the stability of HBA under reaction conditions, even at 170 ºC or in the presence of pure supports employed in this study. Therefore, HBA hydrogenation to 1,3-BDO practically occurs only in the presence of catalysts.

Table 2. HBA conversion obtained in the blank tests and experiments with the supports. Parameters: P = 70 bar, $m_{SiO2} = m_{TiO2} = 150$ mg, t = 5.0 h.

Experiment/Sample	T (ºC)	X_{HBA} (%)
Blank	130	**0**
Blank	150	**2.3**
Blank	170	**2.7**
TiO_2	150	**1.4**
SiO_2	150	**2.0**

In the presence of Ru, hydrogen is known to cleave C-C bonds [12-14], which could explain the formation of 2-PrOH, a C_2 compound, from HBA. Given that H_2 has low solubility in water at low pressure [35], it would be expected that increasing its pressure would facilitate 2-PrOH

production. Interestingly, however, the data showed a progressive decrease in selectivity towards 2-PrOH ($S_{2\text{-PrOH}}$) when the pressure was increased from 35 to 70 bar. In other work, it was found that increasing the H_2 pressure had an effect of diminishing the hysteresis of the isotherms for adsorption of H_2 on carbon-doped Ru [40]. Therefore, high pressure may have favored the spillover of hydrogen from the metallic surface to the carbon support, partially suppressing the presence of H atoms on metal-metal neighbors, which could be responsible for the cleaving of C-C to form 2-PrOH [13]. In addition, possible changes in the form of hydrogen adsorption on Ru at high pressure might have favored selective hydrogenation towards 1,3-BDO.

It is noteworthy that previous studies concerning 1,3-BDO conversion have reported the formation of 2-PrOH and 2-ButOH [15-18], so it is possible that 1,3-BDO was produced and underwent further conversion, under the reaction conditions employed. Nevertheless, the results clearly showed that very high H_2 pressure was required to improve 1,3-BDO selectivity.

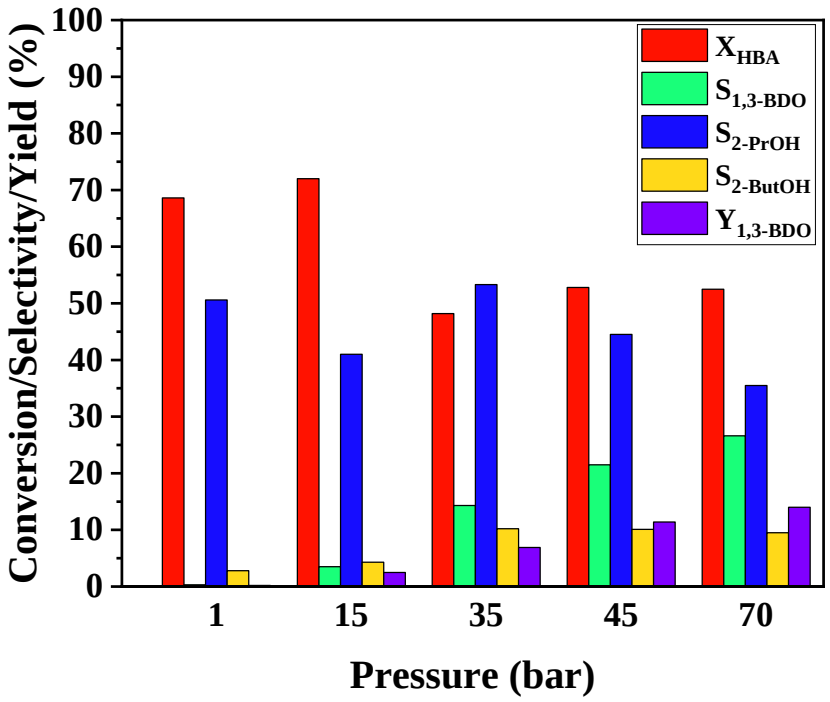

Figure 6. Effect of reaction pressure on HBA conversion (X_{HBA}), selectivity towards 1,3-BDO ($S_{1,3\text{-BDO}}$), 2-propanol ($S_{2\text{-PrOH}}$), and 2-butanol ($S_{2\text{-ButOH}}$), and 1,3-BDO yield ($Y_{1,3\text{-BDO}}$), using the 5.0Ru/C catalyst. Conditions: T = 130 ºC, m_{cat} = 150 mg, and t = 5.0 h.

The high 3-hydroxybutyric acid (HBA) conversion obtained at lower pressure suggested that side reactions occurred, possibly starting with an HBA dehydrogenation pathway, given the lower activity with increase of the H_2 pressure (and, therefore, its solubility in water). Even with H_2 at 1 bar, the major liquid product obtained was 2-PrOH, suggesting that it may have been formed in a route involving dehydrogenation followed by C-C cleavage, catalyzed by Ru/C [12-14], since blank tests confirmed the stability of HBA under the reaction conditions (Table 2). The C-C cleavage route would then be inhibited when the pressure was increased, because modification of the electronic properties of Ru changed the form of H_2 adsorption or dissociation.

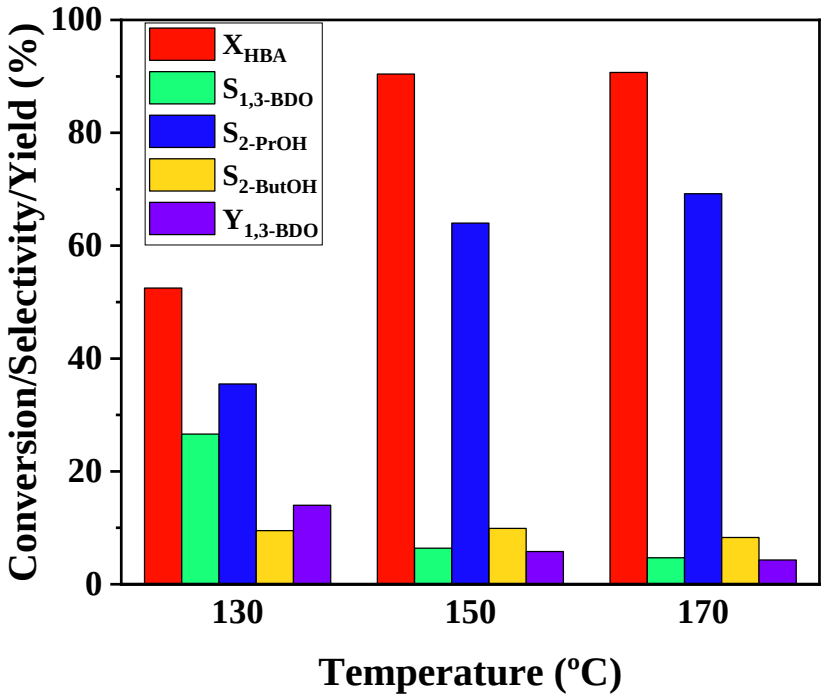

Figure 7. Effect of reaction temperature on HBA conversion (X_{HBA}), selectivity towards 1,3-BDO ($S_{1,3\text{-BDO}}$), 2-propanol ($S_{2\text{-PrOH}}$), and 2-butanol ($S_{2\text{-ButOH}}$), and 1,3-BDO yield ($Y_{1,3\text{-BDO}}$), using the 5.0Ru/C catalyst. Conditions: P = 70 bar, m_{cat} = 150 mg, and t = 5.0 h.

Aiming to optimize the 1,3-BDO yield, an H_2 pressure of 70 bar was selected in the next experiments. Raising the reaction temperature (Figure 7) positively influenced HBA conversion, but there was a notable decline in 1,3-BDO selectivity, leading to lower yields that approached

zero at 170 ºC. In all the experiments, the main side products identified were again 2-PrOH and 2-ButOH, with their concentrations increasing with temperature. This revealed the occurrence of a hydrogenolysis reaction to form 2-PrOH by C-C cleavage, which could occur from HBA or 1,3-BDO [13-16] and was favored by higher temperature. These results highlighted the high activity of the 5.0Ru/C catalyst, consistent with the high amount of Ru in this sample. Therefore, temperatures of 130 and 150 ºC were selected for the experiments with different catalysts and supports. It is notable that in the absence of any catalyst (blank tests), HBA was stable even at 170 ºC, with conversion below 3%, showing that both the main and side reactions were catalyzed by Ru/C. In addition, the selectivity towards 2-ButOH did not appear to be greatly influenced by the reaction temperature.

Effects of Ru loading and nature of the support

Having selected the reaction temperatures and pressure, the production of 1,3-BDO was optimized considering the effects of Ru loading and the nature of the support, using the catalysts supported on TiO_2 and SiO_2. The results (Figures 8 and 9) showed that the reaction side products were the same as those obtained using the commercial catalyst (Figure 8). The tests performed at 130 ºC (Figure 8(a)) highlighted the superior HBA conversion capability of the 0.1Ru/SiO_2 catalyst (X_{HBA} = 27%), compared to the Ru/TiO_2 catalysts, achieving HBA conversion comparable to that obtained with the 2.0Ru/TiO_2 sample (X_{HBA} = 25%). The highest 1,3-BDO selectivity at 130 ºC was obtained with the 2.0Ru/TiO_2 catalyst ($S_{1,3\text{-}BDO}$ = 38%), while the commercial 5.0Ru/C catalyst ($S_{1,3\text{-}BDO}$ = 27%) was less selective towards 1,3-BDO than the 0.1Ru/SiO_2 and 2.0Ru/TiO_2 systems ($S_{1,3\text{-}BDO}$ = 33 and 38%, respectively).

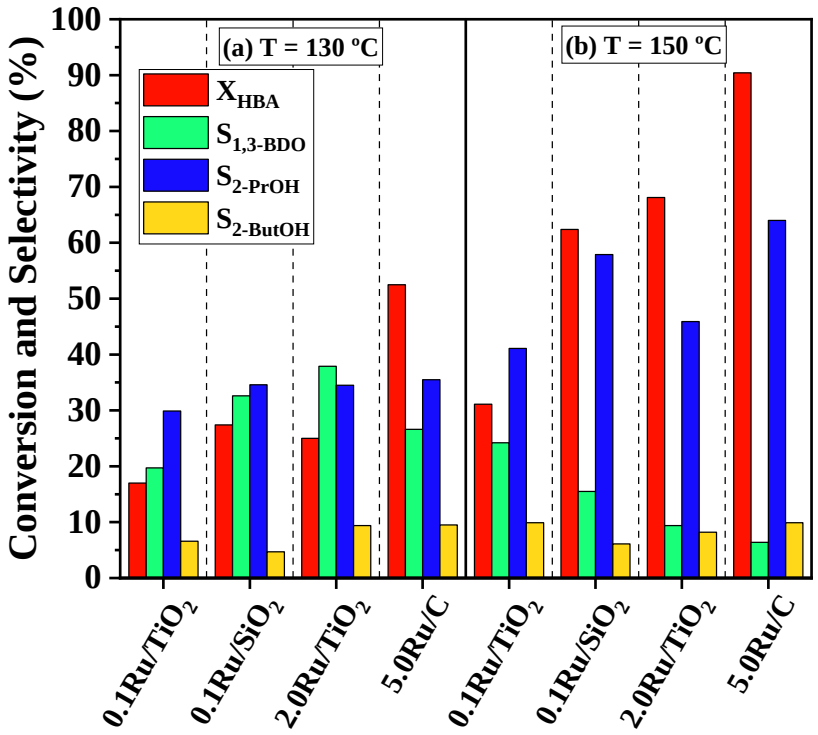

Figure 8. Effects of Ru content and support type on HBA conversion ($X_{HBA\ \%}$) and selectivity to 1,3-BDO ($S_{1,3\text{-BDO}}$), 2-propanol ($S_{2\text{-PrOH}}$), and 2-butanol ($S_{2\text{-ButOH}}$), at **a)** 130 ºC and **b)** 150 ºC. Conditions: P = 70 bar, m_{cat} = 150 mg, and t = 5.0 h.

When the reaction temperature was increased from 130 to 150 ºC (Figure 8(b)), the HBA conversion increased almost proportionally for all the samples, except the 2.0Ru/TiO_2 catalyst, but the selectivity profile changed significantly. In this case, the highest 1,3-BDO selectivity ($S_{1,3\text{-BDO}}$ = 24%) was obtained with 0.1Ru/TiO_2, followed by 0.1Ru/SiO_2 ($S_{1,3\text{-BDO}}$ = 15%), while substantial decreases occurred for the other samples. For the TiO_2-supported samples, higher Ru loading had a substantial effect on HBA conversion, which increased from 31% with 0.1Ru/TiO_2 to 68% with 2.0Ru/TiO_2, due to the higher concentration of active sites for H_2 adsorption on the support surface.

The overall increase in HBA conversion and decrease in 1,3-BDO selectivity observed with increase of the temperature from 130 to 150 ºC was in accordance with the results obtained using the commercial 5.0Ru/C catalyst (Figure 7), so the hydrogenolysis reaction forming 2-PrOH was also favored by increase of the temperature, when the synthesized catalysts supported on TiO_2 and SiO_2 were used. At 150 ºC, all the catalysts except 0.1Ru/TiO_2 showed a sharp drop in selectivity.

The results indicated that the larger Ru particles present in the 0.1Ru/SiO_2 catalyst were highly active in HBA conversion, although much of the activity was related to the hydrogenolysis reaction leading to 2-PrOH. This could be explained in terms of the geometric and electronic effects that were related to the Ru particle size and the nature of the support. It has been reported previously that H_2 can undergo heterolytic dissociation over metal-support interfaces, especially in the presence of a Lewis acid-base pair, and that this type of dissociation can promote the selective hydrogenation of polar groups, such as C=O, instead of C-C bonds [41, 42], which could enhance selectivity towards 1,3-BDO and hinder hydrogenolysis to 2-PrOH. Therefore, it is possible that the 0.1Ru/TiO_2 surface possessed more metal-oxide interfacial sites, compared to the SiO_2-supported counterpart, with the highly dispersed Ru (as evidenced by XRD and HRTEM) and the partially reduced TiO_{2-x} acting as Lewis acid and base, respectively.

Since the heterolytic H_2 dissociation mainly occurred on single metal atoms or very small and dispersed nanoparticles [42] of the 2.0Ru/TiO_2 catalyst, for which the Ru particles were significantly larger (1.8 ± 0.7 nm), compared to the 0.1Ru/TiO_2 catalyst (0.9 ± 0.4 nm), this type of H_2 adsorption could have been hindered, resulting in significantly lower selectivity towards 1,3-BDO (Figure 8(b)). This was in agreement with the results obtained using the 5.0Ru/C catalyst at different pressures (Figure 6), where the higher selectivity towards 2-PrOH at lower pressures could be ascribed to H_2 not spilling over to the support, consequently undergoing homolytic dissociation at metal-metal neighbors, favoring C-C cleavage. A previous theoretical study of H_2 adsorption over Ru clusters supported on TiO_2 found that spillover from the metal to the oxide mainly occurred at high H coverage of Ru particles [43]. Therefore, selective 1,3-BDO formation should be favored at high H_2 pressure, due to spillover to the support and the formation of interfacial sites between highly dispersed Ru nanoparticles and the partially reduced oxide, promoting the heterolytic dissociation of H_2.

1,3-Butanediol stability

Having recognized the challenge of obtaining high selectivity towards 1,3-BDO, product stability tests were performed, considering the effects of the support, the catalysts, and the reaction conditions on the 1,3-BDO conversion. Blank tests were also carried out in the absence of any catalyst. In these experiments, the reactor was loaded with aqueous 1,3-BDO solutions,

maintaining the reaction conditions studied previously. The results are shown in Figure 9. Firstly, the effects of H_2 pressure on 1,3-BDO conversion and product selectivity were evaluated using the commercial 5.0Ru/C catalyst (Figure 9(a)), which showed that increase of the pressure had a positive effect on product stability, in accordance with the 1,3-BDO selectivity profile observed in the initial catalytic tests (Figure 6). The products obtained were again 2-PrOH and 2-ButOH, suggesting that side reactions started from the 1,3-BDO product, although the possibility of side reactions involving HBA and resulting in 2-PrOH and 2-ButOH could not be discarded.

The blank tests (Figure 9(b)) highlighted the stability of 1,3-BDO under the reaction conditions, even at 200 ºC, indicating that the conversion in fact occurred over the supports and the catalysts, or involved a cooperative effect of both. In the tests with the synthesized catalysts and supports (Figure 9(b)), the temperature was set at 150 ºC to enable a better correlation between the data obtained and the selectivity profile (Figure 8(b)). The experiment with pure TiO_2 revealed activity in 1,3-BDO degradation (11%), while this was not observed with SiO_2, possibly due to differences in the acid-base properties of the materials. However, there was a dramatic difference in activity when a very small amount of Ru was incorporated, with the 0.1Ru/SiO_2 and 0.1Ru/TiO_2 materials presenting 99% and 17% 1,3-BDO conversion, respectively. Accordingly, the 0.1Ru/TiO_2 catalyst also showed the highest 1,3-BDO selectivity at 150 ºC, among all the materials (Figure 8(b)). Only when the Ru content on TiO_2 was increased to 2.0% did the catalyst present HBA conversion activity close to that of 0.1Ru/SiO_2.

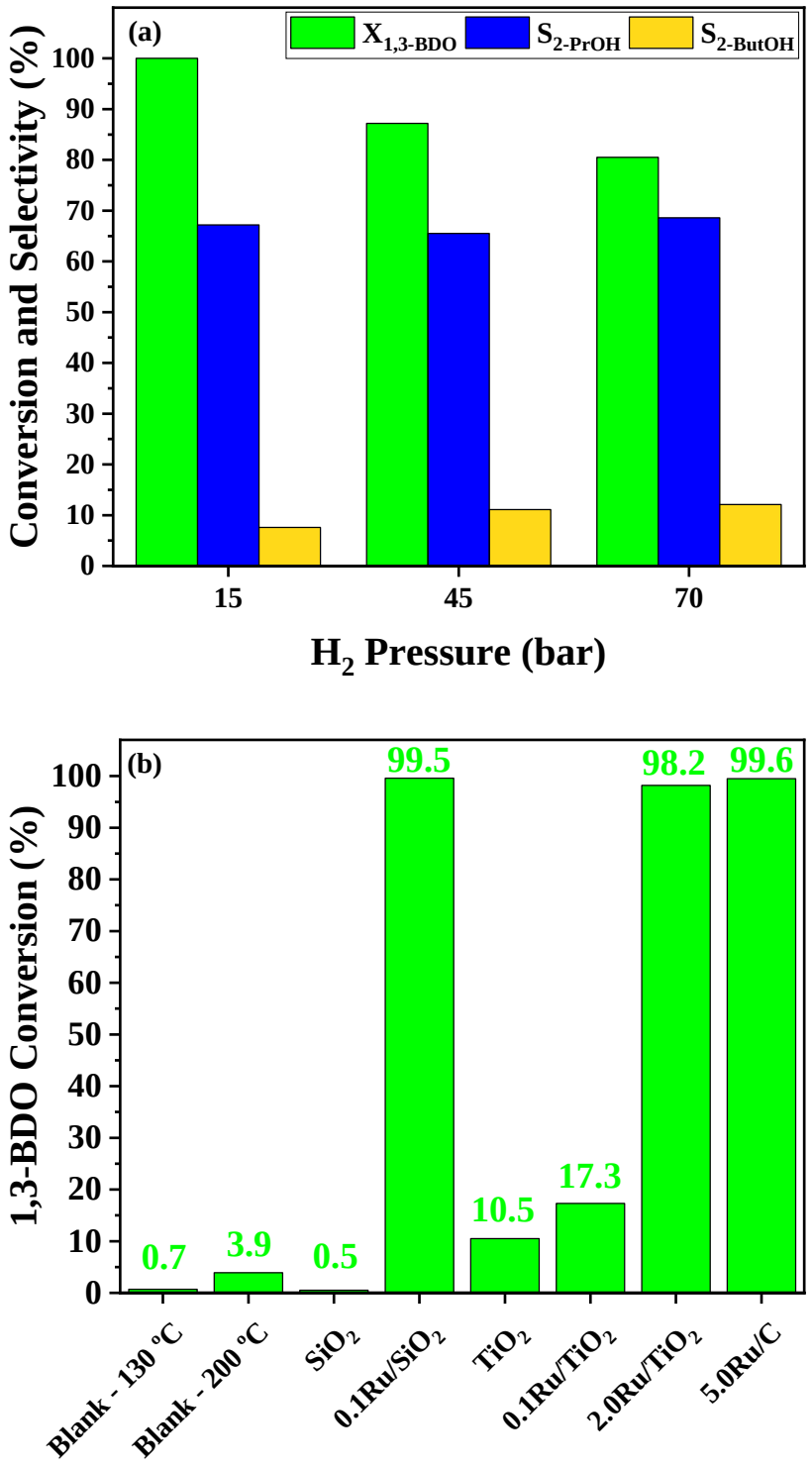

Figure 9. Results of the 1,3-BDO conversion experiments: **(a)** Effects of H_2 pressure on 1,3-BDO conversion and selectivity to 2-propanol and 2-butanol. Conditions: T = 130 ºC, m_{cat} = 150 mg (5.0Ru/C), and t = 5.0 h. **(b)** 1,3-BDO conversions obtained using the different supports and

catalysts. Conditions: T = 150 ºC (except for the blank tests), P = 70 bar, m_{cat} = 150 mg, and t = 5.0 h.

The data indicated that two distinct effects promoted the 1,3-BDO conversion, namely the nature of the support and the amount of Ru in the catalytic systems. It has been reported that the presence of weak acid sites, characterized by hydroxyl groups on the SiO_2 surface, may promote the dehydration reaction during the formation of butadiene from ethanol [10]. The first step proposed for the formation of 2-butanol was dehydration to the corresponding unsaturated alcohol, with subsequent hydrogenation of the C=C bond to form 2-butanol. The authors also reported that in an inert atmosphere, the rate of 1,3-BDO conversion increased linearly with the amount of exposed Cu^0 in bifunctional Cu-Mg-Al catalysts. However, the presence of saturated alcohols was not detected, as expected, since the experiments were performed in the absence of hydrogen. Analogously, the results obtained in the present work were suggestive of an effect of the acid properties of SiO_2 in the 0.1Ru/SiO_2 sample, whereas for the 2.0Ru/TiO_2 and 5.0Ru/C systems, the high amounts of Ru influenced the 1,3-BDO conversion. The 0.1Ru/TiO_2 catalyst presented intermediate performance, due to the low amount of Ru and a contribution from TiO_2.

These results confirmed that Ru on SiO_2 was more prone to side reactions, as observed previously in the HBA hydrogenation experiments at 150 ºC, and corroborated the formation of different active sites by distinct metal-oxide interactions. This could suggest that 1,3-BDO conversion occurred more easily over larger particles, as a dramatic difference in particle size was observed between Ru supported on SiO_2 and TiO_2 (Figure 5). The effect of selectivity loss due to large particles promoting undesirable side reactions has been reported previously, for example in the hydrogenation of furfural [37]. Given the stability of 1,3-BDO in the blank tests (Figure 9(b)), it could be inferred that in all the HBA hydrogenation experiments, the desired 1,3-BDO product was formed over the Ru catalysts, but was further converted by side reactions, resulting in the formation of 2-PrOH and 2-ButOH.

Mechanistic investigation

To further assess the reactions starting from 1,3-BDO, a mechanistic study was carried out, modifying the reaction conditions and the HPLC parameters. The investigation was performed by hindering 1,3-BDO degradation, preventing further conversion of intermediate compounds. The objective was to identify the pathway leading from 1,3-BDO to 2-PrOH and 2-ButOH.

Based on organic chemistry theory and previous reports concerning 1,3-BDO conversion [9-19], standard solutions of possible intermediates were prepared and analyzed by HPLC, where the aim was to identify the retention times (t_R) of the compounds, which depend on the structures of the molecules. The t_R values were then correlated with the signals observed in the procedures described below. However, this identification method could result in false positives, since different compounds may present very similar retention times. Therefore, additional HPLC analyses were performed with the oven temperature (T_{oven}) changed from 65 ºC (the temperature typically used in the analyses) to 30 ºC, to confirm the assignments by observing the shifts in the analyte retention times. Hence, the assignment was only made if the signal matched that for the standard solution, at both oven temperatures.

Three additional catalytic tests were performed, using the commercial 5.0Ru/C catalyst: (a) 1,3-BDO conversion under pure argon at 1 bar; (b) 1,3-BDO hydrogenation at 1 bar; and (c) 4-hydroxy-2-butanone (4H2B) hydrogenation at 70 bar. The resulting conversions and the liquid product distributions are shown in Table 3. The chromatograms obtained are shown in Figure 10, where the solid lines represent analyses at T_{oven} = 65 ºC and the dotted lines correspond to the analyses at T_{oven} = 30 ºC. Table 4 shows the retention times for the standard solutions, at both temperatures.

Qualitative analyses by gas chromatography revealed that methane was produced from both HBA hydrogenation and 1,3-BDO conversion, under the same reaction conditions. This suggested that the liquid products were, in part, further hydrogenated to methane over the catalysts.

Table 3. Conversions and liquid product distributions obtained in the different tests: **(a)** 1,3-BDO conversion under an inert atmosphere at 1 bar; **(b)** 1,3-BDO hydrogenation at 1 bar; and **(c)** 4H2B hydrogenation at 70 bar. X is the 1,3-BDO or 4H2B conversion.

		Liquid product distribution (mol/L)			
Test	**X (%)**	**4H2B**	**1,3-BDO**	**2-PrOH**	**2-ButOH**
(a)	28	0.0069	0.072	0.00039	0.00090
(b)	53	0.00038	0.047	0.031	0.0021
(c)	100	0	0.016	0.051	0.0021

Conditions: 5.0Ru/C catalyst, T = 130 ºC, m_{cat} = 150 mg, and t = 5 h.

In the first test (a), where the conversion of 1,3-BDO was performed in the absence of hydrogen, the different products identified were 4-hydroxy-2-butanone (4H2B), acetone, butanone, and 2-butanol (Figure 10(a)), since the retention times were very close to those of the standards, under both oven conditions (Table 4). The sharp peaks at t_R = 19.2 min (65 ºC) and t_R = 22.1 min (30 ºC) could be attributed to 1,3-BDO (the reactant, in this case). Interestingly, the 5.0Ru/C catalyst converted 28% of 1,3-BDO (Table 3(a)) without H_2, producing 4H2B, butanone, and a very small amount of acetone, which had not been observed in the experiments performed up to this point. It has been reported that 4H2B may be formed by dehydrogenation of the secondary hydroxyl group of 1,3-BDO [14, 19], but it is also susceptible to dehydration, hydrogenation, and cleavage of the C-C bond, in the presence of metallic active sites. On the other hand, it is possible that butanone could be produced from dehydration of the secondary hydroxyl of 1,3-BDO. The small acetone signal suggested a minor contribution of the route with C-C cleavage of 4H2B. Nonetheless, only very small amounts of 2-PrOH and 2-ButOH were observed, so experiment (a) alone was unable to clarify whether 4H2B and butanone were intermediates of 1,3-BDO conversion, under HBA hydrogenation conditions.

Table 4. Retention times (t_R) for the standard solutions analyzed by HPLC with RID, at T_{oven} = 30 and 65 ºC. The chromatograms are shown in Figure 11.

Compound	**$t_{R\_65\ ºC}$ (min)**	**$t_{R\_30\ ºC}$ (min)**
4H2B	(●) 18.17	(●) 23.27
1,3-BDO	(⌘) 19.25	(⌘) 22.05

Acetone	(■) 21.40	(■) 27.84
2-Propanol	(□) 24.30	(□) 26.80
Butanone	(❖) 26.30	(❖) 35.50
2-Butanol	(◆) 31.08	(◆) 35.20

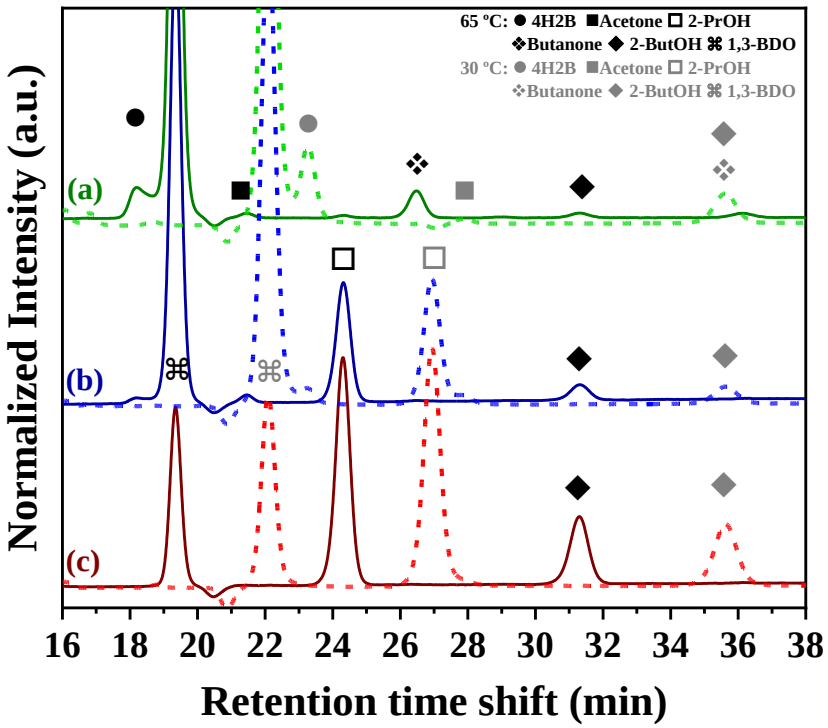

Figure 10. Chromatograms obtained in the different tests: **(a)** 1,3-BDO conversion under an inert atmosphere at 1 bar; **(b)** 1,3-BDO hydrogenation at 1 bar; and **(c)** 4-hydroxy-2-butanone (4H2B) hydrogenation at 70 bar. Solid lines: analyses at T_{oven} = 65 ºC. Dotted lines: analyses at T_{oven} = 30 ºC. The icons are also shown in Table 4. Conditions: 5.0Ru/C catalyst, T = 130 ºC, m_{cat} = 150 mg, and t = 5.0 h.

The next test, experiment (b) (Figure 10(b)), was carried out using the same conditions as test (a), but with 1 bar of H_2, instead of an inert atmosphere. The 1,3-BDO conversion increased to 53%, while 4H2B was present in a very small amount (Table 3(b)), indicating that it was

produced, but was further converted into other products. The intense 2-PrOH peak (Figure 10(b), t_R = 24.3 min) suggested cleavage of the C-C bond of 4H2B to form acetone (observed in a small quantity), followed by hydrogenation to 2-PrOH. Since this feature was not identified in test (a), it could explain the formation of 2-PrOH in the catalytic hydrogenation of HBA under 70 bar of H_2. In addition, the absence of butanone indicated that it may have been further hydrogenated to 2-ButOH (0.0021 mol/L), as shown in Table 3(b). This finding was consistent with 4H2B and butanone being highly active under an H_2 atmosphere, providing an explanation for the fact that these compounds were not observed previously in the HBA hydrogenation.

Lastly, in test (c), the hydrogenation of 4H2B was performed under 70 bar of H_2, to evaluate 2-PrOH production (Figure 10(c)). As expected, 4H2B was highly reactive, being completely converted in 5 h of reaction, forming mainly 2-PrOH. The results further supported the hypothesis that 4H2B was an intermediate in the conversion of 1,3-BDO to 2-PrOH. In this experiment, the formation of 1,3-BDO was observed, which would be expected to occur by hydrogenation of the 4H2B carbonyl group. However, the 2-PrOH concentration was three times higher than that of 1,3-BDO, indicating a predominance of C-C cleavage, compared to carbonyl hydrogenation, even under 70 bar of H_2. In addition, there was a substantial quantity of 2-ButOH, possibly formed by 1,3-BDO dehydration to butanone, followed by hydrogenation to 2-ButOH, or even successive hydrogenations of 4H2B to butanone and 2-ButOH. With the current data, it was not possible to distinguish between these two possible routes. Although 2-PrOH was produced in this test, no acetone was detected, suggesting that it was probably rapidly hydrogenated to the alcohol [19].

Additionally, a single 2-ButOH hydrogenation test carried out at P_{H2} = 70 bar over the Ru/C system resulted in relatively low conversion (15%), showing that the compound was more stable, under the reaction conditions, compared to 4H2B (Table 3(c)) and butanone, which appeared to be rapidly hydrogenated, even at P_{H2} = 1 bar.

The data obtained in the mechanistic investigation enabled the proposal of a pathway for 1,3-BDO conversion (Figure 11). The results indicated that 1,3-BDO conversion started with dehydrogenation of the secondary hydroxyl group, yielding 4H2B, followed by a C-C cleavage pathway to acetone and further hydrogenation to 2-PrOH. The route for 2-ButOH formation remained unclear, but possible mechanisms were (i) dehydration of 1,3-BDO to butanone, followed by hydrogenation, (ii) successive hydrogenations of 4H2B, or (iii) a combination of both.

The absence of formaldehyde and methanol in all the experiments could be explained in terms of further hydrogenation reactions leading to methane, which was detected by GC analyses.

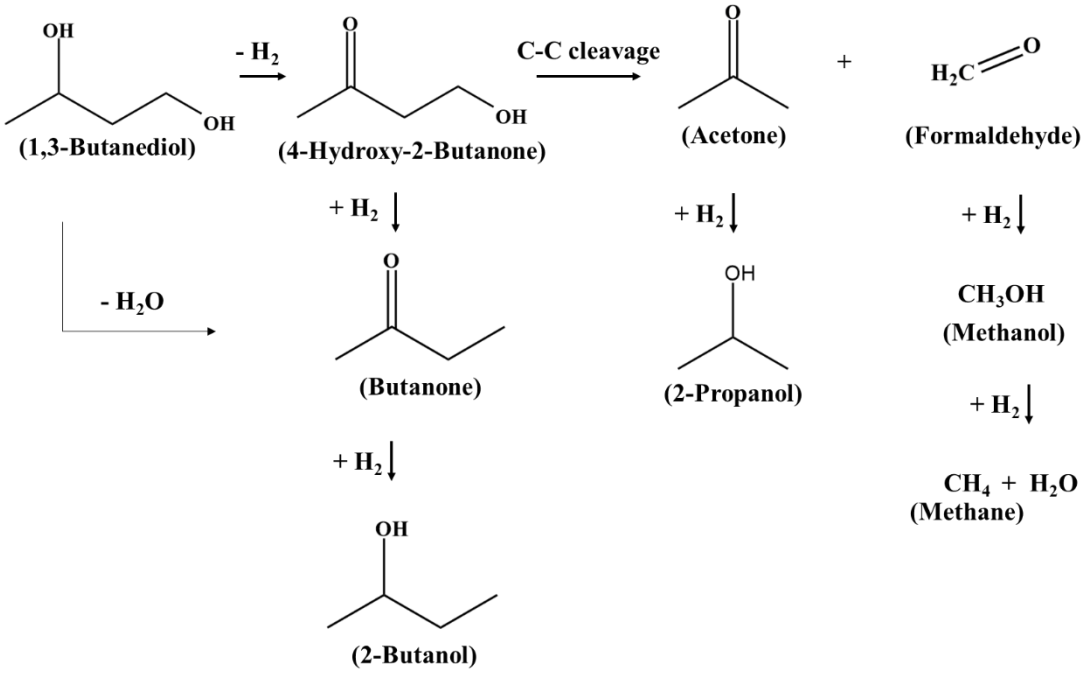

Figure 11. Proposed reaction routes for 1,3-BDO conversion over Ru catalysts, under high-pressure HBA hydrogenation conditions.

Under similar reaction conditions, it has been demonstrated that lactic acid and/or 1,2-propanediol can undergo analogous side reactions. Over Ru catalysts, the usual major side products of lactic acid hydrogenation to 1,2-propanediol are ethanol, 1-propanol, and propionic acid, suggesting the occurrence of C-C bond cleavage, with the secondary hydroxyl group being more prone to side reactions [21, 22, 39]. Both effects were observed in the present work with HBA and 1,3-BDO, considering the products obtained. Differently, when using Cu-based catalysts, the reported side products were a mixture of compounds originating from both the primary and secondary hydroxyls [38]. Therefore, it is likely that the nature of the active phases could also play a role in the mechanisms for HBA and 1,3-BDO.

Finally, it should be mentioned that the available literature regarding mechanisms of 1,3-BDO conversion describes catalytic tests performed in the gas phase and under higher temperature

conditions [17, 19]. The results obtained here corroborate the findings of these previous studies, while also suggesting the occurrence of similar pathways in the aqueous phase. All the products observed here probably resulted from reactions starting with the secondary hydroxyl of 1,3-BDO. It was demonstrated previously that the primary group could also undergo parallel reactions, but under the HBA hydrogenation conditions studied here, the secondary hydroxyl was much more prone to side reactions, compared to the primary hydroxyl.

CONCLUSION

A novel aqueous phase hydrogenation of 3-hydroxybutyric acid to 1,3-butanediol was studied using Ru catalysts supported on SiO_2, TiO_2, and C. Characterization analyses revealed that Ru was highly dispersed on TiO_2, forming very small nanoparticles, while larger particles were observed on SiO_2 and C, possibly due to weaker interactions with these supports. Preliminary catalytic tests with the commercial 5.0Ru/C catalyst showed that high H_2 pressures were required to optimize 1,3-butanediol production, which could have been due to hydrogen spillover to the support, inhibiting the C-C cleavage pathway. In addition, increasing the temperature favored the hydrogenolysis reaction leading to 2-propanol.

For the synthesized systems, the larger particles present on Ru/SiO_2 were more active in 3-hydroxybutyric acid conversion, but promoted the C-C cleavage reaction, while the small particles present on Ru/TiO_2 seemed to selectively hydrogenate the C=O group, possibly due to heterolytic H_2 dissociation at the interface between Ru and partially reduced TiO_{2-x}. Product stability tests revealed that 2-propanol and 2-butanol were formed by degradation of 1,3-butanediol, under the reaction conditions, especially over the catalysts with high Ru loadings and larger particles, although side reactions involving the acid reactant could not be disregarded. Finally, the results of a mechanistic study suggested that the 1,3-butanediol conversion involved the 4-hydroxy-2-butanone intermediate, which underwent hydrogenation to 2-butanol and C-C hydrogenolysis to 2-propanol. The present work reports a novel catalytic process to add value to 3-hydroxybutyric acid, highlighting the encountered challenge of selectively forming the diol, while inhibiting its further conversion to side products.

REFERENCES CHAPTER I

1. Rosenboom, Jan-Georg, Robert Langer, and Giovanni Traverso. "Bioplastics for a circular economy." Nature Reviews Materials 7.2 (2022): 117-137.
2. Tokiwa, Yutaka, and Charles U. Ugwu. "Biotechnological production of (R)-3-hydroxybutyric acid monomer." Journal of biotechnology 132.3 (2007): 264-272.
3. Tokiwa, Yutaka, and Buenaventurada P. Calabia. "Review degradation of microbial polyesters." *Biotechnology letters* 26 (2004): 1181-1189.
4. Chen, Oliver, et al. "Tolerability and safety of a novel ketogenic ester, bis-hexanoyl (R)-1, 3-butanediol: a randomized controlled trial in healthy adults." *Nutrients* 13.6 (2021): 2066.
5. Gascoyne, Joshua Luke, et al. "Engineering Cupriavidus necator H16 for the autotrophic production of (R)-1, 3-butanediol." *Metabolic engineering* 67 (2021): 262-276.
6. Bloom, Paul D., et al. "Process for producing 1, 3-butanediol and for optionally further producing (R)-3-hydroxybutyl (R)-3-hydroxybutyrate." U.S. Patent No. 11,078,140. 3 Aug. 2021.
7. Yun, Yang Sik, et al. "The importance of Brønsted acid sites on CO bond rupture selectivities during hydrogenation and hydrogenolysis of esters." *Journal of Catalysis* 411 (2022): 212-225.
8. Turek, T., D. L. Trimm, and N. W. Cant. "The catalytic hydrogenolysis of esters to alcohols." *Catalysis Reviews—Science and Engineering* 36.4 (1994): 645-683.
9. Jing, Fangli, et al. "Direct dehydration of 1, 3-butanediol into butadiene over aluminosilicate catalysts." *Catalysis Science & Technology* 6.15 (2016): 5830-5840.
10. Duan, Hailing, Yasuhiro Yamada, and Satoshi Sato. "Future prospect of the production of 1, 3-butadiene from butanediols." *Chemistry Letters* 45.9 (2016): 1036-1047.
11. Lee, Jeong Hwan, and Suk Bong Hong. "Dehydration of 1, 3-butanediol to butadiene over medium-pore zeolites: Another example of reaction intermediate shape selectivity." *Applied Catalysis B: Environmental* 280 (2021): 119446.
12. Flaherty, David W., David D. Hibbitts, and Enrique Iglesia. "Metal-catalyzed C–C bond cleavage in alkanes: effects of methyl substitution on transition-state structures and stability." *Journal of the American Chemical Society* 136.27 (2014): 9664-9676.

13. Kühne, Benjamin, et al. "Mechanistic study on–C–O–and–C–C–hydrogenolysis over Cu catalysts: identification of reaction pathways and key intermediates." *Catalysis Science & Technology* 8.3 (2018): 755-767.
14. Lutz, Marius DR, and Bill Morandi. "Metal-catalyzed carbon–carbon bond cleavage of unstrained alcohols." *Chemical reviews* 121.1 (2020): 300-326.
15. Ichikawa, Naoki, et al. "Catalytic reaction of 1, 3-butanediol over solid acids." *Journal of Molecular Catalysis A: Chemical* 256.1-2 (2006): 106-112.
16. Sato, Satoshi, et al. "Dehydrogenation of 1, 3-butanediol over Cu-based catalyst." *Journal of Molecular Catalysis A: Chemical* 272.1-2 (2007): 164-168.
17. Sato, Satoshi, et al. "Catalytic reaction of 1, 3-butanediol over rare earth oxides." *Applied Catalysis A: General* 328.2 (2007): 109-116.
18. Diez, Veronica Karina, et al. "Gas-phase conversion of 1, 3-butanediol on single acid–base and Cu-promoted oxides." *Catalysis today* 213 (2013): 18-24.
19. Torresi, Pablo Antonio, et al. "Conversion of diols by dehydrogenation and dehydration reactions on silica-supported copper catalysts." *Applied Catalysis A: General* 458 (2013): 119-129.
20. Lee, Jong-Min, et al. "Direct Hydrogenation of Biomass-Derived Butyric Acid to n-Butanol over a Ruthenium–Tin Bimetallic Catalyst." *ChemSusChem* 7.11 (2014): 2998-3001.
21. Zhang, Zhigang, James E. Jackson, and Dennis J. Miller. "Aqueous-phase hydrogenation of lactic acid to propylene glycol." *Applied Catalysis A: General* 219.1-2 (2001): 89-98.
22. Liu, Kaituo, et al. "Hydrogenation of lactic acid to 1, 2-propanediol over Ru-based catalysts." *ChemCatChem* 10.4 (2018): 810-817.
23. Jang, Tae Young, et al. "Catalytic conversion of lactic acid into propylene glycol over various metals supported on silica." *Research on Chemical Intermediates* 37 (2011): 1275-1282.
24. Nelson, Ryan C., et al. "Experimental and theoretical insights into the hydrogen-efficient direct hydrodeoxygenation mechanism of phenol over Ru/TiO2." *ACS catalysis* 5.11 (2015): 6509-6523.
25. Toba, Makoto, et al. "Synthesis of alcohols and diols by hydrogenation of carboxylic acids and esters over Ru–Sn–Al2O3 catalysts." *Applied Catalysis A: General* 189.2 (1999): 243-250.

26. Mendes, M. J., et al. "Hydrogenation of oleic acid over ruthenium catalysts." *Applied Catalysis A: General* 217.1-2 (2001): 253-262.
27. Silva, Adriana M., et al. "Selective hydrogenation of dimethyl adipate on titania-supported RuSn catalysts." *Applied Catalysis A: General* 353.1 (2009): 101-106.
28. Bickley, Roger I., et al. "A structural investigation of titanium dioxide photocatalysts." *Journal of solid state chemistry* 92.1 (1991): 178-190.
29. Martínez Tejada, Leidy Marcela, et al. "In-situ Raman spectroscopy study of Ru/TiO2 catalyst in the selective methanation of CO." *Journal of Raman Spectroscopy* 47.2 (2016): 189-197.
30. Barbier Jr, J., et al. "Total oxidation of acetic acid in aqueous solutions over noble metal catalysts." *Journal of Catalysis* 177.2 (1998): 378-385.
31. Srivastava, Vivek. "Active heterogeneous Ru nanocatalysts for CO 2 hydrogenation reaction." *Catalysis Letters* 146 (2016): 2630-2640.
32. Faroldi, Betina M., John F. Múnera, and Laura M. Cornaglia. "In situ characterization of phase transformation and reactivity of high surface area lanthanum-based Ru catalysts for the combined reforming of methane." *Applied Catalysis B: Environmental* 150 (2014): 126-137.
33. Naldoni, Alberto, et al. "Effect of nature and location of defects on bandgap narrowing in black TiO2 nanoparticles." *Journal of the American Chemical Society* 134.18 (2012): 7600-7603.
34. Tauster, S. J. "Strong metal-support interactions." *Accounts of Chemical Research* 20.11 (1987): 389-394.
35. Zhu, Zhiwei, et al. "An accurate model for estimating H2 solubility in pure water and aqueous NaCl solutions." *Energies* 15.14 (2022): 5021.
36. Golubović, A, et al. “Raman study of the variation in anatase structure of TiO_2 nanopowders due to the changes of sol-gel synthesis conditions”. *Journal of Sol-Gel Science and Technology* 49 (2009): 311 – 319
37. Zuo, Lu-Jie, et al. “High-temperature Synthesis of Carbon-Supported Bimetallic Nanocluster Catalysts by Enlarging the Interparticle Distance”. *Inorgarnic Chemistry* 61 (2022): 2719-2723.
38. Simonov, Mikhail N., Irina L. Simakova, Valentin N. Parmon. “Hydrogenation of lactic acid to propylene glycol over copper-containing catalysts”. *Reaction Kinetics and Catalysis Letters* 97 (2009): 157-162.

39. Jang, Hyuk, et al. “Hydrogenation of lactic acid to propylene glycol over a carbon-supported ruthenium catalyst”. *Journal of Molecular Catalysis A: Chemical* 380 (2013) 57-60
40. Saha, Dipendu, and Shuguang Deng. "Hydrogen adsorption on ordered mesoporous carbons doped with Pd, Pt, Ni, and Ru." *Langmuir* 25.21 (2009): 12550-12560.
41. Jing, Yaxuan, and Yanqin Wang. "Heterolytic dissociation of H2 and bond activation: Spotting new opportunities from a unified view." *Chem Catalysis* 3.3 (2023).
42. Aireddy, Divakar R., and Kunlun Ding. "Heterolytic dissociation of H2 in heterogeneous catalysis." *ACS Catalysis* 12.8 (2022): 4707-4723.
43. Chen, Hsin-Yi Tiffany, Sergio Tosoni, and Gianfranco Pacchioni. "Hydrogen adsorption, dissociation, and spillover on Ru10 clusters supported on anatase TiO2 and tetragonal ZrO2 (101) surfaces." *ACS Catalysis* 5.9 (2015): 5486-5495.

CHAPTER II: OPTIMIZING PARAMETERS FOR MODULATION EXCITATION COUPLED WITH PHASE SENSITIVE DETECTION EXPERIMENTS IN STANDARD IN SITU DRIFTS SYSTEMS

ABSTRACT

In situ Diffuse Reflectance Infrared Fourier Transform Spectroscopy (DRIFTS) is among the most established and widely applied techniques in the study and rational design of catalysts, however, the presence of strong spectator signals in the spectra collected at steady state frequently limits the useful information obtained. While Modulation excitation coupled with phase sensitive detection (ME-PSD) is a powerful tool to improve spectra quality and differentiate spectators from active species, the experiments require rapid gas exchanges and sampling rate, so the vast majority of published studies employ specialized spectrometers and low-dead-volume reaction cells that are not standard in many laboratories. In this contribution we aimed at expanding the availability of the technique by evaluating the practicality of performing ME-PSD-DRIFTS experiments with a commercially available system. Using the CO_2 hydrogenation reaction as a case study, we identified and optimized three fundamental parameters required to overcome the limitations of standard equipment. The selection of inert gas was found to be critical, it was demonstrated that Ar is more suitable than He to switch from CO_2, as significant differences in properties such as refractive index during reactant modulation generate systematic artifacts. To achieve low residence time, a successful strategy was diluting the reactants flow to allow high flow rate control while modulating only a small fraction of the stream, preventing physical shocks in the system that lead to baseline shifts. Finally, we revealed that a minimum sampling rate of 19 spectra per cycle is essential for proper PSD processing, which can be accomplished by adjusting the number of scans.

INTRODUCTION

The study of catalysts requires investigation of its superficial and structural properties not only after synthesizing the materials, but most importantly, at the conditions in which the catalyst will be applied in a chemical reaction. This is achieved by in situ characterization, one of the pillars of modern research aiming at rational design of improved catalysts [1,2]. Among the several

available techniques for in situ characterization of catalytic surfaces and structures, Diffuse Reflectance Infrared Fourier Transform Spectroscopy (DRIFTS) is possibly the most well established and widely employed, providing relevant information on active sites and adsorbed species during catalytic and adsorption processes, with the possibility of employing realistic industrially relevant conditions with relative ease [3-5].

One of the main challenges when employing in situ FTIR to the study of chemical intermediates in reactions pathway arises from the inherent limitations of the technique. Active species are often present in minor quantities and become hidden by dominating spectator signals. Also, the catalyst surface may change dynamically during activation processes and the reaction itself, generating background shifts, while random noise is sometimes a persistent issue in certain samples. Hence, the resulting signals almost always contain contributions from these detrimental effects along with actual interesting reaction intermediates [6-8]. The limitations mentioned may also render band assignment difficult, at times unfeasible.

Among the transient techniques developed in the past years with the advancements of in situ spectroscopy applied to catalysis, Modulation Excitation (ME) coupled with Phase Sensitive Detection (PSD) has risen as a powerful tool to overcome this hardship [8]. In modulation excitation spectroscopy a periodic perturbation of an external parameter (such as reactant concentration, temperature and pressure) is performed at a defined frequency, while spectra are collected rapidly in this quasi-steady state to track the changes in the spectra caused by the stimulation [9]. The obtained time-resolved dataset is then subjected to PSD processing, which effectively filters out static signals from background and spectators while selectively improving the signals of active species. The technique was originally implemented by Baurecht and Fringeli [10], later made more available by Srinivasan et al. [7] and is currently being refined [11] and employed in state-of-the-art research in heterogeneous catalysis [12-15, 40]. Here we demonstrate the practicality of using standard in situ DRIFTS equipment to perform these experiments.

Properly performing ME-PSD-DRIFTS experiments requires time-resolved collection of spectra and rapid gas exchanges inside the reaction cell, which may be difficult to achieve with standard FTIR cells due to high void volume (long residence time). Hence several homemade low dead volume cells have been developed over the years [16-20] and applied in the studies of highly relevant chemical reactions such as CO oxidation [21,22], CO_2 hydrogenation [13,14,23,24] and

methanol steam reforming [25]. Nonetheless, most of these accessories are still not commercially available and are difficult to replicate, hindering the wide implementation of the technique. While a few research groups have successfully performed ME analyses using commercial cells [21,26,27], there is little information regarding the preliminary tests and optimization used to guarantee adequate experiment conditions and reliable results [7], as detailing these procedures would certainly be out of scope in most catalysis studies presenting several ex and in situ characterization results.

Motivated by the great opportunities the ME-PSD-DRIFTS technique offer, here we demonstrate its successful application using a standard commercially available DRIFTS system with large void volume reaction cell and a relatively easy to reproduce gas line setup. The CO_2 hydrogenation reaction over a Cu/SiO_2 catalyst was selected for the study. By providing a protocol for optimization of experimental conditions with systematic analysis of the individual impact of several parameters such as flow rate and sampling rate, we hope to make this powerful technique more readily accessible to the broader catalysis community.

METHODOLOGY

Equipment setup

The schematics of the system built for the Modulation Excitation – Phase Sensitive Detection – DRIFTS (ME-PSD-DRIFTS) experiments are presented in Figure 1. Pictures of the system, gas lines and the multiposition valve are exhibited in Figure 2. In this case the CO_2 concentration was modulated. The stainless-steel gas lines connect each cylinder to a Mass Flow Controller (MFC), in the case of Ar the lines connect to two separate MFCs, in order to simultaneously introduce the inert gas into a multiposition valve (Vici Valco, EMTMA-CE) and dilute the H_2 flow, which bypasses the valve and it is constantly being fed to the DRIFTS cell.

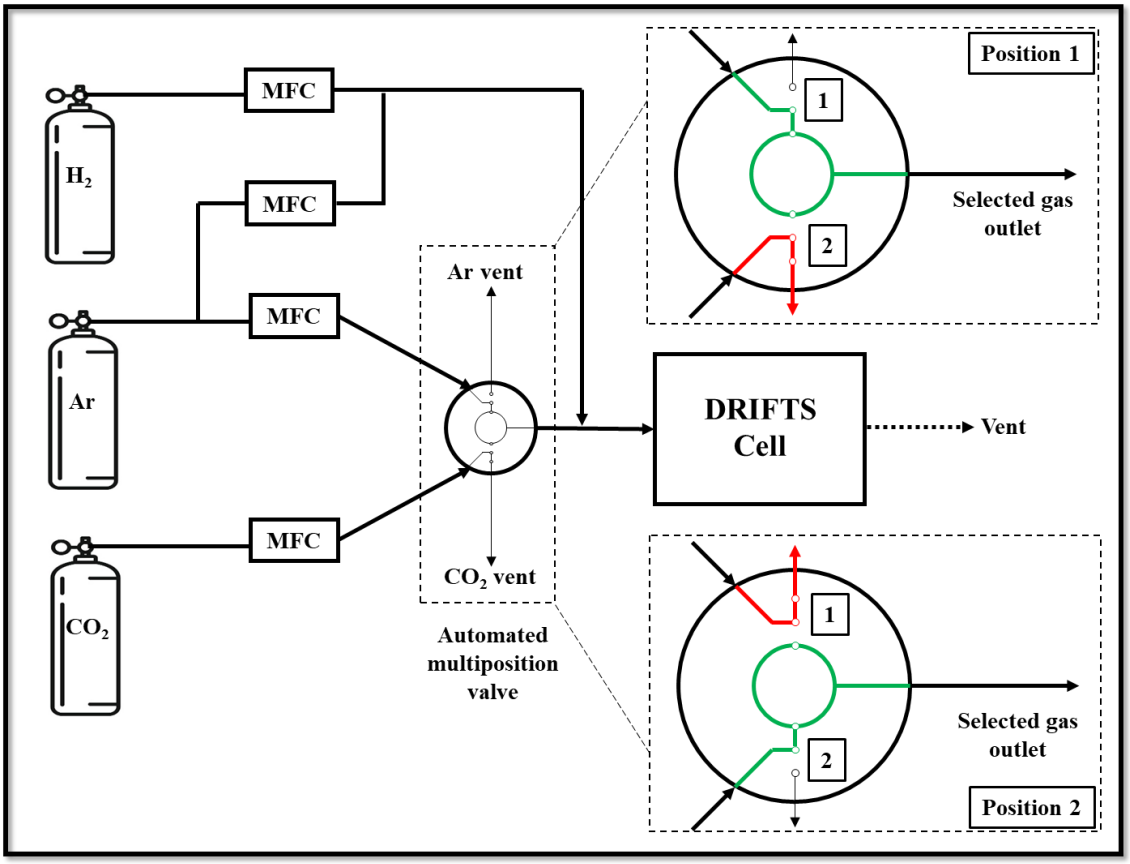

Figure 1. Schematics of the system designed for ME-PSD-DRIFTS experiments.

With the multiposition valve it is possible to rapidly switch between two distinct gas flows, in this case Ar and CO_2. As shown in Figure 1, while the valve is set to position 1, Ar is being fed to the DRIFTS cell while CO_2 is vented, conversely, when the valve is switched to position 2, the opposite happens. The valve was automated to precisely switch positions after a determined amount of time passes, corresponding to half a modulation cycle period, that is, a full cycle is the sum of time spent in each position. The exiting flow from the multiposition valve is then mixed with the H_2/Ar flow and is introduced into the spectrometer (Thermo Scientific, Nicolet iS50 FT-IR), equipped with a Praying Mantis (Harrick) optical system and standard commercial High-temperature reaction chamber (Harrick), the dome used has CaF_2 windows. The length of the gas line connecting the valve outlet and spectrometer was made very short to minimize void volume, allowing rapid gas exchanges.

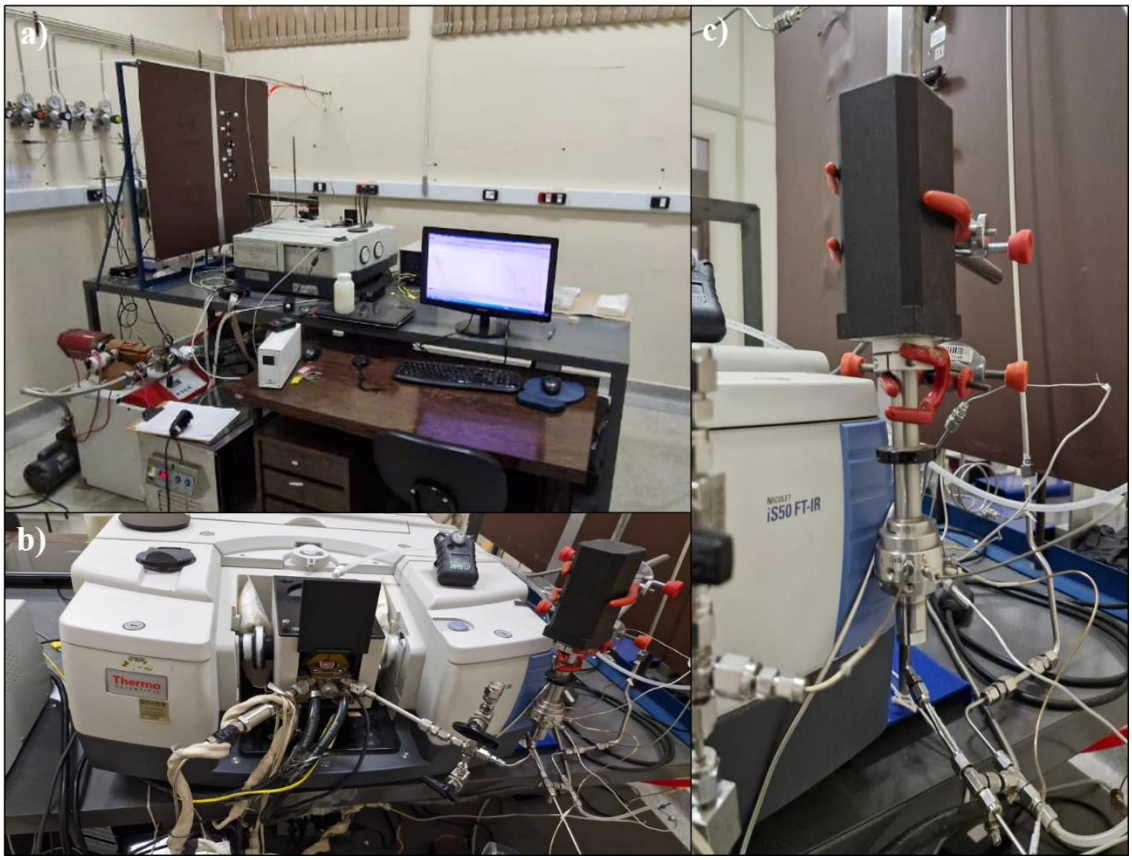

Figure 2. System designed for ME-PSD-DRIFTS experiments

Experiment parameters

The designed system was evaluated under catalytic CO_2 hydrogenation to methanol reaction conditions. A high surface area silica-supported copper catalyst (Cu/SiO_2) with 5% Cu loading was selected for the experiments, the sample was prepared by homogeneous deposition precipitation (HDP), a procedure known to yield metal nanoparticles highly dispersed over the SiO_2 support [28-30], suitable for infrared spectroscopy analyses with good signal-to-noise ratio and resulting spectra relatively easy to interpret. With these conditions, the study could focus on optimizing the modulation-excitation parameters.

In a typical experiment, approximately 35 mg of glass wool (Êxodo Científica) were introduced in the DRIFTS cell sample holder, which was then filled with catalyst powder without packing. The sample surface was then smoothly flattened and the mirrors aligned to maximize the

infrared signal. The Mercury-Cadmium-Telluride (MCT) detector chamber was filled with liquid nitrogen.

Prior to the experiments, the catalyst was reduced at 300 ºC for 1h under H_2/Ar flow. CO_2 hydrogenation to methanol tests were carried out at 200 and 250 ºC, hence, background spectra were collected at these temperatures while cooling down the system after reduction. After the system cooled to 200 ºC and background was collected, the flow was switched to CO_2: $3H_2$ and spectra were collected every minute with 4 cm^{-1} resolution and 64 scans. When the reaction reached steady state, 24 modulation excitation cycles were performed by periodically switching the flow from CO_2: $3H_2$ to Ar: $3H_2$ while spectra were collected rapidly in series mode, with 8 or 16 scans per spectrum, in order to obtain enough experiment points to properly describe the fluctuations in signal intensities. Afterwards, the temperature was raised to 250 ºC and the process described was repeated.

The optimization parameters studied in this work were the inert gas (He and Ar), total reactants flow (20 and 100 mL/min), number of scans per spectrum (8 and 16 scans) and modulation period (50, 100 and 200 s).

Phase sensitive detection data processing

The dataset obtained in the modulation excitation experiments consists of a series of time-resolved spectra collected during the cycles with period T. The first few cycles, typically 3 to 5, were discarded due to equilibration time (dummy periods), resulting in N valid cycles. For each infrared frequency (wavenumber), the intensity profile I(t), (Equation 1) contains contributions from static signals such as background and spectators (I_{static}), time-dependent active signals ($I_{active}(t)$) and random noise ($I_{noise}(t)$).

$$I(t) = I_{static} + I_{active}(t) + I_{noise}(t) \quad (1)$$

The phase sensitive detection (PSD) analysis isolates the active signal by filtering out the static contribution and minimizing noise. This was achieved by extracting the Fourier component of the

signals through numerical integration, that is, the signal intensity I(t) was projected onto a reference wave R(t, ϕ) (Equation 2) by integrating over the period T using the trapezoidal rule for each valid cycle n and then averaging the results to improve the signal-to-noise ratio.

$$R(t,\phi_{PSD}) = \sin(k\omega_{mod}t + \phi_{PSD}) \quad (2)$$

$$I_{PSD}(\phi_{PSD}) = \frac{2}{T}\sum_{n=1}^{N}\left[\int_{0}^{T} I(t)\cdot R(t,\phi_{PSD})dt\right] \quad (3)$$

Where k is the harmonic order (k = 1 for the fundamental frequency and k > 1 for higher harmonics) and $\omega_{mod} = 2\pi/T$ is the modulation frequency.

With this procedure, the orthogonality of the sine function of the reference wave ensures the integral is zero for the constant static contributions (Equation 4) and a finite value for the active signals, which will also present a phase lag that gives kinetic information about the corresponding active species. The noise contribution is effectively minimized by averaging the results over several n cycles (Equation 5). The obtained filtered signal $I_{PSD}(\phi_{PSD})$ is the response in the phase domain, calculated at discrete phase shifts ϕ_{PSD}(0 to 360º, with 10º step), as presented in Equation 6.

$$\int_{0}^{T} I_{static}\cdot \sin(k\omega_{mod}t + \phi_{PSD})dt = 0 \quad (4)$$

$$\sum_{n=1}^{N}\left[\int_{0}^{T} I_{noise}(t)\cdot \sin(k\omega_{mod}t + \phi_{PSD})dt\right] \sim 0 \quad (5)$$

$$I_{PSD}(\phi_{PSD}) = \frac{2}{T}\sum_{n=1}^{N}\left[\int_{0}^{T} I_{active}(t)\cdot R(t,\phi_{PSD})dt\right] \quad (6)$$

To preserve the positive sign of the angle ϕ in the integral, the phase angle results were reported as ϕ_{PSD} = 360º - delay, that is, signals peaking farther to the right correspond to species with faster kinetics. Finally, to match the modulation period start the $CO_{2(g)}$ was transposed to peak at 0º, then the whole phase-resolved spectra was transposed accordingly.

RESULTS AND DISCUSSION

Steady state analysis

Before starting the ME experiments, in-situ DRIFT spectra of the Cu/SiO_2 catalyst surface were recorded every minute until the reaction reached steady-state, which took approximately 90 minutes. Typical spectra obtained in the experiments are presented in Figure 3. As previously reported for Cu/SiO_2 catalysts during CO_2 hydrogenation to methanol [31-34], the species observed here were bidentate formate bound to Cu (b-HCOO-Cu) at 2931, 2851, 1542 and 1351 cm^{-1}, CO-Cu^+ at 2130 cm^{-1} and CO-Cu^0(111) at 2077 cm^{-1} [31,35].

The appearance of b-HCOO-Cu is likely due to hydrogenation of CO_2 adsorbed on SiO_2, although it cannot be discarded the possibility of the species originating from CO [36], which may be formed by CO_2 dissociation on the Cu/Cu^+ surface. Given the experiments were performed at atmospheric pressure and the low methanol selectivity of Cu/SiO_2 catalysts, no methoxy species were detected, nonetheless, the presence of formate in detriment of carboxyl points methanol synthesis from CO_2 would proceed through the formate pathway [37]. Raising the temperature to 250 ºC did not cause significant changes to the spectrum.

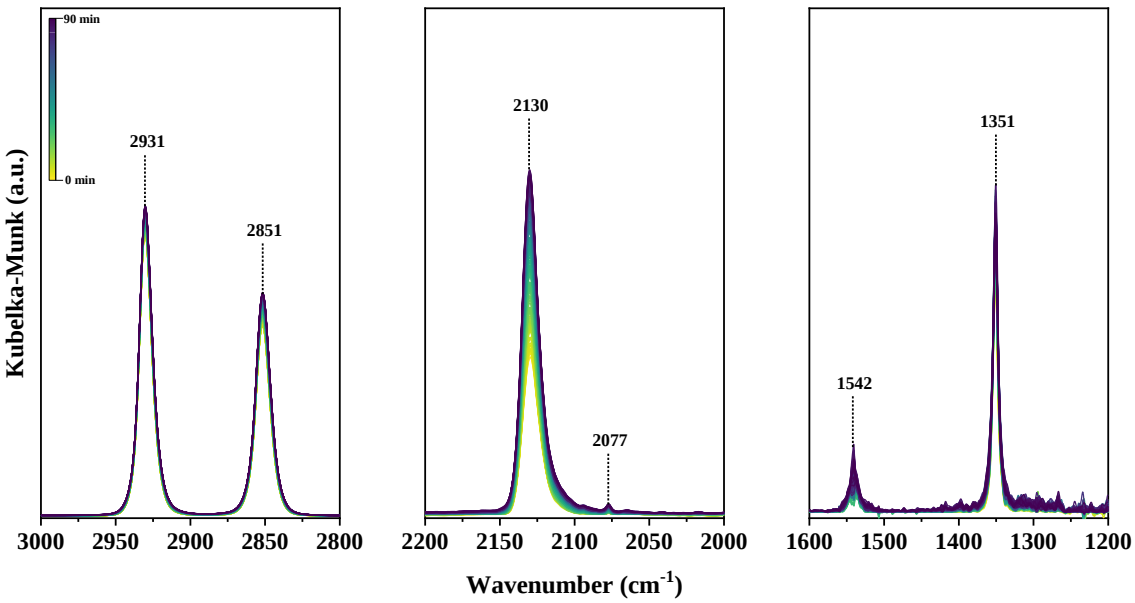

Figure 3. In-situ DRIFTS spectra collected during CO_2 hydrogenation over the Cu/SiO_2 catalyst until steady state was reached. Reactions parameters: T = 200 ºC, 10 mL/min CO_2 + 30 mL/min H_2 + 60 mL/min Ar.

Inert gas selection

When the reaction reached steady state, the flow was periodically switched from CO_2 + $3H_2$ to an inert gas + $3H_2$, maintaining the total flow constant. The inert gases evaluated were He and Ar, the phase resolved spectra obtained after PSD processing are presented in Figures 4 and 5 for experiments at 200 and 250 ºC, respectively. The lines correspond the spectra collected at each phase angle from 0 to 360º, with 10º angle step. The signal intensity scale is different for each region of the spectra, but were normalized in this case to show the spectra quality and resolution. Overall, the ME experiments show the signals of all species observed at the steady state responded to modulation and therefore are active in the reaction.

Regarding the inert gas choice, at 200 ºC (Fig. 4) the regions 3100 – 2700 and 2200 – 2000 cm^{-1} did not present significant differences between the gases apart from a minor improvement in baseline with Ar. On the other hand, the 1600 – 1200 cm^{-1} region changed drastically, with several extra bands appearing when He was employed. The differences in spectra obtained with each gas were far more notable when raising temperature to 250 ºC (Fig. 5), which promoted the reverse

water gas shift (RWGS) reaction, resulting in the appearance of broad $CO_{(g)}$ signals in the region 2200 – 2000 cm^{-1}, making the CO-Cu^{+} (2130 cm^{-1}) signal broad with He, hindering the resolution of the CO-Cu^{0} band (2077 cm^{-1}) when compared to the spectra obtained using Ar. As for the 1600 – 1200 cm^{-1} region, switching CO_2 to He generated several overlapping signals, making the attribution of bands unfeasible.

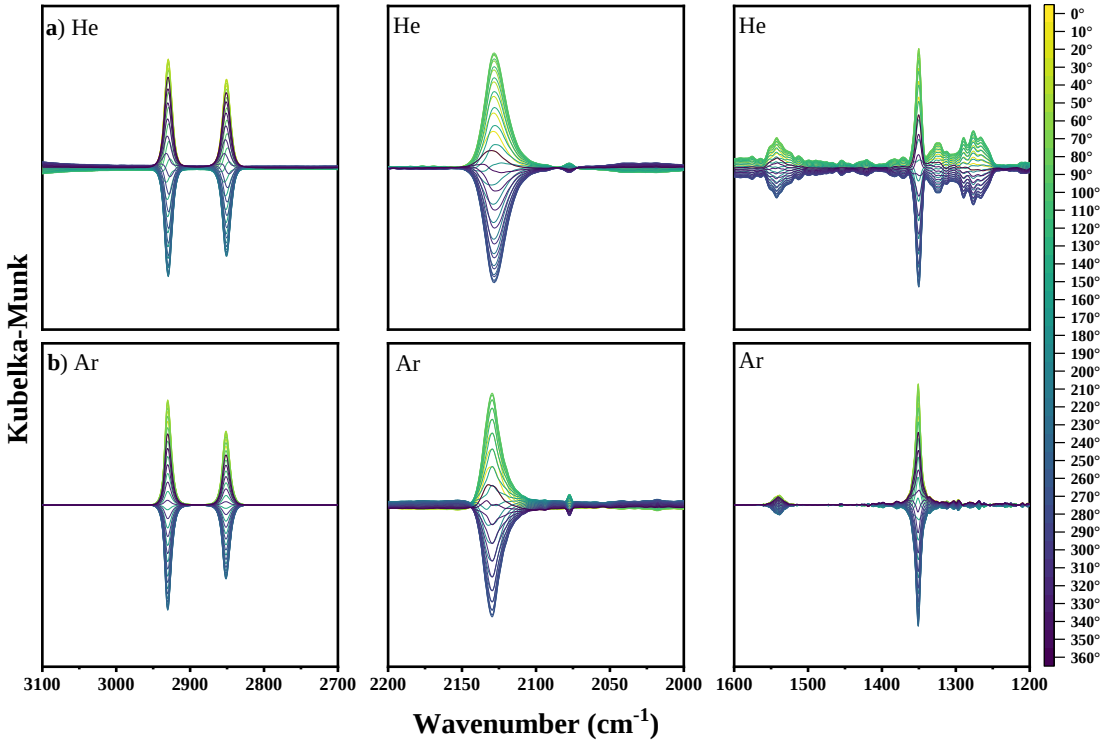

Figure 4. Phase-resolved in situ ME-PSD-DRIFTS spectra collected during CO_2 hydrogenation over the Cu/SiO_2 catalyst using the inert gas **(a)** He and **(b)** Ar. Reactions parameters: T = 200 ºC, 10 mL/min CO_2 + 30 mL/min H_2 + 60 mL/min inert.

Although the total flow was kept constant during the experiments, CO_2 and He have very different physical properties such as refractive index and thermal conductivity, which causes the poor-quality spectra obtained. Prior to the experiments, the background spectrum was collected when cooling the system from the reduction to the reaction temperatures under an inert + $3H_2$ flow. If the inert gas is He, every time it is switched to CO_2, the infrared optical pathway undergoes a drastic change in comparison to the medium inside the cell during background spectrum recording,

creating temporary baseline shifts that disappear when the flow is switched back to He and the medium refractive index is again very similar to when the background was collected. Hence the baseline shift in this case is periodic, with frequency similar to the modulation, causing the shifts to be regarded as active signals during PSD processing and generating the systematic artifacts. Raising the temperature further increases the difference in refractive index and generates more artifacts, as seen in Figure 5, which could also be caused by cell windows slightly expanding/contracting due to the high thermal conductivity of He. Conversely, it was observed that switching between CO_2 and Ar greatly minimized these effects, as the gases have similar refractive index. In this sense, it is very likely that if H_2 was the modulating reactant, He would be more suitable than Ar as the inert gas.

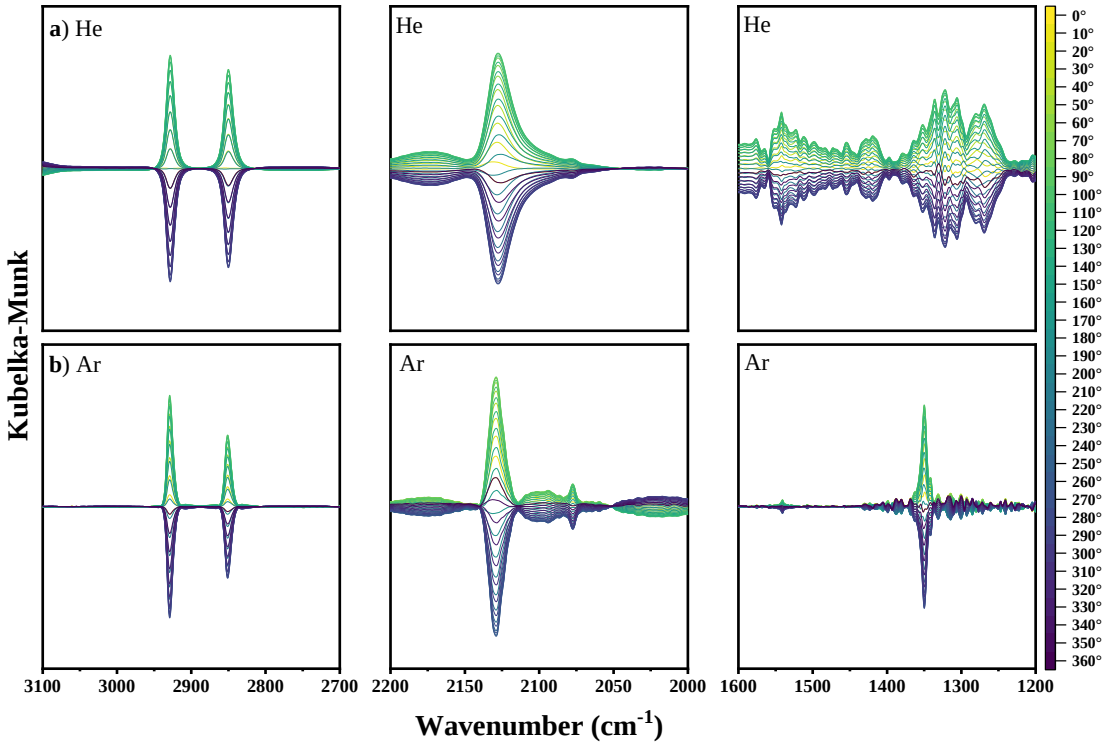

Figure 5. Phase-resolved in situ ME-PSD-DRIFTS spectra collected during CO_2 hydrogenation over the Cu/SiO_2 catalyst using the inert gas **a)** He and **b)** Ar. Reactions parameters: T = 250 ºC, 10 mL/min CO_2 + 30 mL/min H_2 + 60 mL/min inert.

Therefore, it was demonstrated the choice of inert gas is critical for ME experiments when using standard DRIFTS cells with large void volume, which may not be an issue in previous works with the technique being employed in homemade cells designed specifically to minimize void volume [7,13,16,18].

Gas flow rate optimization

The ME technique requires rapid gas exchanges, so another concern when dealing with large dead volume is the gas residence time in the system [16]. Using Ar as inert gas, experiments were performed at 250 ºC under different total flows rates, the results are presented in Figure 6.

In the first experiment (Fig. 6a), using 20 mL/min total flow rate, there were several artifact bands at 1600 – 1200 cm^{-1} and intense baseline shifts at 2200 – 2000 cm^{-1}, negatively impacting band attribution and generating misleading results that could be interpreted as hidden active signals in the steady state. This was likely caused by longer a washout time of the reaction cell than a half modulation period when using low gas flow rate, therefore CO_2 may have been present in the cell at all times as the flow was insufficient to fully carry the reactant and clear CO_2 before the valve turn. Hence it was observed that higher flow rates are necessary for proper modulation in large void volume cells.

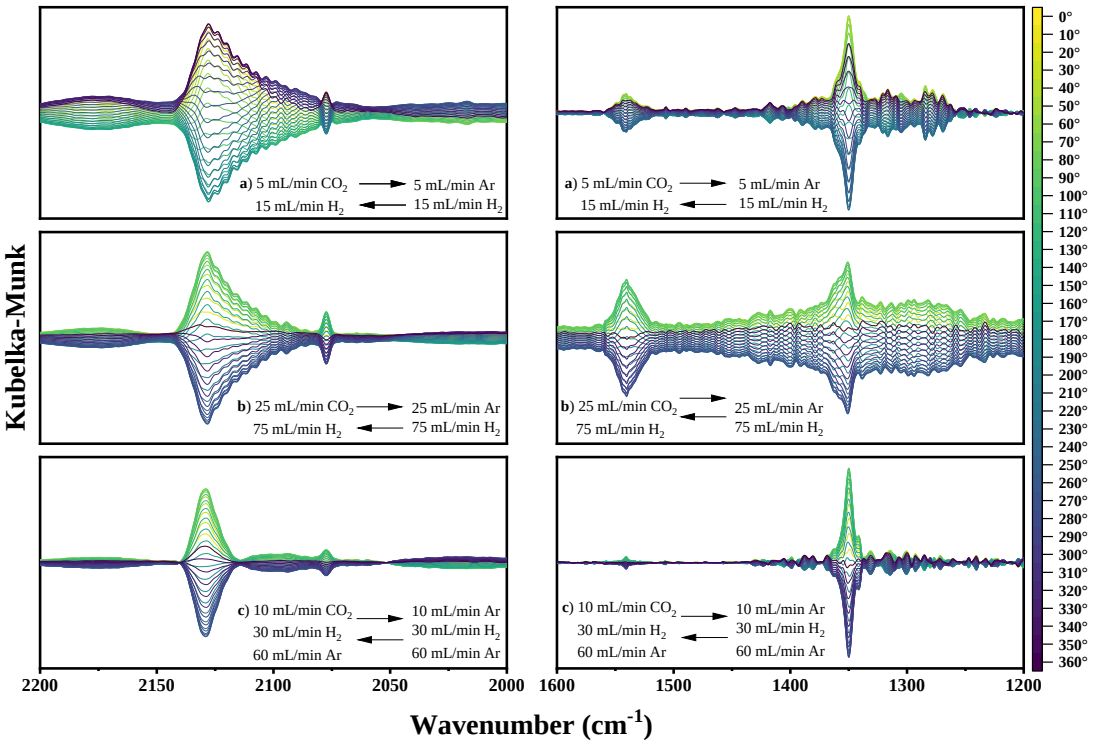

Figure 6. Phase-resolved in situ ME-PSD-DRIFTS spectra collected during CO_2 hydrogenation over the Cu/SiO_2 catalyst at 250 ºC under **a)** 5 mL/min CO_2 + 15 mL/min H_2, **b)** 25 mL/min CO_2 + 75 mL/min H_2 and **c)** 10 mL/min CO_2 + 30 mL/min H_2 + 60 mL/min Ar flow.

By increasing the total flow rate to 100 mL/min (Fig. 6b), the residence time issue may be avoided, but switching 25 mL/min from one flow to another also had negative consequences. The 2200 – 2000 cm^{-1} region was improved, showing a more resolved CO-Cu^0 band (2077 cm^{-1}), however, from 1600 to 1200 cm^{-1} the spectra baselines presented severe instability. This is explained by the large amplitude of the perturbation, which may have caused pressure pulses when the valve turned and generated artificial disturbances in the flow or even slightly altering the sample surface, causing the baseline instability due to modifications in the medium. Moreover, the fluctuations are similar to the observed in Figure 5a, so it is also possible that such perturbation amplitude (25% of the total flow) changed the refractive index significantly, even though the exchange is from CO_2 to Ar.

The challenge encountered motivated the design of an additional gas line to introduce Ar along with the H_2 being constantly fed to the reaction cell, as described previously and depicted in

Figure 1, enabling control of high total flow rates while exchanging only a small fraction of the gas flow. Figure 6c exhibits the ME-PSD spectra obtained using 100 mL/min total flow rate, of which 60 mL/min are Ar. In this case the gas exchanges is a perturbation with more brand amplitude, corresponding to 10% of the total flow. It was observed significant improvement with the new setup, the CO bands at the 2200 – 2000 cm^{-1} region are resolved, while the baseline is stable at 1600 – 1200 cm^{-1} and the artifacts intensity was minimized. The results show the total flow rate and the amplitude of the perturbation need to be selected carefully when using standard large volume cells.

It is noteworthy that while this strategy successfully overcame the fluid dynamics and refractive index issues found in this case, it can impose a limitation in residence time, as the experiments may only be viable using high space velocity [7], which may deviate significantly from the parameters commonly employed in catalytic tests at industrially relevant conditions.

Sampling rate and modulation period

An adequate selection of the infrared spectrometer sampling parameters is critical to properly describe the changes in the spectra caused by the perturbation during modulation excitation experiments [7]. There is a trade-off between spectra quality, determined by the resolution and number of scans, and the time required for acquiring samples. Here we fixed the resolution at 4 cm^{-1} to evaluate the effects of number of scans on the PSD processing of spectra collected during ME, the results are presented in Figures 7 and 8.

Firstly, the modulation period was fixed in 100 s (the typical value employed here) and individual experiments were carried out using 8 and 16 scans (Fig. 7). With 8 scans the sampling rate was approximately 19 spectra/min, resulting in 32 spectra/cycle for a period of 100 s, while with 16 scans the rate was 9 spectra/min (19 spectra/cycle). Apart from a slight improvement in the baseline at the region between 2200 and 2000 cm^{-1}, no other significant changes were observed regardless of the sampling rate in this case, showing that 19 points are sufficient for describing the signals profile during a modulation cycle and 16 scans/spectrum is a suitable condition for the experiments.

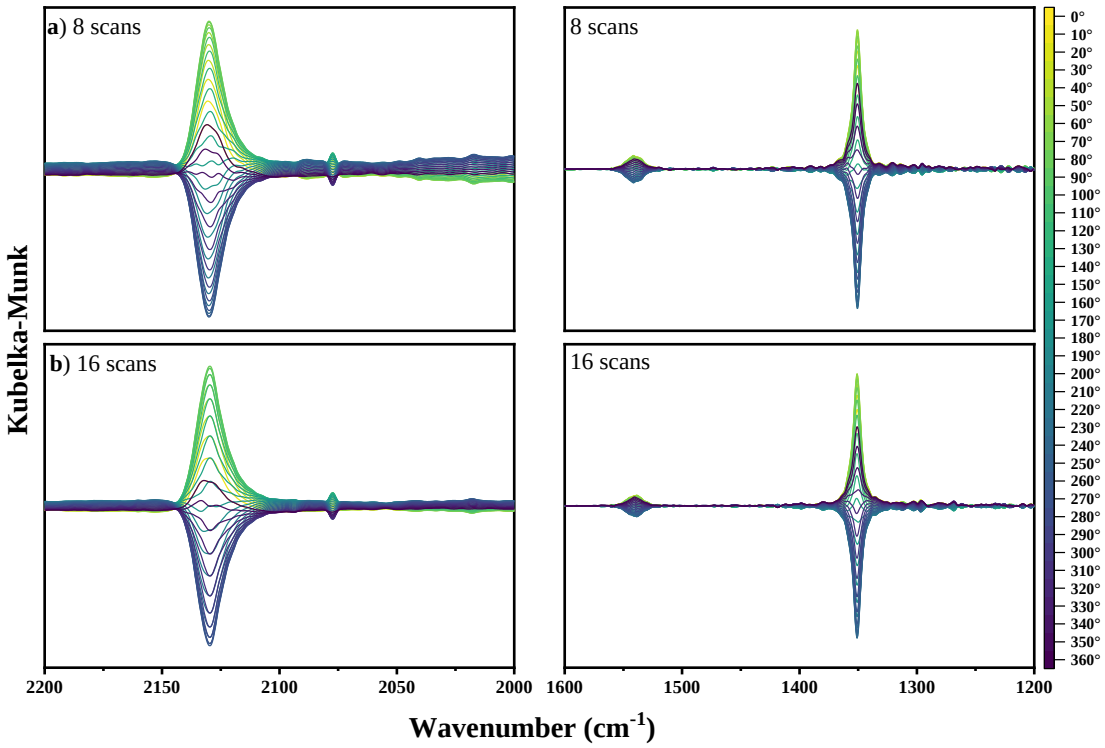

Figure 7. Phase-resolved in situ ME-PSD-DRIFTS spectra collected during CO_2 hydrogenation over the Cu/SiO_2 catalyst at 200 ºC with modulation period of 100s. The spectra were averaged over **a)** 8 and **b)** 16 scans.

On the other hand, when the modulation period was 50 s (7 spectra/cycle) the spectra presented several systematic artifacts over the whole region of interest, including a shouldering at 2114 cm^{-1} (Fig. 8a). Hence, when using short modulation periods (< 100 s) it is likely the samples should be collected with fewer scans to properly track the period changes in the signals. Here the data suggests that at least 19 spectra should be collected for each cycle. It is also possible to change the spectral resolution in order to increase the sampling rate, however, in the case of CO_2 hydrogenation, it has been reported that signals of distinct formate and methoxy species appear at very similar wavenumbers [31,32,37,39].

Moreover, it has been reported previously the possibility of attenuating the signals of faster short-lived species by increasing modulation frequency and/or analyzing signals in higher frequency harmonics [11,15], so it is possible the 2114 cm^{-1} shouldering corresponds to fast Cu-

bound CO species [38] and not an artifact. Nonetheless here we focus on optimizing experimental parameters, so the investigation of short-lived species is out of the scope.

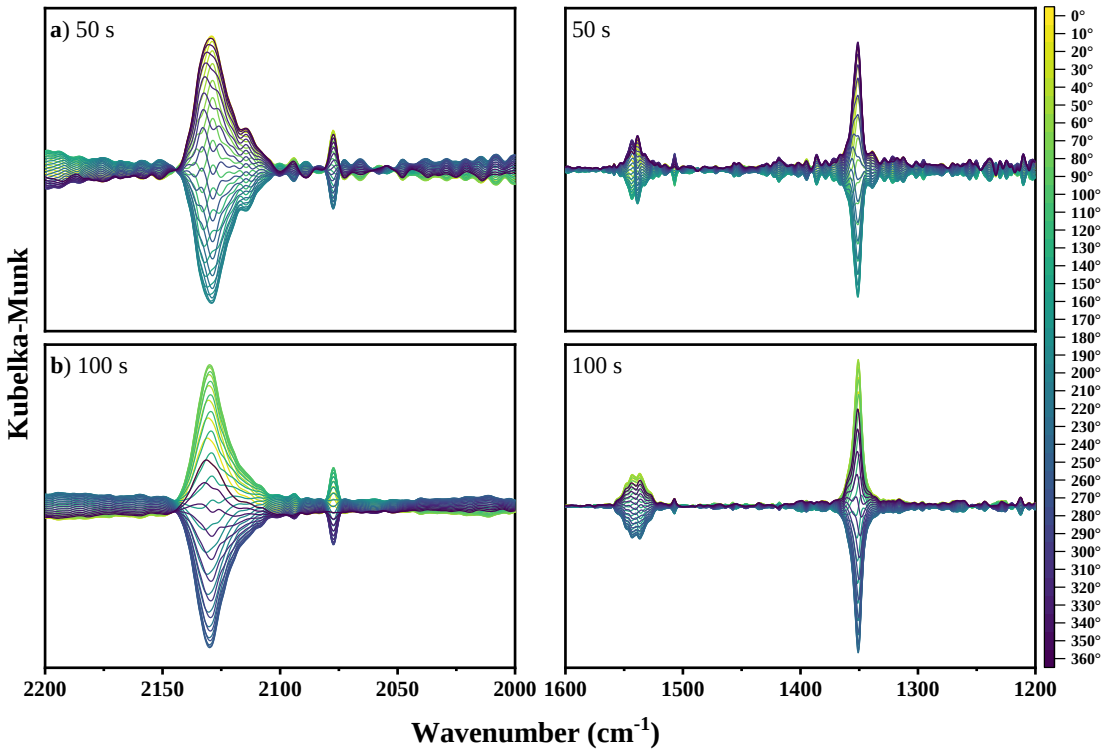

Figure 8. Phase-resolved in situ ME-PSD-DRIFTS spectra collected during CO_2 hydrogenation over the Cu/SiO_2 catalyst at 200 ºC with modulation period of **a)** 50 and **b)** 100 s. The spectra were averaged over 16 scans.

It is worth noticing the modulation frequency must be in the same order of magnitude of the reaction turnover frequency (TOF), which is highly dependent on temperature. Using inappropriate frequencies may lead to weak signal responses or loss of kinetic information due to poor resolution of the active species phase lag, therefore the choice is not arbitrary [7, 9,10,13].

Overall, the results presented here show that performing modulation excitation spectroscopy experiments on standard DRIFTS cells with large volume is viable, but requires careful selection of experimental parameters, as suggested previously [7,26,27]. We have highlighted the impacts of properly adjusting the gas flow rate and using a suitable inert in the

appearance of misleading signals and baseline stability during modulation. The analyses also show how the spectrometer sampling rate must be optimized to preserve the spectra quality while collecting sufficient points to describe the periodic changes in the active species signals.

CONCLUSION

The feasibility of performing in situ Modulation Excitation DRIFTS coupled with Phase Sensitive Detection (ME-PSD-DRIFTS) using a standard, commercially available system was evaluated. The investigation identified three critical aspects affecting data quality in these systems. First, the selection of the inert gas is fundamental. We demonstrated that exchanging CO_2 with He introduced significant systematic artifacts due to a great difference in refractive index and thermal conductivity between the gases. To prevent periodic baseline modulations that can be misleading, Ar must be used as the inert counterpart for CO_2, ensuring the optical path length and thermal environment remain stable during modulation. While high total flow rates are necessary to minimize residence time and prevent signal washout, modulating a large fraction of the flow induces severe baseline shifts. We established that optimal performance is achieved by maintaining an almost constant background of inert gas, modulating only a small fraction of the reactant stream. Lastly, we have shown the minimum sampling rate capable of properly describing the perturbation waveform while preserving signal quality and temporal resolution. It was found that at least 19 spectra must be recorded for each modulation cycle, which can be achieved by adjusting the number of scans collected per spectrum.

By using the CO_2 hydrogenation reaction over a Cu/SiO_2 catalyst as a representative case, we developed a validated experimental protocol for conducting transient kinetic studies using standard instrumentation. By defining the operational boundaries regarding inert gas selection, fluid dynamic control and temporal sampling, we hope to make the powerful ME-PSD-DRIFTS technique more readily accessible to the scientific catalysis community.

REFERENCES CHAPTER II

1. Banares, Miguel A., and Marco Daturi. "Understanding catalysts by time-/space-resolved operando methodologies." *Catalysis Today* 423 (2023): 114255.
2. Zhang, Yulong, et al. "Application of operando spectroscopy on catalytic reactions." *Current Opinion in Chemical Engineering* 12 (2016): 1-7.
3. Grunwaldt, Jan-Dierk, and Alfons Baiker. "In situ spectroscopic investigation of heterogeneous catalysts and reaction media at high pressure." *Physical Chemistry Chemical Physics* 7.20 (2005): 3526-3539.
4. Zaera, Francisco. "In-situ and operando spectroscopies for the characterization of catalysts and of mechanisms of catalytic reactions." *Journal of Catalysis* 404 (2021): 900-910.
5. Li, Xiaodong, et al. "Progress and perspective for in situ studies of CO2 reduction." *Journal of the American Chemical Society* 142.21 (2020): 9567-9581.
6. Meunier, Frederic C., and Alexandre Goguet. "Achievements and challenges in deciphering heterogeneous catalytic reaction mechanisms using operando infrared spectroscopies." *Nature Communications* (2025).
7. Srinivasan, Priya D., et al. "Application of modulation excitation-phase sensitive detection-DRIFTS for in situ/operando characterization of heterogeneous catalysts." *Reaction Chemistry & Engineering* 4.5 (2019): 862-883.
8. Weyel, Jakob, et al. "Modulation Excitation Spectroscopy: A Powerful Tool to Elucidate Active Species and Sites in Catalytic Reactions." *Accounts of Chemical Research* 57.18 (2024): 2643-2652.
9. Urakawa, Atsushi, Thomas Bürgi, and Alfons Baiker. "Sensitivity enhancement and dynamic behavior analysis by modulation excitation spectroscopy: Principle and application in heterogeneous catalysis." *Chemical Engineering Science* 63.20 (2008): 4902-4909.
10. Baurecht, Dieter, and Urs Peter Fringeli. "Quantitative modulated excitation Fourier transform infrared spectroscopy." *Review of scientific instruments* 72.10 (2001): 3782-3792.
11. Marchionni, Valentina, et al. "Increasing the sensitivity to short-lived species in a modulated excitation experiment." *Analytical chemistry* 89.11 (2017): 5801-5809.
12. Kokumai, Tathiana M., et al. "Insights from Modulation-Excitation Spectroscopy into the Role of Pt Geometrical Sites in the WGS Reaction." *ACS Applied Materials & Interfaces* 17.9 (2025): 13221-13231.

13. Al Abdulghani, Abdullah J., et al. "Uncovering the pressure-dependent mechanism of CO2 hydrogenation to methanol on Ga-promoted Cu/ZrO2 using operando modulation-excitation DRIFTS." *Journal of the American Chemical Society* 147.31 (2025): 27438-27448.
14. López-Luque, Iván, et al. "Engineering Peripheral Metal-Oxide Catalysis: Interparticle Spacing in Cu/ZrO2 Catalysts for Methanol Synthesis by CO2 Hydrogenation." *Angewandte Chemie International Edition* 64.37 (2025): e202420126.
15. Have, Iris C. ten, et al. "Uncovering the reaction mechanism behind CoO as active phase for CO2 hydrogenation." *Nature Communications* 13.1 (2022): 324.
16. Patil, Bhagyesha S., et al. "Design, modelling, and application of a low void-volume in situ diffuse reflectance spectroscopic reaction cell for transient catalytic studies." *Reaction Chemistry & Engineering* 4.4 (2019): 667-678.
17. Chiarello, Gian Luca, et al. "Adding diffuse reflectance infrared Fourier transform spectroscopy capability to extended x-ray-absorption fine structure in a new cell to study solid catalysts in combination with a modulation approach." *Review of Scientific Instruments* 85.7 (2014).
18. Aguirre, Alejo, and Sebastián E. Collins. "Selective detection of reaction intermediates using concentration-modulation excitation DRIFT spectroscopy." *Catalysis Today* 205 (2013): 34-40.
19. Li, Binghui, and Richard D. Gonzalez. "Design and construction of a DRIFTS accessory and an in situ heatable sample cell." *Applied spectroscopy* 52.11 (1998): 1488-1491.
20. Fast transient infrared studies in material science: development of a novel low dead-volume, high temperature DRIFTS cell
21. Aguirre, Alejo, et al. "In-Situ DRIFT study of Au–Ir/ceria catalysts: activity and stability for CO oxidation." *Topics in Catalysis* 59.2 (2016): 347-356.
22. del Río, Eloy, et al. "Reversible deactivation of a Au/Ce0. 62Zr0. 38O2 catalyst in CO oxidation: A systematic study of CO2-triggered carbonate inhibition." *Journal of catalysis* 316 (2014): 210-218.
23. Martin, Oliver, et al. "Operando synchrotron X-ray powder diffraction and modulated-excitation infrared spectroscopy elucidate the CO2 promotion on a commercial methanol synthesis catalyst." *Angewandte Chemie International Edition* 55.37 (2016): 11031-11036.

24. Zarfl, Johannes, et al. "DRIFTS study of a commercial Ni/γ-Al2O3 CO methanation catalyst." *Applied Catalysis A: General* 495 (2015): 104-114.
25. Haghofer, Andreas, et al. "Who is doing the job? Unraveling the role of Ga2O3 in methanol steam reforming on Pd2Ga/Ga2O3." *Acs Catalysis* 2.11 (2012): 2305-2315.
26. Kydd, Richard, et al. "Temperature-induced evolution of reaction sites and mechanisms during preferential oxidation of CO." *Journal of catalysis* 277.1 (2011): 64-71.
27. Müller, Philipp, et al. "Mechanistic study on the Lewis acid catalyzed synthesis of 1, 3-butadiene over Ta-BEA using modulated operando DRIFTS-MS." *Acs Catalysis* 6.10 (2016): 6823-6832.
28. Dong, Xiaohuan, et al. "Comparative study of silica-supported copper catalysts prepared by different methods: formation and transition of copper phyllosilicate." *Catalysis Science & Technology* 6.12 (2016): 4151-4158.
29. Du, Hong, et al. "Catalytic furfural hydrogenation to furfuryl alcohol over Cu/SiO2 catalysts: A comparative study of the preparation methods." *Fuel Processing Technology* 193 (2019): 221-231.
30. Wang, Shurong, et al. "Highly active and selective Cu/SiO2 catalysts prepared by the urea hydrolysis method in dimethyl oxalate hydrogenation." *Catalysis Communications* 12.13 (2011): 1246-1250.
31. Fisher, Ian A., and Alexis T. Bell. "In-situ infrared study of methanol synthesis from h2/co2over cu/sio2and cu/zro2/sio2." *Journal of Catalysis* 172.1 (1997): 222-237.
32. Wu, Congyi, et al. "Inverse ZrO2/Cu as a highly efficient methanol synthesis catalyst from CO2 hydrogenation." *Nature communications* 11.1 (2020): 5767.
33. Millar, Graeme J., Colin H. Rochester, and Kenneth C. Waugh. "Infrared study of the adsorption of formic acid on silica-supported copper and oxidised copper catalysts." *Journal of the Chemical Society, Faraday Transactions* 87.9 (1991): 1491-1496.
34. Bando, Kyoko Kitamura, et al. "In-situ FT-IR study on CO2 hydrogenation over Cu catalysts supported on SiO2, Al2O3, and TiO2." *Applied Catalysis A: General* 165.1-2 (1997): 391-409.
35. Zhang, Diyu, et al. "Characterization of CO Adsorbed to Clean and Partially Oxidized Cu (211) and Cu (111)." *The Journal of Physical Chemistry C* 127.50 (2023): 24158-24167.

36. Fisher, Ian A., and Alexis T. Bell. "In situ infrared study of methanol synthesis from H2/CO over Cu/SiO2and Cu/ZrO2/SiO2." *Journal of Catalysis* 178.1 (1998): 153-173.
37. Kattel, Shyam, et al. "Optimizing binding energies of key intermediates for CO2 hydrogenation to methanol over oxide-supported copper." *Journal of the American Chemical Society* 138.38 (2016): 12440-12450.
38. Caldas, Paula CP, et al. "The structure of the Cu–CuO sites determines the catalytic activity of cu nanoparticles." *ACS catalysis* 7.4 (2017): 2419-2424.
39. Binet, Claude, and Marco Daturi. "Methanol as an IR probe to study the reduction process in ceria–zirconia mixed compounds." *Catalysis today* 70.1-3 (2001): 155-167.
40. Silva Sousa, Leonardo da, et al. "Identification of Transient Intermediates and Active Species in Atomic CZA Catalysts for CO2 Hydrogenation to Methanol." *Journal of the American Chemical Society* 147.47 (2025): 43295-43316.

CHAPTER III: IDENTIFYING CO_2 HYDROGENATION ACTIVE SPECIES OVER Cu-ZrO_2/SiO_2 AND Cu/ZrO_2 CATALYSTS WITH IN SITU MODULATION EXCITATION-DRIFTS

ABSTRACT

CO_2 hydrogenation to methanol over Cu catalysts arises as a promising technology in the current need to minimize anthropogenic carbon emission. Despite significant advancements with Cu-Zr systems, key mechanistic aspects remain matters of controversy. Here we addressed these topics on Zr-promoted and supported Cu nanoparticles systems with catalytic tests at industrially relevant conditions and in situ modulation excitation-phase sensitive detection-DRIFTS. The results indicate the formate pathway is the main reaction mechanism for methanol synthesis and dispersed Zr nanoparticles partially inhibit the reverse water gas shift reaction activity on the promoted samples, while bulk ZrO_2 renders Zr-bound formates a spectator behavior. It was observed fast CO_2 conversion to active formates bound to Cu surfaces and sites near the Cu-Zr interfaces, the latter likely being observed experimentally for the first time. The data suggests an optimal Cu-Zr catalyst should present interfacial sites while avoiding bulk ZrO_2 effects. Further hydrogenation of formate to methoxy and hydrolysis of Zr-bound methoxy to methanol were found to be the rate-controlling steps at the conditions employed. Additionally, faster reduction of Cu-bound methoxy species with nearby adsorbed H was also detected. The findings help clarifying the current ongoing debate regarding the active species involved in CO_2 hydrogenation, highlighting the challenges and opportunities to further enhance methanol production with Cu-Zr catalysts.

INTRODUCTION

Our current global production system and form of organizing society have caused atmospheric CO_2 concentration to reach a level unprecedented in the past 800,000 years [1]. Since the beginning of the industrial revolution, CO_2 concentration has risen from 280 ppm in the 1800s to 423 ppm in 2024, with yearly increase rate in the past 60 years being approximately 100 times higher than in the years prior to industrialization. The results are severe damaging effects on the

environment through greenhouse effect and climate change, namely rapid global warming, extreme climate events including deadly heat waves, sea levels rising and ocean acidification [2]. The scenario has caused great concern in scientists and environmentalists, pushing governments of several nations to form pacts such as the Paris Agreement, among other initiatives, to support the development of clean energy alternatives and mitigate carbon emissions [3]. Nonetheless little has been achieved over the last years, as annual emission rate, atmospheric CO_2 concentration and global temperature records are constantly being surpassed [4]. The difficulties encountered have been ascribed to the persistent dependency on fossil fuel, which is highlighted by the main sources of CO_2: energy, transportation and industry (totalizing 80% of emissions) [5]. Furthermore, the current processes for producing clean energy and capturing atmospheric carbon are costly, so the challenge of developing new technologies arises in an emergency state.

Among the various strategies proposed to mitigate anthropogenic CO_2 emissions, catalytic CO_2 hydrogenation has emerged as a promising route for chemical valorization of the greenhouse gas [6,7]. By reacting CO_2 with renewable hydrogen, this process enables the synthesis of value-added chemicals such as methanol, dimethyl ether, and hydrocarbons, thereby contributing to both carbon recycling and the development of sustainable chemical processes. In particular, methanol is a key platform chemical and energy carrier with broad applications [8]. Copper-based catalysts are among the most studied systems for CO_2 hydrogenation [6, 9, 10], owing to their ability to activate hydrogen and facilitate the hydrogenation of intermediates [11,12]. However, the activity of Cu catalysts is highly dependent on the choice of support and promoter materials, which influence not only metal dispersion and morphology but also the rates adsorption, activation, and conversion of reactants and intermediates [13-15]. The $CuO/ZnO/Al_2O_3$ catalyst, employed in methanol synthesis from syngas, has been widely investigated [6, 16-20], showing high activity resulting from the synergy between the components. Conversely, this system promotes CO production through the reverse water gas shift (RWGS) reaction and is prone to deactivation due to strong interaction of Al_2O_3 acid sites with water generated in the process [21,22].

In this context, great enhancements in catalyst activity have been achieved with the incorporation of ZrO_2 as promoter and support [23-29]. The beneficial effects are ascribed to weak surface hydrophilicity [30], availability of basic sites [31] and oxygen vacancies [32] with high CO_2 adsorption capability, inhibition of byproducts CO and CH_4 [33] and strong metal-support

interaction [34], stabilizing dispersed Cu nanoparticles and generating highly active Cu-ZrO_2 interfaces [35,36]. ZrO_2 supports and Cu/ZrO_2 catalysts have been prepared by several synthesis methods [37-40] and advancements employing ZrO_2 as promoter have also been achieved [41]. While the supported and promoted systems have been extensively characterized with ex [24, 42] and in situ techniques [35,43,44] and investigated with density functional theory [45-48], there is currently an ongoing debate regarding the CO_2 hydrogenation mechanisms leading to CO and CH_3OH [23,28,44,45,49-51].

Early papers reported methanol synthesis from CO_2 follows the formate pathway [52,53], with the main intermediates bound to ZrO_2 surfaces. While some results published later are in agreement [28,37,49], others challenged this idea arguing the Zr-bound species are actually spectators and the reaction takes place through the RWGS mechanism generating CO, then hydrogenation to methanol [45,54], it has also been proposed it is possible to unlock a dual channel consisting of both routes [23]. More recent works on inverse catalysts ascribed the catalytic activity to fast Cu-bound formate species, with the Zr counterparts participating less in the reaction [50,51] and a third type of active formate has been envisaged [55,56]. On the other hand, the RWGS reaction may proceed via a carboxyl intermediate or direct CO_2 dissociation [57]. Here we addressed these controversial topics by investigating the mechanism over Zr-promoted and supported catalysts using transient Diffuse Reflectance Infrared Fourier Transform Spectroscopy (DRIFTS).

The difficulty in drawing accurate conclusions when studying reaction pathways with DRIFTS arise from dominating spectator signals, background shifts and in some cases poor signal-to-noise ratio, resulting in misleading data [58-60]. Furthermore, in situ DRIFT spectra of CO_2 hydrogenation often contain overlapped signals, causing conflicting band attribution on the available literature [23,45,50,52]. In this sense, modern state-of-the-art catalysis research is currently employing transient techniques such as Modulation Excitation-Phase Sensitive Detection (ME-PSD) [20,44,49,60], which consists in the rapid acquisition of spectra while performing a periodic perturbation of a reaction parameter, then the PSD processing effectively minimizes static contributions and random noise, significantly enhancing the spectra and providing insight into the relative kinetics of actual reaction intermediates [59,60].

We uncovered with ME-PSD-DRIFTS the actual formate pathway intermediates while no contribution from the carboxyl pathway was detected, and proposed the methoxy production and subsequent hydrolysis to methanol are the rate-determining steps. The bulk properties of ZrO_2 were found to influence the activity of Zr-bound species. Furthermore, for the first time the intermediate related to interfacial sites was revealed experimentally on the Cu/ZrO_2 catalyst and the RWGS reaction was observed to proceed by direct CO_2 dissociation on the copper surface and decomposition of formate species. The findings help clarifying some mechanistic aspects, provide insight on the challenges and opportunities in further optimizing Cu-Zr systems and highlight the need of transient methodologies for a deeper understanding of reaction pathways with infrared spectroscopy.

METHODOLOGY

Synthesis of supports and catalysts

The catalysts studied here were copper supported on SiO_2 (Cu/SiO_2), a series of ZrO_2-promoted Cu/SiO_2 systems and Cu/ZrO_2. For the synthesis of SiO_2 initially 25 g of Tetraethylortosilicate (TEOS) (98%, Sigma-Aldrich) were dissolved in 75 mL of ethanol (99.5%, ACS Científica). Then 6 mL of HNO_3 (65.0%, Synth) were added under stirring, followed by the dropwise addition of NH_4OH aqueous solution (27.0%, Synth) until a gel was obtained. Afterwards the product was filtered and washed with deionized water three times, dried at 100 ºC overnight and calcined under air flow at 500 ºC (3ºC/min) for 5 hours.

The Cu/SiO_2 catalysts were prepared by homogeneous deposition precipitation (HDP) assisted by urea hydrolysis [24,45,61,62]. First $Cu(NO_3)_2{\cdot}xH_2O$ (99.999%, Sigma-Aldrich) was dissolved in 200 mL of deionized water at concentration calculated to obtain catalysts with 5 wt% Cu loading. Urea (99.0 – 100.5%, Sigma-Aldrich) at a concentration 30 times the concentration of $Cu(NO_3)_2$ and 2 g of the prepared SiO_2 were added under vigorous stirring at room temperature. The mixture was then heated to 90 ºC (1 ºC/min) to hydrolyze urea very slowly, kept at this condition until pH reached 8, then aged for 2 hours. The obtained material was centrifuged and washed three times, dried at 100 ºC for 24 hours and calcined under air flow at 350 ºC (1 ºC/min) for 5 hours.

Incorporation of ZrO_2 was performed by incipient wetness impregnation on the prepared Cu/SiO_2 samples [24], the amounts of $ZrO(NO_3)_2 \cdot xH_2O$ (99%, Sigma-Aldrich) were selected to obtain final $Cu\text{-}yZrO_2/SiO_2$ catalysts, y being the ZrO_2 loadings (y = 1, 5, 10 and 20 wt%). The supports' effective pore volume was estimated with the wet point technique, which consists of adding water drops of known volume to the support and homogenizing the sample after each drop, repeating the process until saturation. In this procedure, the ZrO_2 precursor was dissolved in deionized water, using a volume equal to the pore volume estimated, the solution was then added to the dried Cu/SiO_2 catalyst dropwise. The obtained slurry was dried at 100 ºC overnight and calcined under air flow at 350 ºC (1 ºC/min) for 5 hours.

For the Cu/ZrO_2 system, the ZrO_2 support was synthesized by a hydrothermal route. Initially $ZrO(NO_3)_2$ was dissolved in deionized water under stirring at room temperature followed by the addition of three times the Zr precursor mass of the surfactant Pluronic P-123 (PEG-PPG-PEG, Sigma-Aldrich). The mixture was heated to 50 ºC to fully dissolve P-123 and NH_4OH was slowly added until pH reached 7. Afterwards the mixture was transferred to a Teflon-lined stainless-steel autoclave and the system was kept in the oven at 100 ºC for 24 hours. The solid was then dried and calcined under air flow at 350 ºC (1 ºC/min) for 5 hours. Lastly, the Cu/ZrO_2 catalyst was prepared by the HDP method and calcined as described previously. The synthesized Cu/SiO_2, $Cu\text{-}yZrO_2/SiO_2$ and Cu/ZrO_2 catalysts are denoted as CS, C-yZS and CZ, respectively.

X-ray diffraction

X-Ray Diffraction analyses were performed with the synthesized supports and catalysts in a Miniflex 600 diffractometer (Rigaku) using CuKα radiation with $2\theta = 10 - 70^o$ (0.07 step). Samples were characterized after calcination and after the catalytic tests.

Catalytic tests

The catalytic activity was measured at industrially relevant conditions in a FlowCat (H.E.L.) reaction system. Firstly 400 mg of catalyst were loaded in a stainless-steel tubular reactor (i.d. = 12 mm), reduced under pure H_2 flow (25 $mL.min^{-1}$) for 1 hour at 300 ºC, then cooled to 225

ºC for the reaction. The flow was then switched to a $H_2/CO_2/N_2$ (27/9/4 mL.min^{-1}) commercial mixture (White Martins) to purge remaining H_2 in the system, N_2 was used as internal standard. The reactor was pressurized to 30 bar and kept at this condition for 8 hours to ensure steady state. Products were analyzed by on-line Gas Chromatography (GC Agilent 8860) equipped with Flame Ionization and Thermal Conductivity Detectors (FID and TCD). CO_2 conversion, products selectivity and methanol Space-Time Yield (STY) were calculated with Equations 1, 2 and 3, respectively.

$$X_{CO2}(\%) = \frac{A^0_{CO2} - A_{CO2}\omega}{A^0_{CO2}}.100 \quad (1)$$

$$S_i(\%) = \frac{\beta_i}{\beta_{CO2}} \frac{A_i\omega}{(A^0_{CO2} - A_{CO2}\omega)}.100 \quad (2)$$

$$STY\ (g_{CH3OH}/kg_{cat}.h) = \frac{F_{CO2}X_{CO2}S_{CH3OH}}{m_{cat}} \quad (3)$$

Where A^0_{CO2} and A_{CO2} are the CO_2 GC areas before and during the reaction, respectively, $\omega = A^0_S/A_S$ is the ratio between the N_2 (internal standard) areas before and during the reaction, β_i is the internal standard calibration coefficient of compound i, A_i is the GC area obtained for product i (i = CO, CH_3OH and CH_4), F_{CO2} is the CO_2 reactant flow and m_{cat} the catalysts' mass used in the tests.

CH_3OH adsorption DRIFTS

The setup used in all Diffuse Reflectance Infrared Fourier Transform Spectroscopy (DRIFTS) experiments of the present work was the following: Nicolet iS50 FT-IR (Thermo Scientific) spectrometer, equipped with Praying Mantis optical system Harrick and High-temperature chamber (Harrick), dome with CaF_2 windows and liquid nitrogen-cooled Mercury-Cadmium-Telluride (MCT) detector. The gas switches were performed with a multiposition valve (Vici Valco, EMTMA-CE).

CH_3OH adsorption/desorption was monitored with DRIFTS. Initially, the mounted samples were reduced in situ under 75% H_2/Ar flow at 300 ºC for 1 hour, the system was then cooled to 200 ºC and background spectrum was collected. Subsequently, the samples were cooled to room temperature and CH_3OH vapor was introduced in the cell using a syringe and septum gas line. After purging the system at room temperature for 30 min with Ar, the reactor was heated to 200 ºC and spectrum was acquired with 4 cm^{-1} resolution and 64 scans.

In situ modulation excitation-phase sensitive detection-DRIFTS

The in situ modulation excitation measurements were performed employing the sample preparation method and optimized conditions discussed in Chapter II.

Prior to the experiments, the catalysts were reduced at the conditions described in the previous section. The system was cooled to 200 ºC and background spectrum was collected after a period of stabilization, the flow was then switched to H_2/CO_2/Ar (30/10/60 $mL.min^{-1}$) and spectra were acquired every minute with 4 cm^{-1} resolution and 64 scans until steady state was reached. Afterwards, 24 modulation cycles were carried out by periodically switching the flow from H_2/CO_2/Ar to Ar/CO_2/Ar every 50 s (full cycle period T = 100 s), keeping the total flow constant to avoid baseline shifts, while spectra were rapidly collected in series mode with 16 scans per spectrum.

The phase sensitive detection data processing is briefly described by Equation 4. For each wavenumber, the time-dependent signal I(t) was projected onto a reference sine wave with the modulation frequency ($\omega_{mod} = 2\pi/T$), filtering out static signals. The noise was minimized by averaging N valid cycles.

$$I_{PSD}(\phi_{PSD}) = \frac{2}{T}\sum_{n=1}^{N}\left[\int_{0}^{T} I(t)\cdot \sin(\omega_{mod}t + \phi_{PSD})\,dt\right] \quad (4)$$

The obtained filtered signal $I_{PSD}(\phi_{PSD})$ is in the phase domain, determined at discrete phase shifts ϕ_{PSD} (0 to 360º, 10º step), the angle is reported as ϕ_{PSD} = 360º - delay, so maximum intensity at higher angles denote faster formation rate [59].

RESULTS AND DISCUSSION

X-ray diffraction

To investigate the mechanism of CO_2 hydrogenation over Cu and ZrO_2 nanoparticles and the synergy between these species, the synthesis methods employed aimed at highly dispersed catalysts resistant to sintering at reaction conditions, with well-defined active sites and homogeneous structures. In this sense, X-ray diffraction (XRD) analysis gives basic information on the phases obtained after synthesis procedures and hints on the dispersion of nanoparticles on the supports.

The X-ray diffractograms obtained for the prepared supports and catalysts after calcination and after the catalytic tests are presented in Figures 1a and 1b, respectively. For the SiO_2 support only a broad peak was observed at 22.3º, indicative of an amorphous material with no defined lattice structure [63-65]. No Cu diffraction lines were detected for any SiO_2-supported catalyst, showing the HDP synthesis procedure was effective in the formation of highly dispersed nanoparticles, with crystallite diameter below the XRD detection limit (~3 nm). The diffractograms of the C-ZS catalysts also indicate highly dispersed ZrO_2 over the SiO_2 matrix and suggest the formation of amorphous ZrO_2 [67], as a broad signal appeared at 30.9º and intensified with Zr loading, becoming prominent at 20% (C-20ZS).

For a more direct comparison between the C-ZS and CZ systems, we attempted to synthesize an amorphous ZrO_2 support with the assistance of a surfactant [66,67], thus avoiding effects of crystalline phases [68] and increasing the oxide surface area. The characteristic broad signal at 30.9º shows the material is predominantly amorphous, apart from a small diffraction line at 50.6º which could be attributed to tetragonal (200) planes [40]. The CZ catalyst diffractogram presented small features at 35.6 and 38.8º, assigned to monoclinic CuO (ICDD 01-080-0076), indicating larger Cu crystallites on the ZrO_2 structure, likely due to the lower surface area of this support in comparison to SiO_2.

Regarding the post-reaction samples (Fig. 1b), the diffractograms of the CS and C-ZS catalysts with Zr loading up to 5% presented a small bump at 36.8º, previously attributed to Cu_2O [62]. In all samples except CS, short broad signals at 43.3º and 50.5º were detected and assigned to the (111) and (211) planes of cubic Cu^0 (ICDD 01-089-2838), respectively. The lines became

more apparent in the CZ profile, plausibly a result of sintering during reduction. It may be also inferred that ZrO_2 facilitates complete copper reduction, evidenced by the disappearance of the Cu_2O line in the C-20ZS and CZ catalysts diffractograms [28, 69].

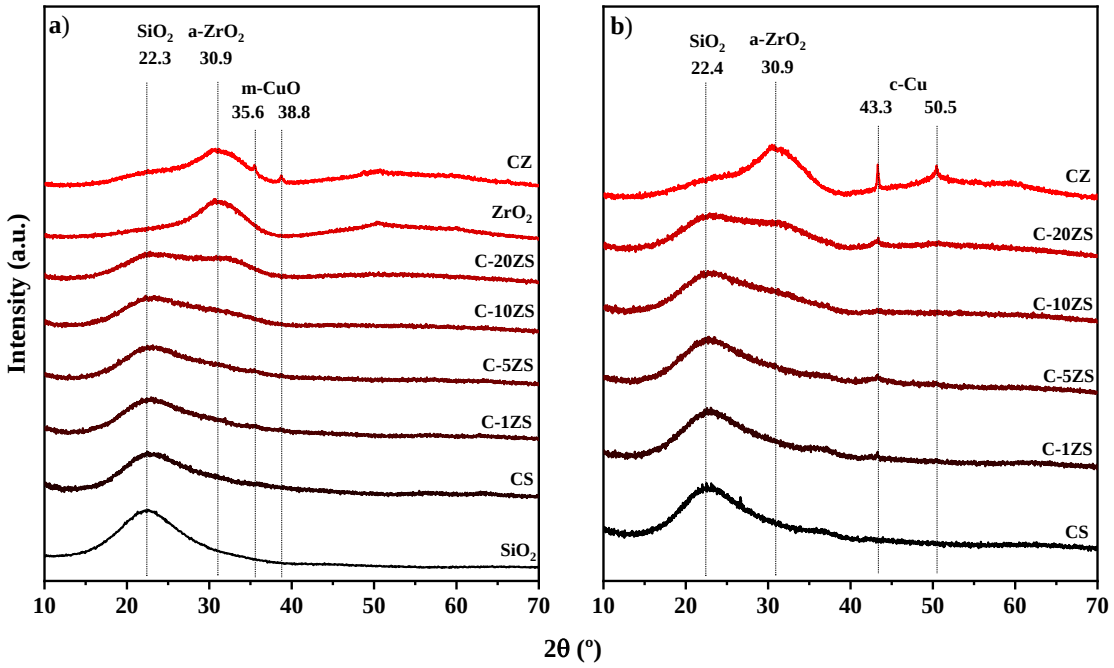

Figure 1. X-Ray Diffractograms obtained for the **a)** supports and catalysts after calcination and **b)** after catalytic test.

Overall, the XRD results envisage monoclinic CuO and amorphous ZrO_2 nanoparticles highly dispersed on the SiO_2 matrix, while larger ones formed on the ZrO_2 support. The nanoparticles were relatively resistant to sintering during reduction, as suggested by the absence of intense and sharp Bragg reflections on the post-reaction samples diffractograms. Moreover, it is likely that Cu^0 and Cu^+ species coexist after reduction especially on the C-ZS catalysts with Zr loading up to 5%, with ZrO_2 promoting CuO reduction to Cu^0 [70]. Nevertheless, partial oxidation of Cu^0 due to exposition to atmosphere during sample preparation cannot be discarded.

Catalytic activity

The synthesized catalysts were evaluated in the CH_3OH production from CO_2 hydrogenation at relevant industrial conditions (225 ºC and 30 bar), the results obtained at steady state are presented in Figure 2 in terms of CO_2 conversion (blue line), CH_3OH and CO selectivities (red and gray bars, respectively) and CH_3OH space time yield (STY) (green line). Only trace amounts of CH_4 and CH_3OCH_3 were detected in all experiments and therefore were disregarded.

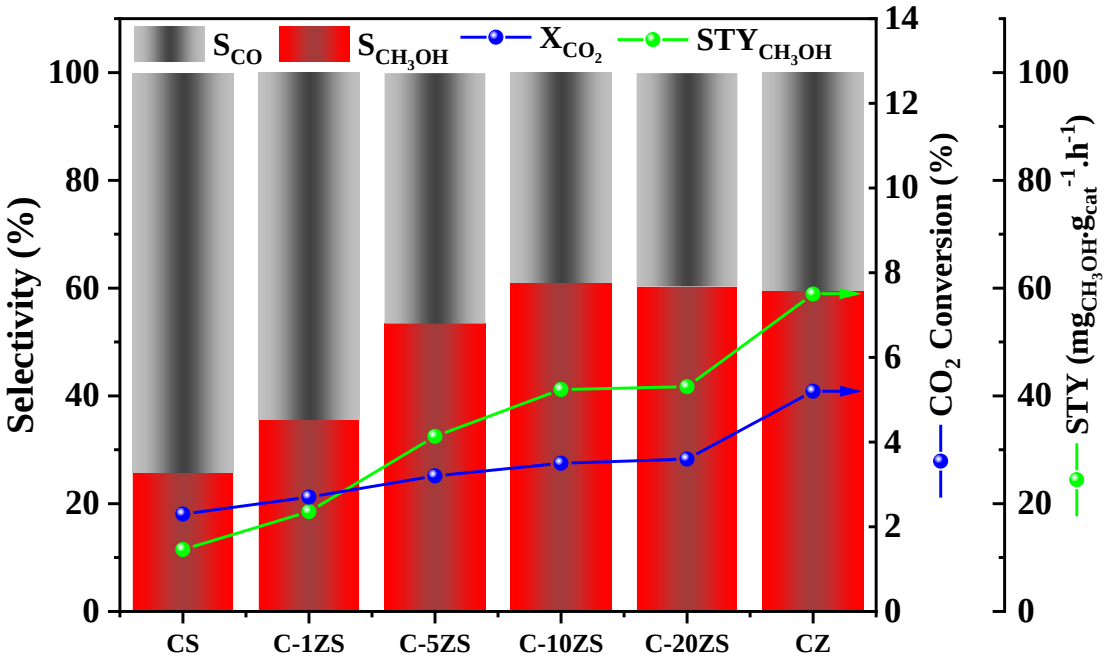

Figure 2. Steady state catalytic activity tests results. Product selectivity (CO: gray bar, CH_3OH: red bar), CO_2 conversion (green line) and CH_3OH STY (red line) obtained for the catalysts at T = 225 ºC, P = 30 bar and GHSV = 6000 $mL.h^{-1}.g_{cat}^{-1}$.

CO_2 conversion was 2 – 3% for the CS and C-ZS catalysts and 5% for the CZ sample. The values are much lower than the equilibrium conversion at these conditions [71], so the data reflects the intrinsic catalytic activity and not the thermodynamic limitation. The low CH_3OH selectivity obtained with the Cu/SiO_2 catalyst (26%) was enhanced continuously with the incorporation of Zr loadings up to 10 wt%, reaching 60% for the C-10ZS sample. Further increasing loading did not

have an impact on products distribution. Methanol STY (green line) followed a similar trend, with the highest value obtained for the CZ catalyst (59 $g_{CH3OH}.kg_{cat}^{-1}.h^{-1}$) due to the higher CO_2 conversion observed for this sample.

The catalytic activity is in accordance with the XRD results (Fig. 1), as ZrO_2 appears to facilitate complete copper reduction and Cu^0 species have the role of activating H_2 [11,12]. The beneficial role of ZrO_2 promotion in CH_3OH production observed here is in agreement with several previous studies [23,24,41]. Despite the lack of further structure and surface characterization in the present work, previous studies on similar Cu/ZrO_2 catalyst attribute the activity enhancement mainly to the presence of basic sites for CO_2 adsorption [24,70] and synergistic effects caused by strong metal-support interaction, generating Cu nanoparticles close to oxygen vacancies [37,72] and $Cu\text{-}ZrO_2$ interfaces [43,45,69].

Even though these catalysts have been extensively characterized and investigated previously, there is still no consensus on key factors governing the reaction mechanism [23,45,49-51,55,56], which would be fundamental for further optimization of CH_3OH yields over $Cu\text{-}ZrO_2$ systems. In the following sections we addressed some of these topics.

CH_3OH adsorption DRIFTS

CH_3OH adsorption/desorption experiments were performed and monitored with DRIFTS to gain insight on the interaction of methanol with the supports and catalysts [73] and later facilitate band attributions of in situ tests. The spectra obtained after adsorption at room temperature followed by desorption at 200 ºC are presented in Figure 3. The 3900 – 3500 cm^{-1} region (Fig. 3a) shows CH_3OH binds to hydroxyls when adsorbed on the ZrO_2 support and CZ catalyst, the negative signals at 3765/3744 and 3685 cm^{-1} were attributed to terminal (t-OH) and bridged (b-OH) hydroxyls of ZrO_2 [74-76], respectively. Conversely, no hydroxyl bands were observed on the spectra of the SiO_2 and CS samples, even though it is likely that silanol (Si-OH) groups are present in the support structure.

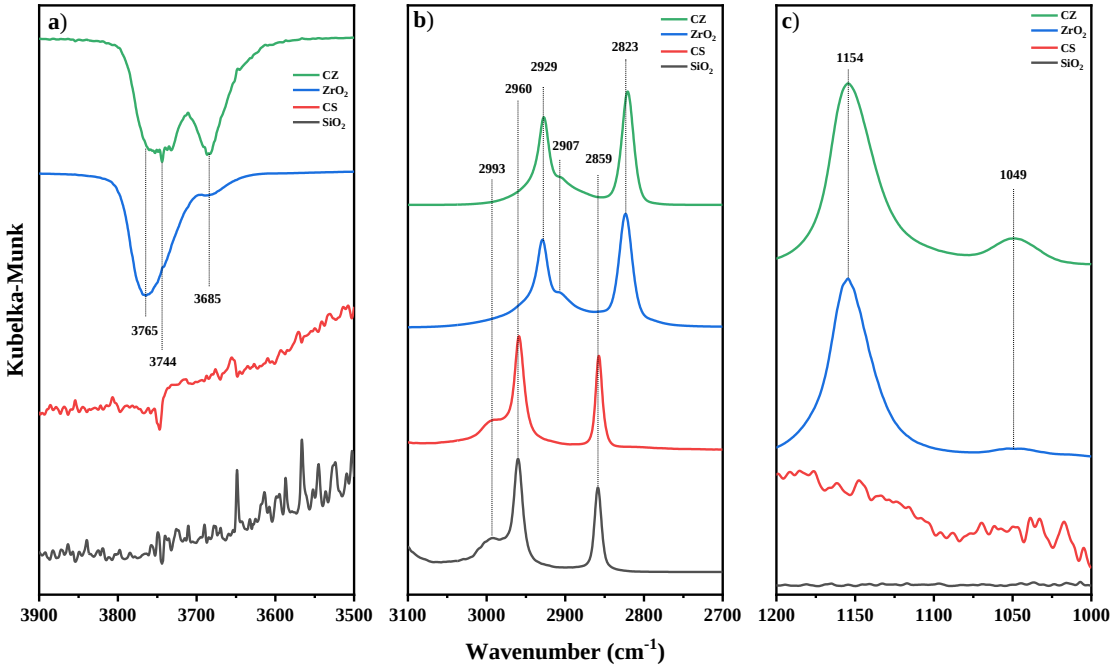

Figure 3. DRIFT spectra obtained after CH_3OH desorption at 200 ºC of the samples SiO_2, ZrO_2, CS and CZ in the regions **a)** 3900 – 3500, **b)** 3100 – 2700 and **c)** 1200 – 1000 cm^{-1}. The signals were normalized at each region of the spectrum.

In the C-H and C-O stretching regions (Figs. 3a and 3b, respectively) adsorbed methoxy signals were observed at 2993/2960/2859 cm^{-1} and 2929/2907/2823/1154 cm^{-1} for the SiO_2 and ZrO_2 samples, respectively. The band at 1049 cm^{-1} has been previously attributed to gas-phase methanol [49,51] but also to methoxy species [45,50]. The supports and corresponding catalysts presented very similar spectra, suggesting methoxy either does not bind to Cu or the surface species are short-lived [53], therefore the bands were attributed to methoxy bound to the oxides (CH_3O-Si and CH_3O-Zr) [45,50-53,73].

Reaction mechanism investigation with in situ ME-PSD-DRIFTS

To help elucidate the ongoing debate regarding active surface species during CO_2 hydrogenation over Cu/ZrO_2 systems, the reaction mechanism over the synthesized catalysts was studied with ME-PSD-DRIFTS, which allows distinguishing intermediates from spectators and

provides information on the relative kinetics of surface species. Given the ambient pressure limitation of the setup available at the time of research, the tests were carried out at 200 ºC, as it was recently reported with ME-PSD that lowering temperature has an effect similar to increasing pressure on the reaction mechanism [49], so the data can be better related to the catalytic tests results at high pressure and 225 ºC. The modulation cycles were performed after the reaction reached steady state during in situ DRIFTS experiments, which took approximately 90 - 120 min depending on the sample. The obtained spectra are presented in Figures 4 to 10, the top and bottom panels exhibit the steady state and ME-PSD spectra, respectively.

ZrO_2-promoted Cu/SiO_2 catalysts

Initially the CS catalyst was evaluated as control data (Fig. 4), which was fundamental in this case to identify Cu-bound species, as the signals may overlap with CH_3O-Zr species in the C-H stretching region when studying Cu/ZrO_2 systems [45,52,53]. The bands detected at 2930, 2852, 1540 and 1350 cm^{-1} during steady state and confirmed as active species with ME-PSD were all attributed to HCOO-Cu [50-53]. Regarding the ZrO_2 promoted Cu/SiO_2 catalysts, the results obtained for the samples containing 1 and 10% were very similar to the systems with 5 (Fig. 5) and 20% (Fig. 6) Zr loading, respectively, hence only the latter are presented and discussed. Apart from the previously assigned HCOO-Cu signals, the spectra exhibited bands at 2983, 2895, 1581, 1388 and 1372 cm^{-1} ascribed to active HCOO-Zr (Figs. 5c and 5d) [23,45,50,52]. Additionally, the steady state in situ DRIFTS spectra obtained with the C-20ZS catalyst (Fig. 6a) presented shoulders at 2944 and 2834 cm^{-1}, possibly related to methoxy species [52,53], however these were filtered out by PSD (Fig. 6c).

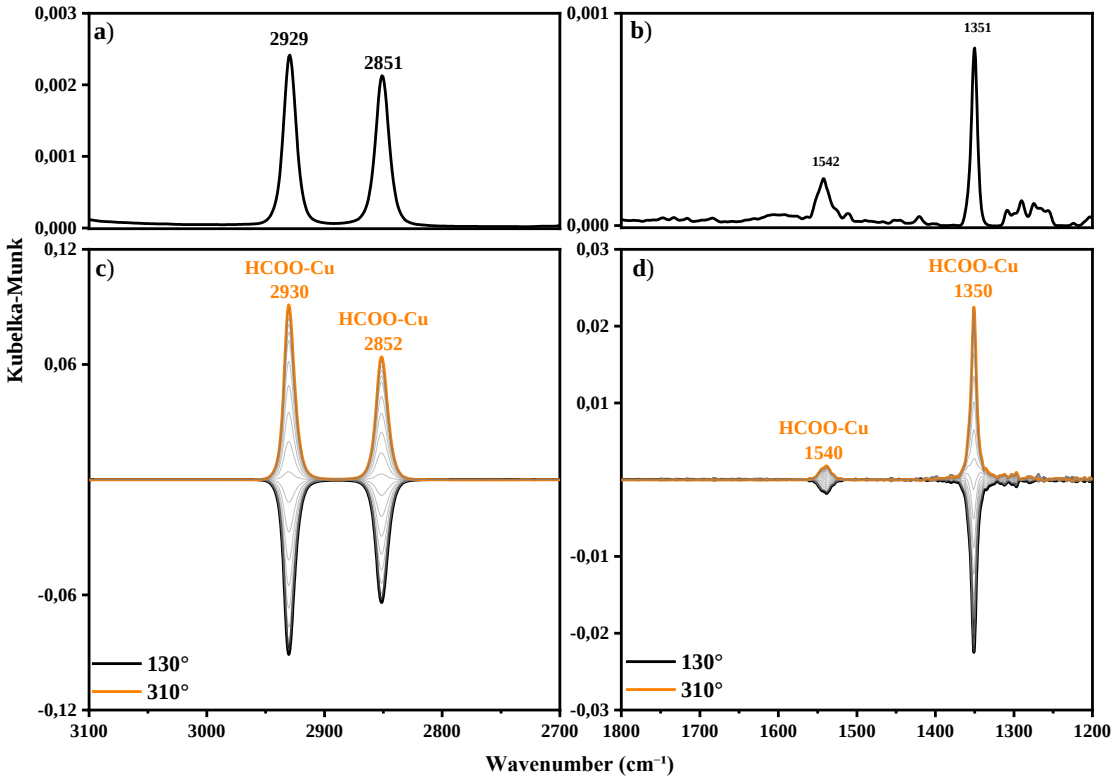

Figure 4. a,b) In situ DRIFT spectrum obtained at steady state CO_2 hydrogenation and **c,d)** Phase resolved spectra obtained from the ME-PSD experiments for the CS catalyst at 200 ºC. The highlighted angles denote the maximum and minimum intensity of the signals. Regions: 3100 – 2700 cm^{-1} (a,c) and 1800 – 1200 cm^{-1} (b,d).

Considering the dissociative $H_{2(g)}$ adsorption mechanism on Cu [11,12], the results obtained for the CS and C-ZS samples envisage CO_2 reacting with hydrogen generating distinct formate species on Cu and ZrO_2 even at low Zr loadings. The absence of active carbonates and bicarbonates indicates CO_2 reacts directly with adsorbed H to form HCOO-Cu and HCOO-Zr, with signals intensity reaching maximum in the ranges 290 - 310º and 280 – 290º, respectively. The high angles observed denotes species rapidly forming on the Cu and ZrO_2 surfaces, likely by a fast Eley-Rideal mechanism (H-Cu + $CO_{2(g)}$ → HCOO-M; M = Cu or Zr) [77,78]. While small $CO_{(g)}$ signals were observed in the spectra of all catalysts, no gas phase methanol was detected with the CS and C-ZS samples and surface methoxy species signals were only barely present at 20% Zr loading (Fig. 6a), but appears to be a spectator at these conditions (Fig. 6c). Hence, we

can conclude increasing H_2 pressure is required to continue the methanol synthesis from the formate pathway, especially considering these catalysts showed low activity (2 - 3%) even during the catalytic tests (Fig. 2) at more favorable conditions. In any case the data is useful to identify and confirm the activity of the distinct formate species, understand CO production through the reverse water gas shift (RWGS) reaction and overall band assignment. In all cases active CO-Cu^+ and CO-Cu^0 were observed (Fig. 9) and will be thoroughly discussed soon, for now it is worth noticing these species are rapidly formed on the Cu and Cu_2O sites detected by XRD (Fig. 1).

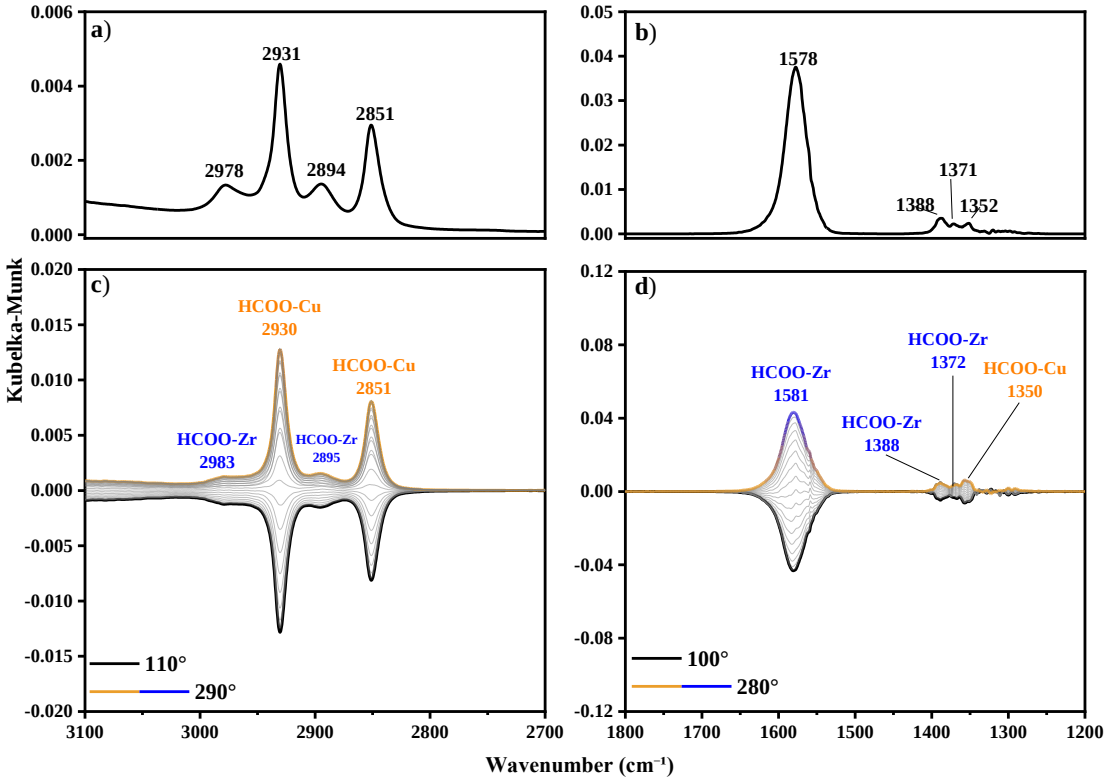

Figure 5. a,b) In situ DRIFT spectrum obtained at steady state CO_2 hydrogenation and **c,d)** Phase resolved spectra obtained from the ME-PSD experiments for the C-5ZS catalyst at 200 ºC. The highlighted angles denote the maximum and minimum intensity of the signals. Regions: 3100 – 2700 cm^{-1} (a,c) and 1800 – 1200 cm^{-1} (b,d).

Having observed the Cu-bound CO and formate species are active on the CS catalyst, one possibility is HCOO-Cu decomposing with nearby adsorbed hydrogen to produce $CO_{(g)}$ via a CO-Cu intermediate (HCOO-Cu + H-Cu → CO-Cu + $H_2O_{(g)}$ + Cu; CO-Cu → $CO_{(g)}$ + Cu), which would be favored at lower pressure. Another possibility is the direct CO_2 dissociation pathway on Cu^0 sites ($CO_{2(g)}$ + Cu^0 → CO-Cu^+) [57]. Given the two fast CO-Cu^x modulating species during CO_2 hydrogenation over the CS sample, it is plausible both routes coexist.

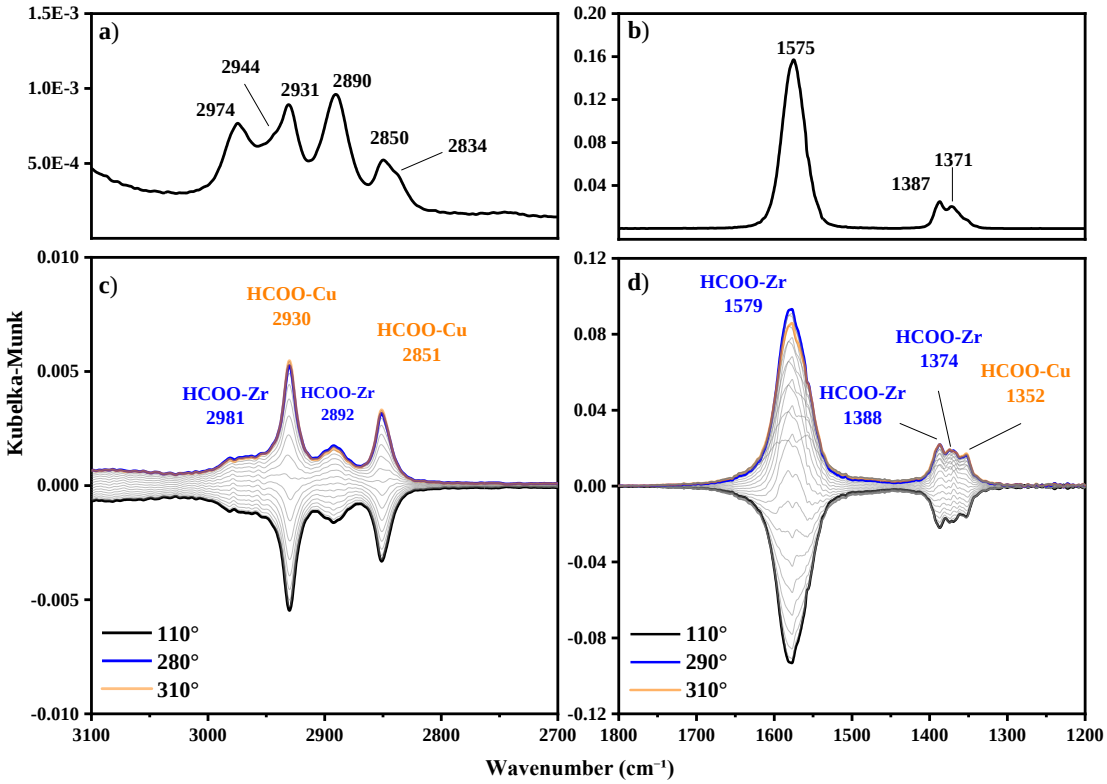

Figure 6. a,b) In situ DRIFT spectrum obtained at steady state CO_2 hydrogenation and **c,d)** Phase resolved spectra obtained from the ME-PSD experiments for the C-20ZS catalyst at 200ºC. The highlighted angles denote the maximum and minimum intensity of the signals. Regions: 3100 – 2700 cm^{-1} (a,c) and 1800 – 1200 cm^{-1} (b,d).

The HCOO-Zr observed for the ZrO_2-promoted samples is often a major point of controversy in previous studies regarding methanol synthesis over Cu/ZrO_2 catalysts. While

frequently observed during steady state in situ infrared spectroscopy, the actual participation of this surface species on the mechanism is debatable [23,45,50,51]. Here we demonstrated its activity over the ZrO_2 promoted catalysts with ME-PSD, but the lack of active methoxy signals still leaves doubts regarding its role on the formate pathway leading to methanol. In the case of the C-ZS systems studied, HCOO-Zr is either converted to CO-Cu leading to $CO_{(g)}$, as discussed previously, or is in equilibrium with HCOO-Cu through spillover [11]. The possibility of CO being the actual source of formates [53] cannot be completely discarded with the current data, although it was evidenced previously with ME-PSD that CO does not participate in methanol synthesis over similar catalysts [49]. Moreover, the PSD analysis indicate HCOO-Cu has faster kinetics than HCOO-Zr, corroborating previous transient studies [50,52,55,56].

Cu/ZrO_2

The results obtained with the CZ catalyst are exhibited in Figures 7 and 8, the C-H and C-O stretching regions at steady state (Figs. 7a and 7b, respectively) presented similar behavior to the C-ZS samples, with intense HCOO-Zr and HCOO-Cu signals dominating the spectrum. The appearance of a shoulder at 1569 cm^{-1} denotes Zr-bound carbonate species [23,52,79]. Differently than the C-ZS samples, however, on other spectral regions (Figs. 8a and 8b) a CH_3O-Zr signal was detected at 1149 cm^{-1} and negative t-OH-Zr and b-OH-Zr bands at 3757 and 3715 cm^{-1} [74-76], respectively, denoting interaction of CH_3OH with hydroxyl groups of ZrO_2, as observed in the adsorption/desorption DRIFTS experiments (Fig. 3). The production of CH_3OH exclusively over the CZ is in line with the catalytic activity observed with this sample (Fig. 2), which despite being marginally higher than the C-ZS systems (5% CO_2 conversion), in this case it was sufficient to produce methoxy and methanol at the employed conditions. While similar in situ DRIFTS data was reported across several studies on Cu/ZrO_2 and inverse ZrO_2/Cu catalysts, the interpretations vary significantly. The CH_3OH synthesis activity was previously attributed to the formate pathway [28,50-52], the RWGS + CO hydrogenation [45] or combination of both [23]. On the other hand, even studies that agree on the formate pathway as the main route have no consensus on the nature of the actual HCOO species intermediate [28,47,50,55,56,].

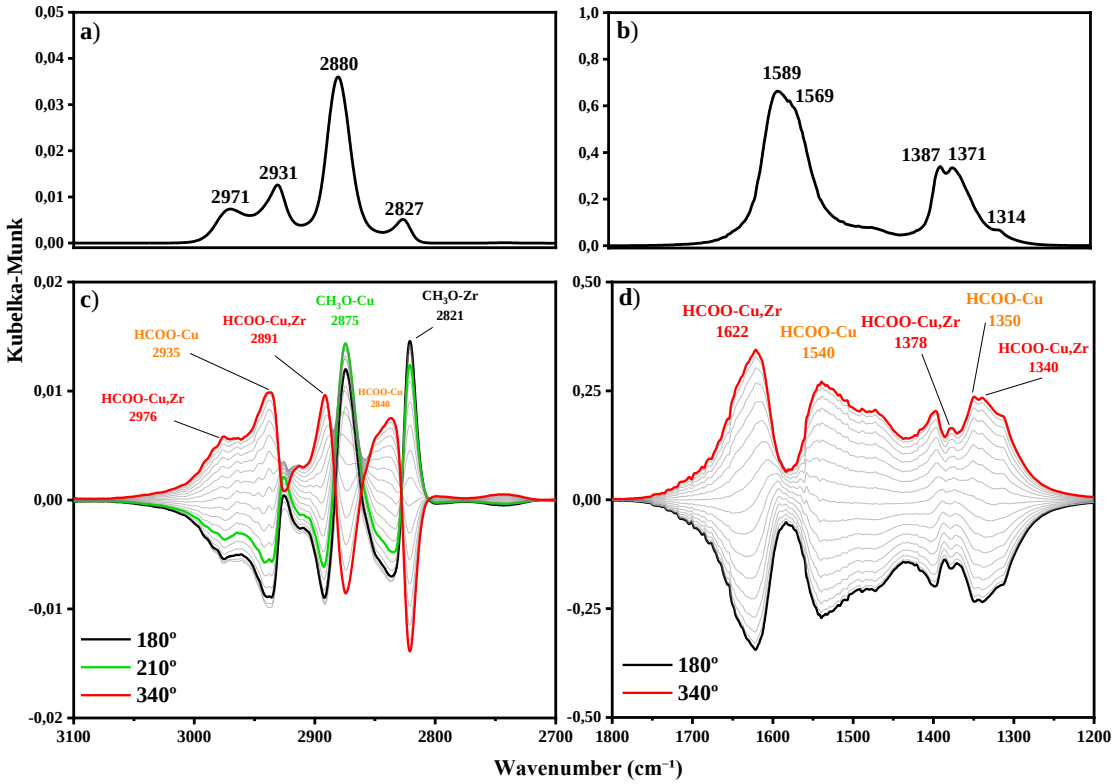

Figure 7. a,b) In situ DRIFT spectrum obtained at steady state CO_2 hydrogenation and **c,d)** Phase resolved spectra obtained from the ME-PSD experiments for the CZ catalyst at 200 ºC. The highlighted angles denote the maximum intensity of the signals. Regions: 3100 – 2700 cm^{-1} (a,c) and 1800 – 1200 cm^{-1} (b,d).

The bottom panels of Figures 7 and 8 depict the ME-PSD spectra obtained for the CZ catalyst. The analysis revealed several modulating signals at the C-H and C-O stretching regions (Figs. 7c and 7d, respectively), the interplay between the active species resulted in complex spectra, including bands reaching maximum intensities at different phase angles. By carefully examining the phase resolved spectra, it was noted the fast active HCOO-Cu species with signals at 2935, 2840, 1540 and 1350 cm^{-1}, similarly to the CS and C-ZS catalysts (Figs. 5 and 6). Conversely, despite being active on the C-ZS samples, in this case the HCOO-Zr species is a spectator, as can be clearly observed by the absence of the intense steady state 1589 cm^{-1} band in the phase resolved spectra. Interestingly, new modulating signals were resolved at 2976, 2891, 1622, 1378 and 1340 cm^{-1} denoting the appearance of a fast-forming active species (peak

maximum at 340º) specifically on the CZ system. The arguments for the attribution of this intermediate will be presented shortly. The spectra also presented active bands related to CH_3O-Zr at 2821 and 1152 [28,45,50], CH_3O-Cu at 2875 [53], $CH_3OH_{(g)}$ at 1036 [49] and t-OH-Zr at 3766 cm^{-1} [74,75]. The hydroxyl region (3900 – 3500 cm^{-1}) of the CS and C-ZS catalysts only presented the $CO_{2(g)}$ overtone bands.

It was recently reported evidence for the coexistence of three distinct formate species over Cu/ZrO_2 catalysts by means of quantitative analysis of the decaying rate of the signals during transient DRIFTS experiments [55,56], it was proposed HCOO-Cu as the main intermediate, while two Zr-bound formate species contribute less to methanol production. In fact, CH_3OH selectivity is often ascribed to HCOO-Cu in previous studies [20,50,52]. In this sense the present data corroborates the fast activity of the Cu-bound species and HCOO-Zr being a spectator [45], not contributing in the formate pathway leading to CH_3OH over the CZ sample. On the other hand, the new active signals observed in the C-H and C-O stretching regions (Figs. 7c and 7d) appear to be as important to the mechanism as HCOO-Cu, denoted by the high phase angle of the signals (340º), indicating rapidly forming surface species.

The bands at 2976, 2891, 1378 and 1340 cm^{-1} correspond to a contribution of the C-H bending and O-C-O asymmetric stretching ($\delta(CH) + \nu_{as}(OCO)$), the C-H stretching ($\nu(CH)$), the $\delta(CH)$ and the symmetric O-C-O ($\nu_s(OCO)$) vibration modes, respectively, of formate species, usually attributed to bidentate HCOO-Zr. Given HCOO-Zr in this case is not present in the phase resolved spectra and the HCOO-Cu signals are well stablished here supported by the presented data and literature, Figs. 7c and 7d point to the appearance of a third formate species. We propose this formate is located near the Cu-ZrO_2 interface, as envisaged previously [35,36,55,80,81] and denoted here as HCOO-Cu,Zr. The key for this assignment was the intense band observed in the C-O stretching region at 1622 cm^{-1} (Fig. 7d). While this signal was previously ascribed to Zr-bound bicarbonate (HCO_3-Zr) [52,82], the spectra obtained here lack other relevant bicarbonate bands and, most important, its assignment would not explain the 2976 and 2891 cm^{-1} modulating signals, as this species do not possess C-H stretching vibration modes. Hence it is more plausible the 1622 cm^{-1} signal correspond to the $\nu_{as}(OCO)$ mode of formates.

In this context a good candidate for assigning these bands was monodentate Zr-bound formate (m-HCOO) [37], which would be aligned with recently published ME-PSD-DRIFTS data

showing active Al_2O_3-bound m-HCOO species on the $Cu/ZnO/Al_2O_3$ catalyst [20]. It could be argued the 2957 and 2845 cm^{-1} m-HCOO-Zr signals are present in the C-H stretching region (Fig. 7c), given the poor resolution specially between 2930 and 3000 cm^{-1}, likely due to the presence of $CH_3OH_{(g)}$ [83]. However, the ν_{as}(OCO) mode band at 1622 cm^{-1} (Fig. 7d) is severely red-shifted in relation to what was previously reported for m-HCOO-Zr (1663 cm^{-1}) [37]. Additionally, the two bands at 1378 and 1340 cm^{-1} are characteristic of the δ(CH) and ν_s(OCO) vibration modes of bidentate formate species. Furthermore, the splitting peak position value between the asymmetric and symmetric stretching modes ($\Delta\nu = \nu_{as} - \nu_s$) is 282 cm^{-1}, which is in the inferior and superior limits for monodentate and bridging formate, respectively [80]. Hence, the data suggests the interfacial HCOO-Cu,Zr species produces infrared signals similar to bidentate HCOO-Zr with the exception of the ν_{as}(OCO) mode, which is strongly red-shifted due to the perturbation caused by close proximity with Cu nanoparticles, indicating this vibration mode behaves similar to monodentate species.

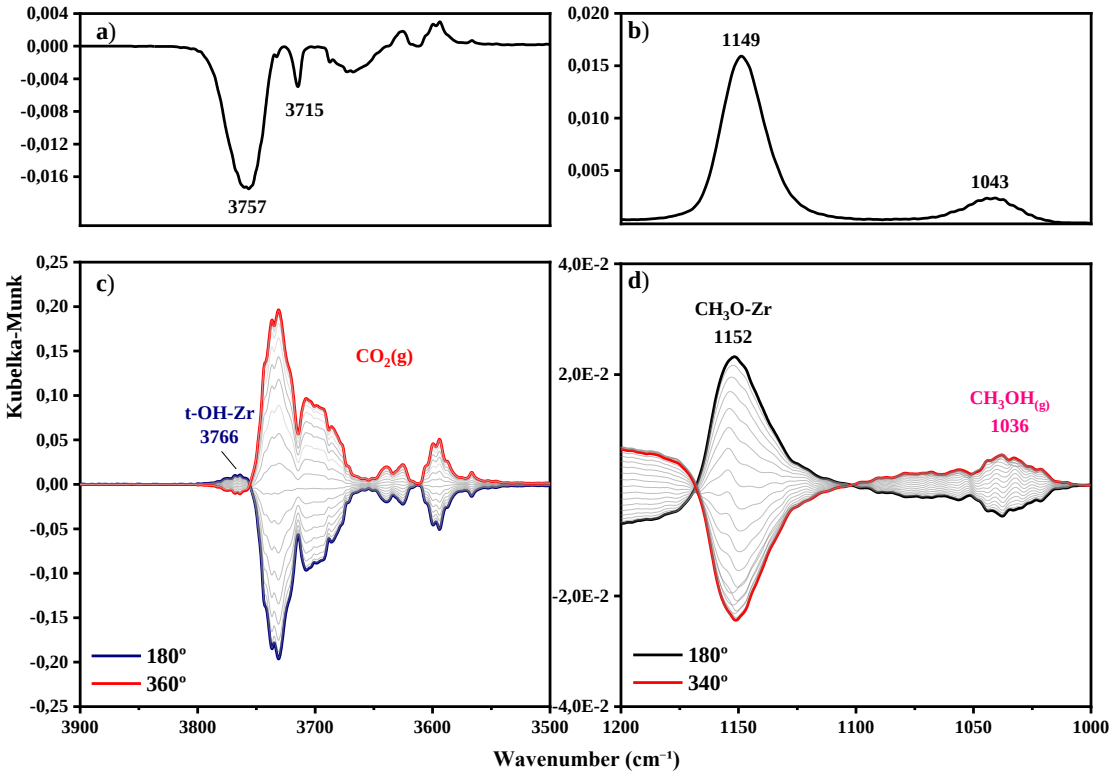

Figure 8. a,b) In situ DRIFT spectrum obtained at steady state CO_2 hydrogenation and **c,d)** Phase resolved spectra obtained from the ME-PSD experiments for the CZ catalyst at 200 ºC. The highlighted angles denote the maximum and minimum intensity of the signals. Regions: 3900 – 3500 cm^{-1} (a,c) and 1200 – 1000 cm^{-1} (b,d).

The ME-PSD spectra obtained with the CZ catalyst (Figs. 7 and 8) also revealed the presence of two distinct methoxy intermediates, CH_3O-Zr (2821 and 1152 cm^{-1}) and CH_3O-Cu (2875 cm^{-1}), the latter was rarely observed previously with conventional in situ DRIFTS [53]. Distinguishing these species was possible due to band position and the phase lag between the signals (210º – 180º = 30º), indicating the production of CH_3O-Cu is faster than the Zr-bound counterpart. The dynamics denoted by the phase angles indicate the formation of HCOO-Cu and HCOO-Cu,Zr is fast (340º) while their hydrogenation to CH_3O-Cu and CH_3O-Zr is much slower (180 and 210º, respectively), being a rate-controlling step in the overall mechanism. It is unclear with the present data whether the formates observed are reduced to specific methoxy or to either species.

Regarding the final step of the pathway, methanol production from methoxy, the region exhibited in Figure 8d presented a fast-forming $CH_3OH_{(g)}$ signal at 1036 cm^{-1} (340º), which could be clearly differentiated from CH_3O-Zr in this case as the species are out of phase. On the other hand, the spectra also showed slow-forming t-OH-Zr at 3766 cm^{-1} (180º), only observed on the CZ spectra (Fig. 8c), likely involved in the interaction of methanol with the support as observed in the CH_3OH adsorption/desorption DRIFT spectra (Fig. 3). Other hydroxyl species are either spectators or the signals are overwhelmed by the intense $CO_{2(g)}$ overtone bands (Fig. 8c). The conversion of methoxy to methanol and its velocity is also a matter of controversy in previous research. While some studies found methoxy species are hydrolyzed to $CH_3OH_{(g)}$ with water generated in the RWGS reaction pathway [49,52], others propose its hydrogenation by adsorbed hydrogen [50,57,84]. Given the distinct CH_3O-Zr and CH_3O-Cu observed here and the coexistence of slow-forming hydroxyls and fast-forming $CH_3OH_{(g)}$, it is more plausible CH_3O-Cu is rapidly reduced by nearby adsorbed H on the copper surface, while CH_3O-Zr is stabilized on t-OH-Zr sites and slowly hydrolyzed to CH_3OH, being another rate-controlling step. The proposed routes are described by Equations 5 and 6.

$$CH_3O\text{-}Cu + H\text{-}Cu \rightarrow CH_3OH_{(g)} + 2Cu \quad (5)$$

$$CH_3O\text{-}Zr + H_2O_{(g)} \rightarrow CH_3OH_{(g)} + t\text{-}OH\text{-}Zr \quad (6)$$

It may be inferred from the data that a short distance between Cu and ZrO_2 was obtained when employing the HDP synthesis method, generating active Cu-ZrO_2 interfacial sites on the CZ catalyst due to strong metal-support interaction [42]. Conversely, the impregnation of ZrO_2 on the CS samples performed without tailoring the support [41], despite achieving high dispersion, may have resulted in ZrO_2 motifs far away from the Cu surface, promoting the formation of HCOO-Zr in detriment of interfacial HCOO-Cu,Zr. Nonetheless, while the results indicate HCOO-Zr is active on the C-ZS catalysts (Figs. 5 and 6), on CZ bulk ZrO_2 appears to stabilize this species [45,85], rendering it a spectator behavior. These findings reflect the CH_3OH selectivity limitation encountered with the synthesized catalysts (Fig. 2), as switching from highly dispersed to bulk ZrO_2 presented the tradeoff of forming active HCOO-Cu,Zr but inhibiting the hydrogenation of HCOO-Zr, which was observed to be active on the C-ZS catalysts. The presence of terminal hydroxyl groups on the support had a role of stabilizing CH_3O-Zr, which is hydrolyzed to $CH_3OH_{(g)}$ slower than the reduction of CH_3O-Cu by adsorbed hydrogen, which may not be the case with dispersed ZrO_2 nanoparticles. To confirm these hypotheses, future studies should perform ME-PSD experiments at higher pressures to investigate the fate of the Zr-bound formate species and interaction of methoxy with hydroxyls on the C-ZS systems at more favorable conditions for methanol production.

CO region

Lastly, we analyze the CO region (2200 – 2000 cm^{-1}) of the spectra obtained with the synthesized catalysts, exhibited in Figure 9. The CS catalyst (Fig. 9a) presented an intense CO-Cu^+ signal at 2130 cm^{-1} [53, 86] at steady state. The ZrO_2 promotion resulted in the appearance of a signal at 2077 cm^{-1} (Figs. 9b-d) attributed to CO bound to metallic Cu(111) [87,88], consistent with the XRD data of post-reaction samples (Fig. 1b). The Cu^+-bound CO signal was not observed

in the C-20ZS and CZ spectra (Figs. 9e,f). Nonetheless, the steady state spectra are significantly distorted due to $CO_{(g)}$ signals, especially for the samples with Zr loading of 10 wt% or more, so more relevant information could only be obtained with ME-PSD-DRIFTS (Figs. 9g-l). On the CS sample the signal of both species peaked at 340º, denoting fast-forming Cu^{+} and Cu^{0}-bound CO. The progressive incorporation of ZrO_2 generated CO species bound to step defects Cu(211) sites (2094 cm^{-1}) [87], lowered the relative band intensity CO-Cu^{+}/CO-Cu^{0} and inhibited the formation of CO-Cu^{+} species, denoted by the phase shift from 350º to 320º for the C-1ZS (Fig. 9h) and C-20ZS (Fig. 9k) catalysts, respectively, disappearing completely on the CZ spectra (Fig. 9l). Conversely, ZrO_2 promoted the fast Cu^{0}-bound CO formation (350 – 360º), with signals becoming dominant with increasing Zr loading.

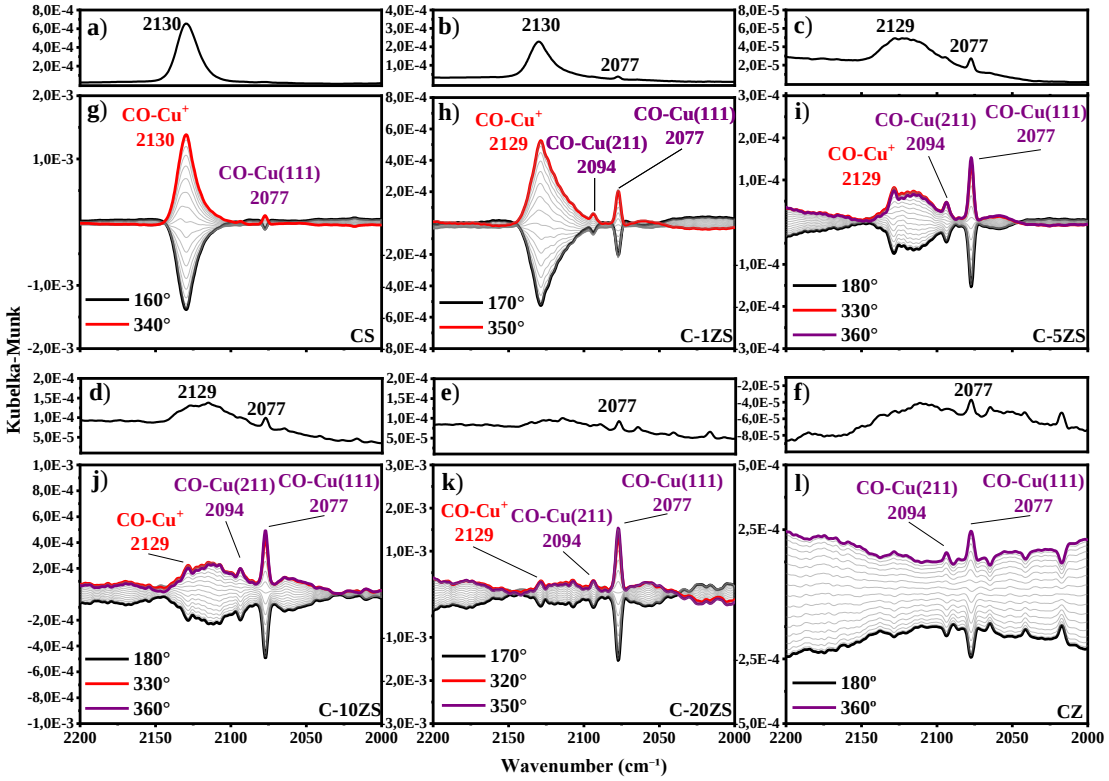

Figure 9. a,b,c – d,e,f) In situ DRIFT spectrum obtained at steady state CO_2 hydrogenation and **g,h,i – j,k,l)** Phase resolved spectra obtained from the ME-PSD experiments for the catalysts **(a,g)** CS; **(b,h)** C-1ZS; **(c,i)** C-5ZS; **(d,j)** C-10ZS; **(e,k)** C-20ZS and **(f,l)** CZ at 200 ºC in the 2200 –

2000 cm^{-1} region. The highlighted angles denote the maximum and minimum intensity of the signals.

The fast-forming adsorbed CO species indicate $CO_{(g)}$ is produced through direct CO_2 dissociation [57] on both Cu^+ and Cu^0 sites. With the data it was possible to observe the effect of ZrO_2 in the oxidation state of copper during the reaction [24,28,70], the progressive lowering of the relative $CO\text{-}Cu^+/CO\text{-}Cu^0$ intensity shows Zr facilitates further reduction of Cu_2O species to metallic Cu [70] and generates step defects. Inhibiting the formation of $CO\text{-}Cu^+$ species effectively lowered CO selectivity obtained with the C-ZS catalysts with Zr loading up to 10% (Fig. 2). Further increasing Zr content did not present this effect due to the fast CO-Cu species observed, with maximum intensity at 350 – 360º indicating almost instantaneous CO_2 dissociation on metallic sites leading to a minimum CO selectivity of 39%, highlighting the challenge of inhibiting the RWGS pathway.

Contrary to what previously proposed [23,45,54], no signals attributable to carboxyl species were observed in any spectra presented here, so the results indicate the RWGS reaction proceeds through direct CO_2 dissociation or formate decomposition to CO [57]. Methanol production over the CZ catalyst through the RWGS reaction followed by CO hydrogenation was not observed at the conditions studied, with the formate pathway being the main route even though Zr-bound formate species are in fact spectators [45]. While the observations for CZ are in agreement with recently reported ME-PSD data at high pressure [49], the ambient pressure limitation still leaves doubts if methanol synthesis via the RWGS and CO hydrogenation route is relevant on the C-ZS systems. It is worth noticing, however, that performing the experiments at low pressure may have facilitated band resolution and clarification of the dynamics of specific surface species, indicating a moderate pressure may be useful to obtain such responses while better reflecting the catalytic activity at industrially relevant conditions.

A representation of the CO_2 hydrogenation mechanism envisioned here is depicted in Figure 10. The overall data gathered in this work reveal key information for deeper understanding of the mechanisms governing CO_2 hydrogenation over $Cu\text{-}ZrO_2$ catalytic systems, contributing to elucidate some controversial topics in state-of-the-art research. The results indicate three different kinds of formate being rapidly produced from CO_2, such species presented different behavior

across the catalysts investigated. HCOO-Cu was observed to be active in all cases and contributes to methanol production on the Cu/ZrO_2 catalyst, HCOO-Zr is active on the ZrO_2-promoted systems (although the exact fate of this species is still unclear on these samples) and a spectator on Cu/ZrO_2, likely due to bulk effects. We proposed HCOO-Cu,Zr located near the Cu-Zr interfaces of Cu/ZrO_2, with activity comparable to HCOO-Cu. At the operating conditions, the rate-controlling steps identified were formate hydrogenation to methoxy species (with CH_3O-Cu production faster than CH_3O-Zr) and slow hydrolysis of methoxy stabilized on terminal OH sites. The fast-forming gas phase methanol denotes the reduction of CH_3O-Cu with nearby adsorbed H is a more favorable route. The ME-PSD-DRIFTS analysis combined with catalytic activity data suggest ZrO_2 promotion can minimize CO_2 dissociation on Cu^+ sites, partially inhibiting the RWGS route, conversely it was demonstrated metallic Cu itself is also a major source of CO, in addition to the fundamental role of dissociating H_2 and generating important formate and methoxy species.

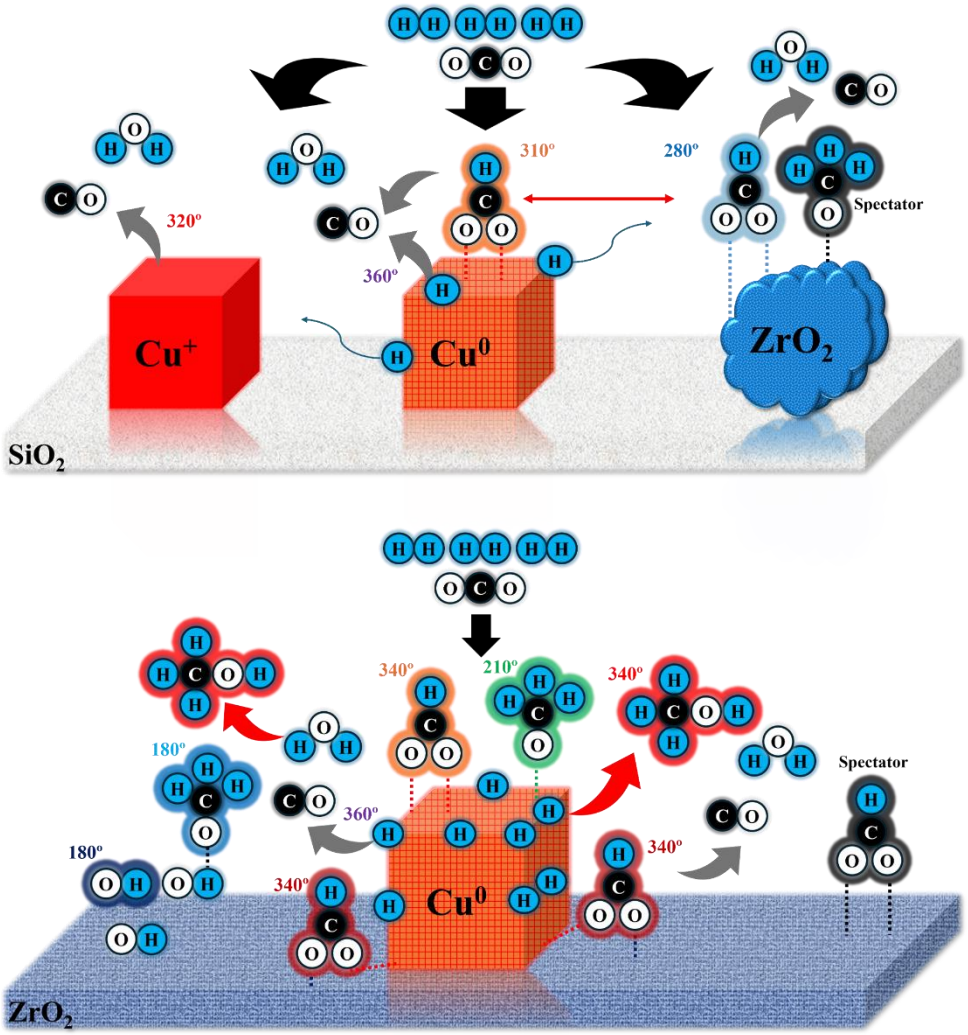

Figure 10. Proposed CO_2 hydrogenation mechanism over ZrO_2-promoted Cu/SiO_2 and Cu/ZrO_2 catalysts. The gray and red curved arrows represent the RWGS and methanol production through the formate pathway, respectively. Higher angles denote faster formation of surface species.

In practical methanol production terms, the Cu/ZrO_2 was the best catalyst among the studied samples, the effect was ascribed to the activity induced by interfacial sites. It is plausible the activity could be further enhanced by preparing catalysts containing high concentration of Cu-Zr interfaces and avoiding bulk ZrO_2 to unlock a possible Zr-bound formate route leading to methoxy and minimize its stabilization on terminal hydroxyl groups.

CONCLUSION

The mechanism of the CO_2 hydrogenation reaction over Zr-promoted Cu/SiO_2 and Cu/ZrO_2 catalysts was investigated with modulation excitation-phase sensitive-detection DRIFTS. The study demonstrates CO is produced through fast CO_2 dissociation on Cu^+ and Cu^0 surfaces. It was found CH_3OH synthesis follows the formate pathway, with no signs of the carboxyl intermediate. While CO_2 conversion to formate is fast, further hydrogenation is highly dependent on the binding site of formate species. The Zr-bound formate was active on the promoted catalyst, although its participation on the formate pathway remains unclear as no methanol was observed, but not on the Zr-supported system, while Cu-bound species was active in all cases. Our main findings show, for the first time experimentally, formate species located near the Cu-Zr interfaces of the Cu/ZrO_2 catalyst, observed here as an active species with kinetics similar to the Cu-bound counterparts in methanol synthesis. It was also demonstrated formate hydrogenation to methoxy followed by its hydrolysis to methanol are the slowest steps at the conditions employed, while a faster methoxy reduction route was detected on Cu surfaces. The data gathered deepens the understanding of the CO_2 hydrogenation reaction pathways over Cu-Zr systems and suggests further optimization of methanol synthesis may be achieved if interfacial sites are obtained in the catalysts while avoiding bulk ZrO_2 to possibly unlock the mechanism of Zr-bound formate species.

REFERENCES CHAPTER III

1. Morgan, Jamie. "Capitalism, climate catastrophe and commoning: Hosseini and Gills on theory of value and what matters now." Globalizations 21.8 (2024): 1610-1627.
2. Kweku, Darkwah Williams, et al. "Greenhouse effect: greenhouse gases and their impact on global warming." Journal of Scientific research and reports 17.6 (2018): 1-9.
3. Gills, Barry, and Jamie Morgan. "Global climate emergency: After COP24, climate science, urgency, and the threat to humanity." Economics and climate emergency. Routledge, 2022. 253-270.
4. Romero-García, Ana Gabriela, et al. "Sustainability assessment in the CO2 capture process: Multi-objective optimization." Chemical Engineering and Processing-Process Intensification 182 (2022): 109207.

5. Nejat, Payam, et al. "A global review of energy consumption, CO2 emissions and policy in the residential sector (with an overview of the top ten CO2 emitting countries)." Renewable and sustainable energy reviews 43 (2015): 843-862.
6. Álvarez, Andrea, et al. "Challenges in the greener production of formates/formic acid, methanol, and DME by heterogeneously catalyzed CO2 hydrogenation processes." *Chemical reviews* 117.14 (2017): 9804-9838.
7. Porosoff, Marc D., Binhang Yan, and Jingguang G. Chen. "Catalytic reduction of CO 2 by H 2 for synthesis of CO, methanol and hydrocarbons: challenges and opportunities." Energy & Environmental Science 9.1 (2016): 62-73.
8. Olah, George A., Alain Goeppert, and GK Surya Prakash. Beyond oil and gas: the methanol economy. John Wiley & Sons, 2018.
9. Tursunov, Obid, Leonid Kustov, and Aleksandr Kustov. "A brief review of carbon dioxide hydrogenation to methanol over copper and iron based catalysts." Oil & Gas Sciences and Technology–Revue d'IFP Energies nouvelles 72.5 (2017): 30.
10. Yuan, Yongning, et al. "A review on the development of catalysts and technologies of CO2 hydrogenation to produce methanol." Chemical Engineering Communications 210.10 (2023): 1791-1821.
11. Jung, Kwang-Deog, and Alexis T. Bell. "Role of hydrogen spillover in methanol synthesis over Cu/ZrO2." Journal of catalysis 193.2 (2000): 207-223.
12. Syzgantseva, Olga, Monica Calatayud, and Christian Minot. "Theoretical study of H2 dissociation on a ZrO2 cluster." Chemical Physics Letters 503.1-3 (2011): 12-17.
13. Schilke, Tobin C., Ian A. Fisher, and Alexis T. Bell. "In SituInfrared Study of Methanol Synthesis from CO2/H2on Titania and Zirconia Promoted Cu/SiO2." Journal of Catalysis 184.1 (1999): 144-156.
14. Millar, Graeme J., Colin H. Rochester, and Kenneth C. Waugh. "Infrared study of the adsorption of formic acid on silica-supported copper and oxidised copper catalysts." *Journal of the Chemical Society, Faraday Transactions* 87.9 (1991): 1491-1496.
15. Jurković, Damjan Lašič, et al. "Effect of copper-based catalyst support on reverse water-gas shift reaction (RWGS) activity for CO2 reduction." *Chemical Engineering & Technology* 40.5 (2017): 973-980.

16. Vanden Bussche, Kurt M., and Gilbert F. Froment. "A steady-state kinetic model for methanol synthesis and the water gas shift reaction on a commercial Cu/ZnO/Al2O3Catalyst." *Journal of catalysis* 161.1 (1996): 1-10.
17. Beck, Arik, et al. "The enigma of methanol synthesis by Cu/ZnO/Al2O3-based catalysts." Chemical Reviews 124.8 (2024): 4543-4678.
18. Behrens, Malte, et al. "The active site of methanol synthesis over Cu/ZnO/Al2O3 industrial catalysts." Science 336.6083 (2012): 893-897.
19. Beck, Arik, et al. "Following the structure of copper-zinc-alumina across the pressure gap in carbon dioxide hydrogenation." Nature Catalysis 4.6 (2021): 488-497.
20. Silva Sousa, Leonardo da, et al. "Identification of Transient Intermediates and Active Species in Atomic CZA Catalysts for CO2 Hydrogenation to Methanol." Journal of the American Chemical Society 147.47 (2025): 43295-43316.
21. Martin, Oliver, et al. "Indium oxide as a superior catalyst for methanol synthesis by CO2 hydrogenation." *Angewandte Chemie* 128.21 (2016): 6369-6373.
22. Twigg, Martyn V., and Michael S. Spencer. "Deactivation of supported copper metal catalysts for hydrogenation reactions." *Applied Catalysis A: General* 212.1-2 (2001): 161-174.
23. Yang, Meng, et al. "Unlocking a Dual-Channel Pathway in CO2 Hydrogenation to Methanol over Single-Site Zirconium on Amorphous Silica." *Angewandte Chemie* 136.4 (2024): e202312292.
24. Fisher, Ian A., Hee Chul Woo, and Alexis T. Bell. "Effects of zirconia promotion on the activity of Cu/SiO2 for methanol synthesis from CO/H2 and CO2/H2." *Catalysis letters* 44.1 (1997): 11-17.
25. Zhu, Yifeng, et al. "Copper-zirconia interfaces in UiO-66 enable selective catalytic hydrogenation of CO2 to methanol." *Nature communications* 11.1 (2020): 5849.
26. Lam, Erwin, et al. "Zr (IV) surface sites determine CH3OH formation rate on Cu/ZrO2/SiO2-CO2 hydrogenation catalysts." *Chinese Journal of Catalysis* 40.11 (2019): 1741-1748.
27. Szummer, A., et al. "Effect of hydrogenation under high pressure on the structure and catalytic properties of Cu–Zr amorphous alloys." *Journal of Molecular Catalysis A: Chemical* 176.1-2 (2001): 205-212.

28. Vergara, Tomás, et al. "On the Structure Sensitivity of CO2 Hydrogenation over Cu/ZrO2: Insights into the Role of the Support and the Active Sites." *ACS Catalysis* 14.18 (2024): 14127-14138.
29. Tada, Shohei, et al. "Cu species incorporated into amorphous ZrO2 with high activity and selectivity in CO2-to-methanol hydrogenation." *The Journal of Physical Chemistry C* 122.10 (2018): 5430-5442.
30. Wambach, Jörg, Alfons Baiker, and Alexander Wokaun. "CO 2 hydrogenation over metal/zirconia catalysts." *Physical Chemistry Chemical Physics* 1.22 (1999): 5071-5080.
31. Arena, Francesco, et al. "Solid-state interactions, adsorption sites and functionality of Cu-ZnO/ZrO2 catalysts in the CO2 hydrogenation to CH3OH." *Applied Catalysis A: General* 350.1 (2008): 16-23.
32. Mao, Donglei, et al. "The influence of the compositions and structures of Cu-ZrO2 catalysts on the catalytic performance of CO2 hydrogenation to CH3OH." *Chemical Engineering Journal* 471 (2023): 144605.
33. Bianchi, Daniel, et al. "Intermediate species on zirconia supported methanol aerogel catalysts: I. State of the catalyst surface before and after the adsorption of hydrogen." *Applied Catalysis A: General* 101.2 (1993): 297-315.
34. Zhao, Huibo, et al. "The role of Cu1–O3 species in single-atom Cu/ZrO2 catalyst for CO2 hydrogenation." *Nature Catalysis* 5.9 (2022): 818-831.
35. Chang, Xiao, et al. "Insight into the role of Cu–ZrO2 interaction in methanol synthesis from CO2 hydrogenation." *Industrial & Engineering Chemistry Research* 61.20 (2022): 6872-6883.
36. Tada, Shohei, et al. "Design of interfacial sites between Cu and amorphous ZrO2 dedicated to CO2-to-methanol hydrogenation." *ACS Catalysis* 8.9 (2018): 7809-7819.
37. Ding, Jieqiong, et al. "ZrO2 Morphology-Dependent Cu–ZrO2 Interfacial Catalysis in CO2 Hydrogenation to Methanol Reaction." *ACS Catalysis* 15.14 (2025): 12386-12394.
38. Oshima, Kazumasa, et al. "Mechanochemical effect in mixing sponge copper with amorphous ZrO2 creates effective active sites for methanol synthesis by CO2 hydrogenation." *The Journal of Physical Chemistry C* 125.15 (2021): 8155-8162.

39. Huang, Yonglong, and Zhengkang Duan. "Research progress on Cu-ZrO2 catalysts: a systematic review of their preparations, doping, and applications." *Journal of Materials Chemistry A* (2025).
40. Garanin, Yuriy, et al. "Influence of precursors and mineralizers on phase formation in ZrO2 nanoparticles synthesized by the hydrothermal method." *Scientific Reports* 15.1 (2025): 26165.
41. Lam, Erwin, et al. "Isolated Zr surface sites on silica promote hydrogenation of CO2 to CH3OH in supported Cu catalysts." *Journal of the American Chemical Society* 140.33 (2018): 10530-10535.
42. Xu, Ming, et al. "Renaissance of strong metal–support interactions." *Journal of the American Chemical Society* 146.4 (2024): 2290-2307.
43. Ding, Jian, et al. "Enhanced selectivity to methanol in CO2 hydrogenation on CuO/ZrO2 catalysts by alkali metal modification." *ChemCatChem* 17.2 (2025): e202401400.
44. López-Luque, Iván, et al. "Engineering Peripheral Metal-Oxide Catalysis: Interparticle Spacing in Cu/ZrO2 Catalysts for Methanol Synthesis by CO2 Hydrogenation." *Angewandte Chemie International Edition* 64.37 (2025): e202420126.
45. Kattel, Shyam, et al. "Optimizing binding energies of key intermediates for CO2 hydrogenation to methanol over oxide-supported copper." *Journal of the American Chemical Society* 138.38 (2016): 12440-12450.
46. Hong, Qi-Jun, and Zhi-Pan Liu. "Mechanism of CO2 hydrogenation over Cu/ZrO2 (212) interface from first-principles kinetics Monte Carlo simulations." *Surface science* 604.21-22 (2010): 1869-1876.
47. Polierer, Sabrina, et al. "On the reactivity of the Cu/ZrO2 system for the hydrogenation of CO2 to methanol: A density functional theory study." *The Journal of Physical Chemistry C* 123.44 (2019): 26904-26911.
48. Liu, Lingna, et al. "Zirconia-modified copper catalyst for CO2 conversion to methanol from DFT study." *Applied Surface Science* 528 (2020): 146900.
49. Al Abdulghani, Abdullah J., et al. "Uncovering the pressure-dependent mechanism of CO2 hydrogenation to methanol on Ga-promoted Cu/ZrO2 using operando modulation-excitation DRIFTS." *Journal of the American Chemical Society* 147.31 (2025): 27438-27448.

50. Wu, Congyi, et al. "Inverse ZrO2/Cu as a highly efficient methanol synthesis catalyst from CO2 hydrogenation." *Nature communications* 11.1 (2020): 5767.
51. Xu, Yangzhi, et al. "Insights into the interfacial structure of Cu/ZrO2 catalysts for methanol synthesis from CO2 hydrogenation: Effects of Cu-supported nano-ZrO2 inverse interface." *Chemical Engineering Journal* 470 (2023): 144006.
52. Fisher, Ian A., and Alexis T. Bell. "In-situinfrared study of methanol synthesis from h2/co2over cu/sio2and cu/zro2/sio2." *Journal of Catalysis* 172.1 (1997): 222-237.
53. Fisher, Ian A., and Alexis T. Bell. "In situ infrared study of methanol synthesis from H2/CO over Cu/SiO2and Cu/ZrO2/SiO2." *Journal of Catalysis* 178.1 (1998): 153-173.
54. Yang, Yong, et al. "Mechanistic studies of methanol synthesis over Cu from CO/CO2/H2/H2O mixtures: The source of C in methanol and the role of water." *Journal of catalysis* 298 (2013): 10-17.
55. Meunier, Frederic C., et al. "Cu-bound formates are main reaction intermediates during CO2 hydrogenation to methanol over Cu/ZrO2." *Angewandte Chemie International Edition* 62.29 (2023): e202303939.
56. Meunier, Frederic C., et al. "Differentiating the reactivity of ZrO2-bound formates formed on Cu/ZrO2 during CO2 hydrogenation." *Catalysts* 12.7 (2022): 793.
57. Grabow, L. C., and M. Mavrikakis. "Mechanism of methanol synthesis on Cu through CO2 and CO hydrogenation." *Acs Catalysis* 1.4 (2011): 365-384.
58. Meunier, Frederic C., and Alexandre Goguet. "Achievements and challenges in deciphering heterogeneous catalytic reaction mechanisms using operando infrared spectroscopies." *Nature Communications* (2025).
59. Srinivasan, Priya D., et al. "Application of modulation excitation-phase sensitive detection-DRIFTS for in situ/operando characterization of heterogeneous catalysts." *Reaction Chemistry & Engineering* 4.5 (2019): 862-883.
60. Weyel, Jakob, et al. "Modulation Excitation Spectroscopy: A Powerful Tool to Elucidate Active Species and Sites in Catalytic Reactions." *Accounts of Chemical Research* 57.18 (2024): 2643-2652.
61. Du, Hong, et al. "Catalytic furfural hydrogenation to furfuryl alcohol over Cu/SiO2 catalysts: A comparative study of the preparation methods." *Fuel Processing Technology* 193 (2019): 221-231.

62. Dong, Xiaohuan, et al. "Comparative study of silica-supported copper catalysts prepared by different methods: formation and transition of copper phyllosilicate." *Catalysis Science & Technology* 6.12 (2016): 4151-4158.
63. Yu, Jiafeng, et al. "Stabilizing Cu+ in Cu/SiO2 catalysts with a shattuckite-like structure boosts CO2 hydrogenation into methanol." *ACS catalysis* 10.24 (2020): 14694-14706.
64. Han, Xue-Qing, et al. "Selective hydrogenation of dimethyl maleate to tetrahydrofuran over Cu/SiO2 catalyst: Effect of Cu+ on the catalytic performance." *Chinese Chemical Letters* 26.9 (2015): 1150-1154.
65. Shawabkeh, Reyad A., et al. "Adsorption of CO2 on Cu/SiO2 nano-catalyst: Experimental and theoretical study." *Applied Surface Science* 586 (2022): 152726.
66. Wu, Yingquan, et al. "Effect of preparation method on ZrO2-based catalysts performance for isobutanol synthesis from syngas." *Catalysts* 9.9 (2019): 752.
67. Dan, Hui, et al. "Preparation of amorphous ZrO2 powders by hydrothermal-assisted sol-gel method." *Inorganic Chemistry Communications* 138 (2022): 109272.
68. Witoon, Thongthai, et al. "CO2 hydrogenation to methanol over Cu/ZrO2 catalysts: Effects of zirconia phases." *Chemical Engineering Journal* 293 (2016): 327-336.
69. Yu, Jiahui, et al. "Cu-ZrO2 catalysts with highly dispersed Cu nanoclusters derived from ZrO2@ HKUST-1 composites for the enhanced CO2 hydrogenation to methanol." *Chemical Engineering Journal* 419 (2021): 129656.
70. Śliwa, Michał, and Katarzyna Samson. "Influence of synthesis parameters on physicochemical properties of CuO/ZrO2 catalysts." *Chemical Papers* 73.11 (2019): 2793-2802.
71. Ahmad, Kaisar, and Sreedevi Upadhyayula. "Greenhouse gas CO2 hydrogenation to fuels: A thermodynamic analysis." *Environmental Progress & Sustainable Energy* 38.1 (2019): 98-111.
72. Samson, Katarzyna, et al. "Influence of ZrO2 structure and copper electronic state on activity of Cu/ZrO2 catalysts in methanol synthesis from CO2." *ACS catalysis* 4.10 (2014): 3730-3741.
73. Binet, Claude, and Marco Daturi. "Methanol as an IR probe to study the reduction process in ceria–zirconia mixed compounds." *Catalysis today* 70.1-3 (2001): 155-167.

74. Ouyang, Feng, and Shuiliang Yao. "Infrared study of ZrO2 surface sites using adsorbed probe molecules. 2. dimethyl ether adsorption." *The Journal of Physical Chemistry B* 104.47 (2000): 11253-11257.
75. Graf, P. O., et al. "New insights in reactivity of hydroxyl groups in water gas shift reaction on Pt/ZrO2." *Journal of catalysis* 262.2 (2009): 181-187.
76. Li, Kongzhai, and Jingguang G. Chen. "CO2 hydrogenation to methanol over ZrO2-containing catalysts: insights into ZrO2 induced synergy." *ACS catalysis* 9.9 (2019): 7840-7861.
77. Quan, Jiamei, et al. "Vibration-driven reaction of CO2 on Cu surfaces via Eley–Rideal-type mechanism." *Nature Chemistry* 11.8 (2019): 722-729.
78. Nakano, Haruhisa, et al. "Structure-dependent kinetics for synthesis and decomposition of formate species over Cu (111) and Cu (110) model catalysts." *The Journal of Physical Chemistry B* 105.7 (2001): 1355-1365.
79. Pokrovski, Konstantin, Kyeong Taek Jung, and Alexis T. Bell. "Investigation of CO and CO2 adsorption on tetragonal and monoclinic zirconia." *Langmuir* 17.14 (2001): 4297-4303.
80. Zhao, Kun, et al. "Identifying reaction species by evolutionary fitting and kinetic analysis: an example of CO2 hydrogenation in DRIFTS." *The Journal of Physical Chemistry C* 123.14 (2019): 8785-8792.
81. Xiong, Wei, et al. "Cu Facet-dependent elementary surface reaction kinetics of CO2 hydrogenation to methanol catalyzed by ZrO2/Cu inverse catalysts." *The Journal of Physical Chemistry Letters* 14.32 (2023): 7229-7234.
82. Jung, Kyeong Taek, and Alexis T. Bell. "The effects of synthesis and pretreatment conditions on the bulk structure and surface properties of zirconia." *Journal of Molecular Catalysis A: Chemical* 163.1-2 (2000): 27-42.
83. Fisher, Ian A., and Alexis T. Bell. "A mechanistic study of methanol decomposition over Cu/SiO2, ZrO2/SiO2, and Cu/ZrO2/SiO2." *Journal of Catalysis* 184.2 (1999): 357-376.
84. Gau, Alina, et al. "Operando spectroscopic monitoring of active species in CO2 hydrogenation at elevated pressure and temperature: steady-state versus transient analysis." *Energy & Fuels* 35.18 (2021): 15243-15246.

85. Feng, Zhendong, et al. "Asymmetric sites on the ZnZrO x catalyst for promoting formate formation and transformation in CO2 hydrogenation." *Journal of the American Chemical Society* 145.23 (2023): 12663-12672.
86. Caldas, Paula CP, et al. "The structure of the Cu–CuO sites determines the catalytic activity of cu nanoparticles." *ACS catalysis* 7.4 (2017): 2419-2424.
87. Zhang, Diyu, et al. "Characterization of CO Adsorbed to Clean and Partially Oxidized Cu (211) and Cu (111)." *The Journal of Physical Chemistry C* 127.50 (2023): 24158-24167.
88. Hadjiivanov, Konstantin I., and Georgi N. Vayssilov. "Characterization of oxide surfaces and zeolites by carbon monoxide as an IR probe molecule." (2002): 307-511.

APPENDIX

Publication: Novel Aqueous-Phase Process for Conversion of 3-Hydroxybutyric Acid to 1,3-Butanediol: Effects of Temperature, Hydrogen Pressure, and Nature of Ru-Supported Catalysts on Selective Hydrogenation

DOI: https://doi.org/10.1021/acsengineeringau.5c00049

ACS Engineering Au > Vol 5/Issue 6 > Article

Open Access

Cite Share Jump to Expand

ARTICLE | September 12, 2025

Novel Aqueous-Phase Process for Conversion of 3-Hydroxybutyric Acid to 1,3-Butanediol: Effects of Temperature, Hydrogen Pressure, and Nature of Ru-Supported Catalysts on Selective Hydrogenation

João Lucas Marques Barros, José Lucas Vieira, Jean Marcel R. Gallo, Carla Ramos Moreira, Adriana Maria da Silva, and José Maria Corrêa Bueno*

Abstract

A novel aqueous-phase hydrogenation reaction was developed for the conversion of 3-hydroxybutyric acid (HBA) to 1,3-butanediol (1,3-BDO) over catalysts composed of Ru supported on TiO_2, SiO_2, and C. Analyses using XRD and Raman spectroscopy indicated strong metal–oxide interactions in the Ru/TiO_2 samples, while weak interactions of Ru with SiO_2 led to crystallization of the Ru species. Preliminary catalytic tests with a commercial Ru/C catalyst showed that higher H_2 pressure and low temperature (130 °C) enabled selective hydrogenation of HBA to 1,3-BDO. Compared to the commercial